

LINKING URBAN MOBILITY PATTERNS WITH DISEASE CONTAGION IN  
URBAN NETWORKS

A Dissertation

Submitted to the Faculty

of

Purdue University

by

Xinwu Qian

In Partial Fulfillment of the

Requirements for the Degree

of

Doctor of Philosophy

December 2018

Purdue University

West Lafayette, Indiana



**THE PURDUE UNIVERSITY GRADUATE SCHOOL**  
**STATEMENT OF APPROVAL**

Dr. Satish V. Ukkusuri, Chair

Lyles School of Civil Engineering

Dr. Joaquín Goñi

School of Industrial Engineering and School of Biomedical Engineering

Dr. Andrew Liu

School of Industrial Engineering

Dr. Shreyas Sundaram

School of Electrical and Computer Engineering

**Approved by:**

Dr. Dulcy M. Abraham

Head of the School Graduate Program

To my parents and my wife.

## ACKNOWLEDGMENTS

I am deeply indebted to my advisor and mentor Dr. Satish Ukkusuri, for his expert supervision, excellent guidance, and endless support throughout my Ph.D. study. It was a great pleasure to work and conduct research under his supervision during the past six and half years.

I would like to express my appreciation to the other three members of my Ph.D. advisory committee: Dr. Andrew Liu, Dr. Shreyas Sundaram, and Dr. Joaquín Goñi. You have provided me extremely valuable suggestions in finalizing the research questions after the preliminary exam and in improving the research frameworks of the dissertation.

Thanks to my former and current lab mates - Xianyuan Zhan, Kein Doan, Samiul Hasan, Feng Zhu, Rodrigo Arango, Wenbo Zhang, Arif Sadri, Hemant Gehlot, Tho Le, and Takahiro Yabe, for their help and support during my Ph.D. study at Purdue. I would like to especially thank Xianyuan and Kein for their mentoring at the early stage of my Ph.D. study. And thanks to my collaborators, Dr. Xin Chen at the University of Dayton, Dr. Lijun Sun at McGill University, and Jiawei Xue at Purdue University, for their contributions to this dissertation.

Finally, my deepest gratitude goes to my dear mother, Aimei Li, and dear father, Guangren Qian, and my better half, Shenmeng Chen, for being with me during the six and half years of my Ph.D. study. This journey would not have been possible if not for them, and I dedicate this milestone to them.

## TABLE OF CONTENTS

	Page
LIST OF TABLES . . . . .	ix
LIST OF FIGURES . . . . .	x
ABSTRACT . . . . .	xiii
1 INTRODUCTION . . . . .	1
1.1 Background . . . . .	1
1.1.1 Urbanization and infectious diseases . . . . .	1
1.1.2 Impact of urban infectious diseases . . . . .	3
1.2 Motivation . . . . .	7
1.2.1 Urban travel . . . . .	7
1.2.2 The era of big data . . . . .	9
1.2.3 Gap in the literature . . . . .	10
1.3 Objectives of the dissertation . . . . .	12
1.4 Organization of the dissertation . . . . .	13
2 EPIDEMIC MODELING . . . . .	17
2.1 The basics . . . . .	17
2.1.1 The susceptible-infectious-recovery (SIR) model . . . . .	17
2.1.2 Disease over the network . . . . .	19
2.2 Literature review on compartment models for epidemic modeling . . . . .	21
2.3 Literature review on disease over networks . . . . .	25
2.4 Summary . . . . .	28
PART I: NETWORK MODEL FOR SPREADING OF INFECTIOUS DISEASES	
3 MODELING DISEASE CONTAGION IN URBAN TRANSPORTATION SYSTEM . . . . .	31
3.1 Introduction . . . . .	31
3.2 Modeling preliminaries . . . . .	34
3.2.1 Notation . . . . .	34
3.2.2 Epidemic modeling . . . . .	34
3.2.3 Mobility model . . . . .	37
3.3 Modeling disease spreading with travel contagion . . . . .	40
3.3.1 The basic model . . . . .	40
1. Notation . . . . .	40
2. System dynamics . . . . .	42
3. Formulation . . . . .	44

	Page
3.3.2	Stability of the transportation system . . . . . 46
3.3.3	Control the spread of disease within transportation system . . . 50
3.4	Verification for the control strategies . . . . . 53
3.4.1	Hybrid automata . . . . . 54
3.4.2	Reachability analysis using Taylor model flowpipe construction . 56
3.5	Results . . . . . 60
3.5.1	Experiment setting . . . . . 60
3.5.2	Case study: 2003 SARS outbreak in Beijing . . . . . 62
3.5.3	The role of contagion within transportation system . . . . . 67
3.5.4	Reachability analysis . . . . . 74
3.6	Conclusion . . . . . 81

## PART II: DISEASE SPREADING IN CONTACT NETWORK

4	METRO CONTACT MODELING . . . . . 83
4.1	Introduction . . . . . 83
4.2	Data . . . . . 85
4.3	Metro contact network . . . . . 87
4.4	Individual based transmission model . . . . . 94
4.4.1	Disease transmission rate . . . . . 95
4.4.2	Individual based transmission model . . . . . 96
4.5	OD-level model . . . . . 99
4.5.1	Equivalence between individual model and the OD level model 101
4.6	Generation model . . . . . 103
4.6.1	Generation rule . . . . . 104
4.6.2	Analytical expression . . . . . 105
4.6.3	Validation . . . . . 106
4.6.4	Parameter fitting . . . . . 107
4.7	Results . . . . . 107
4.7.1	Change of vulnerability over time . . . . . 107
4.7.2	Control the metro network . . . . . 110
	1. Random control . . . . . 110
	2. Target control . . . . . 110
	3. Path-based control . . . . . 110
	4. Station-based control . . . . . 110
	5. Results . . . . . 111
4.7.3	Fitting generation function to MCN . . . . . 112
4.7.4	Discussion . . . . . 116
4.8	Conclusion . . . . . 120

## PART III: MULTIPLEX NETWORKS FOR INFORMATION AND DISEASE PERCOLATION AND CO-EVOLUTION

	Page
5 DISEASE SPREADING WITH LOCAL AND GLOBAL INFORMATION DISSEMINATION IN MULTIPLEX NETWORKS . . . . .	123
5.1 Introduction . . . . .	123
5.2 Notation . . . . .	125
5.3 Assumption . . . . .	125
5.4 UA-SIS model . . . . .	126
5.5 Formulation . . . . .	129
5.5.1 Observation layer . . . . .	129
5.5.2 Disease layer . . . . .	129
5.5.3 Information layer . . . . .	130
5.5.4 Probability of a node in infectious state . . . . .	131
5.6 System equilibrium and stability analysis . . . . .	131
5.6.1 Disease and awareness free equilibrium . . . . .	132
5.6.2 Disease free equilibrium with awareness . . . . .	135
5.6.3 Size of endemic state . . . . .	137
5.7 Numerical experiments . . . . .	139
5.8 Conclusion . . . . .	146
6 CONCLUSION AND FUTURE WORK . . . . .	149
6.1 Conclusion . . . . .	149
6.2 Future work . . . . .	151
REFERENCES . . . . .	153
VITA . . . . .	161

## LIST OF TABLES

Table	Page
1.1 Summary of vital infectious disease outbreaks . . . . .	4
3.1 Table of notation . . . . .	35
3.2 Table of notation . . . . .	41
3.3 Computational efficiency of the Taylor model approach with different parameter settings . . . . .	74
4.1 Summary of metro card transaction data from three major cities in China	86
4.2 Summary statistics of the generated contact networks . . . . .	92
4.3 Table of notation . . . . .	96
4.4 Summary of fitted results and model parameters from K-S test for three cities. . . . .	115
5.1 Table of notation . . . . .	125

## LIST OF FIGURES

Figure	Page
1.1 Total number of worldwide international tourism arrivals from 1995-2015 . . . . .	2
1.2 Annual influenza associated death in United States from 1976-2006. Data source: CDC . . . . .	3
1.3 Prevalent infected diseases in each decade since 1960s . . . . .	4
1.4 Timeline of SARS outbreak [13] . . . . .	5
1.5 Thermal imaging camera used for screening suspicious travelers in Israel during SARS. (source: Getty Image) . . . . .	6
1.6 Relationship between transportation engineering and public health, and the number of studies on each topic since 2013. Data were collected from Google Scholar. . . . .	11
1.7 Dissertation framework . . . . .	14
2.1 Illustration of the SIR model with contagion rate $\beta$ and recovery rate $\gamma$ . (compartment model) . . . . .	17
2.2 Illustration of the SIR model over networks. . . . .	19
3.1 Illustration of the disease contagion process in a 3-patch network . . . . .	43
3.2 Illustration of the passenger dynamics . . . . .	51
3.3 Controlled transportation system . . . . .	53
3.4 A 2-dimensional hybrid automaton . . . . .	56
3.5 Example of a Taylor model $(p(x), [a, b])$ . . . . .	57
3.6 Example of domain contraction . . . . .	57
3.7 An overapproximation for flowpipe/guard intersections . . . . .	60
3.8 Flowpipes for the 2-D hybrid automaton . . . . .	60
3.9 Test network with 3 nodes . . . . .	62
3.10 Networks with three different urban structures . . . . .	62
3.11 Measures were taken in mass transit systems to identify probable cases of SARS in Beijing . . . . .	63

Figure	Page
3.12 The Beijing network with 5 nodes . . . . .	64
3.13 Cumulative SARS cases since April-20, 2013, Beijing, China . . . . .	66
3.14 Daily increases of SARS cases since April-20, 2013, Beijing, China . . . . .	66
3.15 Total infected population over time . . . . .	68
3.16 Total number of infected people in each patch . . . . .	71
3.17 The change of $R_0$ by modeling urban travel . . . . .	72
3.18 Comparison of no-control scheme versus hybrid system setting . . . . .	73
3.19 Accuracy with different cutoff thresholds and Taylor model orders . . . . .	75
3.20 Evaluation of successive errors (in log scale) due to wrapping effect at each time step . . . . .	78
3.21 Accuracy with different cutoff thresholds and Taylor model orders . . . . .	80
4.1 Metro network structures, passenger demand distributions, and passenger travel time distributions of the three cities . . . . .	87
4.2 Probability that two passengers will be on the same train as a function of their gap of arrival time at the station . . . . .	89
4.3 Visualization of sample MCNs from the three cities, with 100, 500, and 1000 passengers from left to right, followed by their degree distributions . . . . .	91
4.4 CCDF of unweighted and weighted degree distributions for MCNs of the three cities. . . . .	94
4.5 Variation of risk level with respect to different time of the day, in all three cities. Both overall risk as well as the risk per individual are presented. . . . .	109
4.6 Evaluations of effectiveness of various control strategies on improving the vulnerability of metro network to infectious diseases. . . . .	112
4.7 Visualization for the goodness of fit of the generation model to the MCNs generated from the smart card data. . . . .	114
4.8 Validation of the generation model by varying train frequency and number of passengers . . . . .	116
4.9 The correlations among travel time, number of contacts, and total contagion duration in MCNs of three cities. . . . .	118
5.1 Illustration of the UA-SIS modeling process. . . . .	127
5.2 Illustration of the UA-SIS information dissemination process. . . . .	128

Figure	Page
5.3 Spreading rate of awareness with the change of individual perception of disease . . . . .	134
5.4 Infectious population (left) and aware population (right) with varying $\beta$ and $p$ . . . . .	139
5.5 The impact of local information on disease spreading dynamics . . . . .	140
5.6 The impact of global information on disease spreading dynamics . . . . .	142
5.7 Comparison between $\lambda_D$ and $\lambda_{DFEA}$ . DFE is achieved when $\lambda < 0$ , otherwise the disease process will reach the endemic state. . . . .	143
5.8 The rate of change for S and I in three different equilibrium states . . . . .	144
5.9 Decay of disease threshold in scale free network with increasing number of nodes (increasing maximum degree). ( $\gamma = -2.5$ ) . . . . .	146

## ABSTRACT

Qian, Xinwu PhD, Purdue University, December 2018. Linking urban mobility patterns with disease contagion in urban networks. Major Professor: Satish V. Ukkusuri.

This dissertation focuses on developing a series of mathematical models to understand the role of urban transportation system, urban mobility and information dissemination in the spreading process of infectious diseases within metropolitan areas. Urban transportation system serves as the catalyst of disease contagion since it provides the mobility for bringing people to participate in intensive urban activities and has high passenger volume and long commuting time which facilitates the spread of contagious diseases. In light of significant needs in understanding the connection between disease contagion and the urban transportation systems, both macroscopic and microscopic models are developed and the dissertation consists of three main parts.

The first part of the dissertation aims to model the macroscopic level of disease spreading within urban transportation system based on compartment models. Non-linear dynamic systems are developed to model the spread of infectious disease with various travel modes, compare models with and without contagion during travel, understand how urban transportation system may facilitate or impede epidemics, and devise control strategies for mitigating epidemics at the network level. The hybrid automata is also introduced to account for systems with different levels of control and with uncertain initial epidemic size, and reachability analysis is used to over-approximate the disease trajectories of the nonlinear systems. The 2003 Beijing SARS data are used to validate the effectiveness of the model. In addition, comprehensive numerical experiments are conducted to understand the importance of modeling travel contagion during urban disease outbreaks and develop control strate-

gies for regulating the entry of urban transportation system to reduce the epidemic size.

The second part of the dissertation develops a data-driven framework to investigate the disease spreading dynamics at individual level. In particular, the contact network generation algorithm is developed to reproduce individuals' contact pattern based on smart card transaction data of metro systems from three major cities in China. Disease dynamics are connected with contact network structures based on individual based mean field and origin-destination pair based mean field approaches. The results suggest that the vulnerability of contact networks solely depends on the risk exposure of the most dangerous individual, however, the overall degree distribution of the contact network determines the difficulties in controlling the disease from spreading. Moreover, the generation model is proposed to depict how individuals get into contact and their contact duration, based on their travel characteristics. The metro data are used to validate the correctness of the generation model, provide insights on monitoring the risk level of transportation systems, and evaluate possible control strategies to mitigate the impacts due to infectious diseases.

Finally, the third part of the dissertation focuses on the role played by information in urban travel, and develops a multiplex network model to investigate the co-evolution of disease dynamics and information dissemination. The model considers that individuals may obtain information on the state of diseases by observing the disease symptoms from the people they met during travel and from centralized information sources such as news agencies and social medias. As a consequence, the multiplex networks model is developed with one layer capturing information percolation and the other layer modeling the disease dynamics, and the dynamics on one layer depends on the dynamics of the other layer. The multiplex network model is found to have three stable states and their corresponding threshold values are analytically derived. In the end, numerical experiments are conducted to investigate the effectiveness of local and global information in reducing the size of disease outbreaks and the synchronization between disease and information dynamics is discussed.

# 1. INTRODUCTION

## 1.1 Background

### 1.1.1 Urbanization and infectious diseases

Urbanization is the process where increasing number of people migrate to urban areas from rural places. It is estimated that over 64% population of developing countries and 86% population of developed countries will reside in urban areas by the end of 2050 [1], which is four times greater than the size of urban population by the end of 20th century. The rapid urbanization process brings more intensive urban activities, vivid land use patterns, the developments of urban infrastructures as well as the economy system. Meanwhile, urban population have access to better sanitary system, cleaner water sources, and well-established system of personal health care. All these benefits signify that urbanization may lead to the society with superior efficiency. But challenges also arise with the fast-growing urban population. There are concerns related to housing, education, energy consumption, urban waste, emission and pollution. The traffic congestion and road accidents are also well-known byproducts of the urbanization process. And significant efforts have been made during the past few decades to address the above-mentioned issues for improving urban efficiency.

However, there is one additional challenge for the urban population, whose consequence is likely to be underestimated, the spread of infectious diseases. The World Health Organization (WHO) has listed urbanization as a major public health challenge in the 21st century. But major efforts were focused on physical activities and mental health [2–4], where researchers were more concerned with the consequences

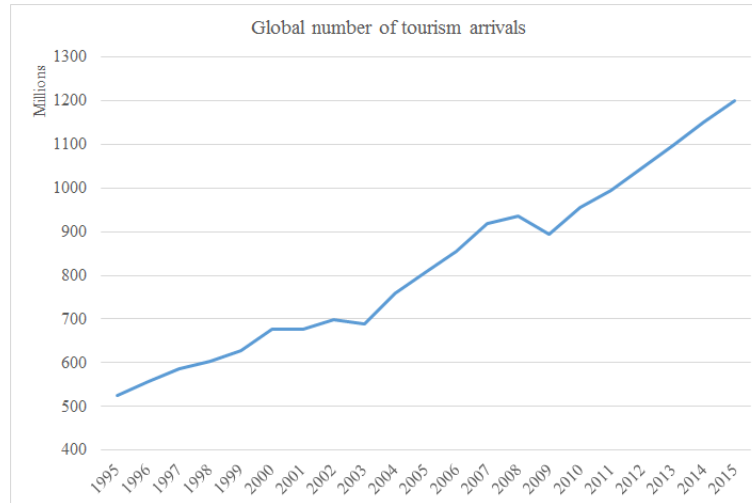


Figure 1.1.: Total number of worldwide international tourism arrivals from 1995-2015

and treatments of road accidents, air pollution, obesity, and mental disorder condition. And various studies have established the connections between urban planning and urban population health, and devised measures for promoting urban public health [5,6]. Under the impression of the availability of vaccines to major communicable diseases, the accessibility to advanced urban health care system, and the development of modern medicine and pharmacy, few studies explored the risk of infectious diseases associated with the vast urban population.

Is infectious disease a major challenge to urban population? Perhaps the current urban society is more vulnerable to the invasion of infectious diseases than any other time in the history, and will be increasingly more vulnerable in the future. Proximity and exposure duration are two deterministic factors for infectious diseases to spread among population, and dense and heterogeneous urban population serve as an ideal catalyst which facilitates the disease spreading process. In addition, the world is more connected with improved accessibility to mobility services, and we have seen more and more frequent world trades and travels taking place over the years. As shown in Figure 1.1, the total number of worldwide tourism arrivals has almost tripled in 2015 than that in 1995. This implies that any local disease outbreaks may easily turn into a global outbreak nowadays, and cause significant panic worldwide. And

our memory of global panic caused by infectious diseases is still fresh, such as the Zika virus epidemic in 2015-2016 [7] and the SARS outbreak in 2002 [8]. Both disease outbreaks are representative examples where local diseases evolve into global endemic, and the disease timeline of 2002 SARS is shown in Figure 1.4. Last but not least, the leading causes of death in low income countries are reported to be lower respiratory infections, HIV/AIDS, malaria, tuberculosis, and diarrhea disease [9], all belonging to infectious diseases. While the most rapid urbanization is expected to take place in low-income developing countries [10], the challenge of infectious disease should be one of the major issues that needs to be properly addressed during urbanization processes in these countries.

### 1.1.2 Impact of urban infectious diseases

Infectious diseases, also known as communicable or transmissible diseases, are transmitted by healthy individual contact with an infected person or virus hosts such as mosquitoes. There are over 200 different types of infectious disease nowadays [11]. It can be as minor as a common cold and flu where a person may be self-cured after several days, or may be as deadly as SARS in 2002 when no effective vaccine nor treatment was available.

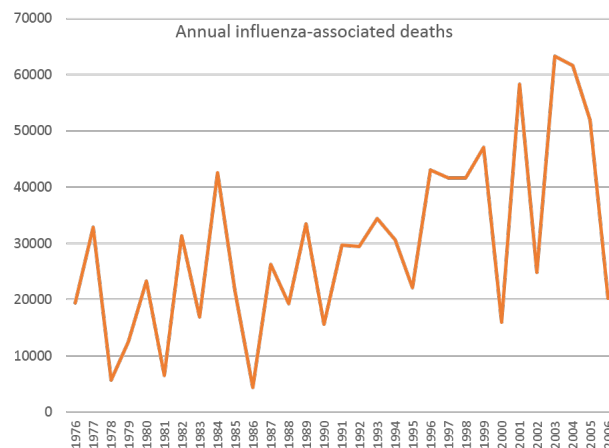


Figure 1.2.: Annual influenza associated death in United States from 1976-2006. Data source: CDC

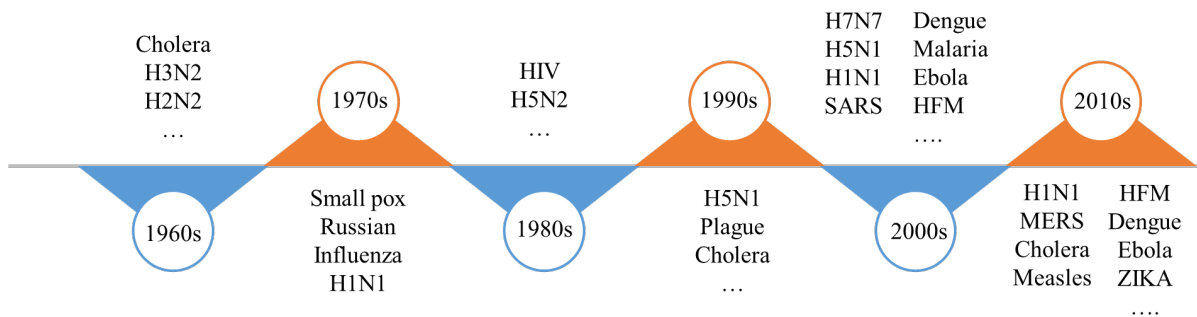


Figure 1.3.: Prevalent infected diseases in each decade since 1960s

Table 1.1.: Summary of vital infectious disease outbreaks

Time	Disease	Spread	Consequence
1850s	Measles	Cough, tears	20 million cases worldwide
1950s	Smallpox	Face-to-Face contact	15 million cases each year, killed 500 million people
...	...	...	...
2003	SARS	Person-to-person	8,273 cases, 775 deaths
2009	H1N1	Person-to-person	300,000 deaths
2012	MERs	Person-to-person	1,000 case reported, 40% death rate
2015	ZIKA	Mosquitoes	1.5 million people infected in Brazil

Even the consequence of flu seems minor as compared to other deadly infectious diseases, the cost of flu when it comes to the most population may become mighty. As presented in Figure 1.2, since 1976, the influenza has taken over 20,000 lives on average each year, and the number of deaths is in an overall growing trend even though the disease can be easily prevented by vaccines or effectively treated. In the year 2015, the flu was reported to account for \$5.8 billion in health care and lost productivity costs, and the pandemic outbreak of flu resulted in the GDP loss between \$34.4 billion and \$45.3 billion [12]. And if we look back into the past five decades, there were numerous infectious diseases which resulted in significant losses of human lives and economy as shown in Figure 1.3. Most of these diseases were transmitted through close human contact, such as measles, small pox, and plague, and led to a large number of infected people and deaths due to limited accessibility to health care infrastructures and underdeveloped modern medicine. Smallpox alone

resulted in 500 million death during 1950s, and latter reappeared in 1970s. But effective vaccines have been developed since then and such infectious diseases are no longer major threats for modern human societies. The real challenges are introduced by the infectious diseases with numerous variants (e.g., H1N1, H5N2, H3N2), having periodical outbreaks, and most importantly, no effective vaccines or treatments being available by the time that the disease was first identified. In this situation, a single case of infected individual may lead to rapid growth of total infected population and rapid synchronization of the disease all over the world.

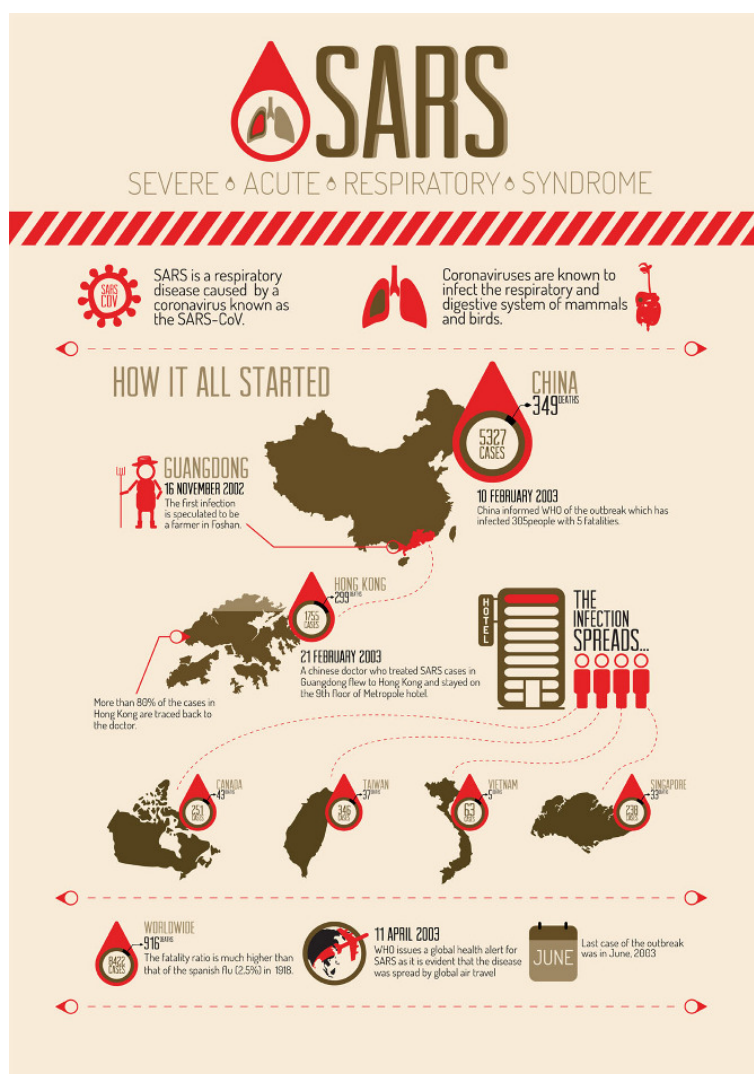


Figure 1.4.: Timeline of SARS outbreak [13]



Figure 1.5.: Thermal imaging camera used for screening suspicious travelers in Israel during SARS. (source: Getty Image)

A notable example of the above mentioned scenario is the 2002 SRAS outbreak (see Figure 1.4). The patient zero was believed to appear in Guangdong Province, China, in November 2002. But not until the next February did people start to pay attention to the disease, when there had been 305 suspicious cases reported and 5 people had already lost their lives. While most of the cases were found local, on February 21, 2003, first case was identified in Hong Kong, which is one the largest cities in the world famous for international trades and travels. Soon SARS outbreaks were reported in many other major cities and countries around the world, including China, Singapore, Vietnam, and Canada. The disease caused significant global panic during its outbreak, and was transmitted at an unprecedented pace over the world. By the time when most of the cities were removed by WHO from the list of areas with recent local transmission, SARS had affected at least 8,000 people worldwide and taken 775 lives, most of them being medical workers. Apparently, the growth of regional and global transportation networks played an important role in the rapid spread of the disease. And during the global SARS outbreaks, we have seen at airports and transit entrances the screening equipment (e.g., the use of thermal imaging cameras, shown in Figure 1.5) being introduced for spotting suspicious travelers, which was

believed to have significant contributions to lower the number of infected population and deaths during the time. Such control procedures have also been used in later global epidemic outbreaks, such as H1N1 and MERS.

As of today, the most reliable and practical method for addressing the invasion of infectious diseases is through vaccination, whose development relies heavily on the advances in pathology, pharmacy, and modern medicines. Vaccines have proven to be effective for many infectious diseases such as smallpox and measles, and have contributed significantly to the eradication of these diseases. Unfortunately, the drawback of vaccination is that it is a reactive strategy, and vaccines are usually developed after significant costs of lives and human efforts being. For disease outbreaks such as SARS and MERS, no effective vaccines were developed in a timely manner, and the best strategy one may adopt is therefore to quarantine suspicious people and prevent them from producing further infections. But quarantine as a proactive action is not an easy task especially in urban areas, considering complex urban land use and activities, large and heterogeneous population, and the rapid global synchronization of newly emerged diseases. The effective implementation of quarantine strategy requires in-depth understanding of the relationship between disease contagion and urban mobility, and hence the structures of urban transportation systems, which is the main objective of the dissertation.

## 1.2 Motivation

### 1.2.1 Urban travel

One of the key driving forces for the spread of infectious disease is intensive urban travels. While we cannot restrain people from traveling, it is important to investigate how people's travel patterns contribute to the disease transmission so that we may build a more resilient urban mobility system against disease contagion. In suburban and rural areas where people are sparsely distributed and have access to limited num-

ber of transportation modes, and the commuting patterns are stable and predictable, the disease dynamics can be easily modeled through the classic compartment model with high level of accuracy [14, 15].

But an entirely different story emerges when it comes to modeling the spread of infectious diseases within urban areas. And there are three notable characteristics of urban travels that motivate the dissertation to explore the relationship between disease transmission and urban transportation systems. First, the fact that urban population are dense and highly heterogeneous violates the key assumption on homogeneous population of the classical compartment model. Second, urban population have access to a wide collection of transportation modes, and each of these modes has its distinct characteristics when associated with the spread of diseases based on its capacity and level of mobility. But most importantly, urban population spend significant amount of time during daily commuting. Recent report suggested that New York City (NYC) residents spent an average of 6 hours and 18 minutes per week for daily commuting [16], while this number is 52 and 51 minutes per day for commuters in Beijing and Shanghai, China, respectively [17]. These statistics suggest that urban population may spend around 10% of their active daily hours in the urban transportation systems. More importantly, since disease contagion is a function of exposure time and proximity, the high population density inside the mass transit system has made the system an ideal place for infectious diseases to be transmitted over the crowd. Taking Hong Kong as an example, the population density is reported to be  $6.69 \times 10^{-3}$  per square meter [18], while the typical population density of a classroom is 0.018 per square meter and that of the office is 0.33 per square meter. However, the metro passenger density may reach 4 people per square meter and that of the bus may be up to 8 passengers per square meter. These clearly imply that people in urban transportation systems may be exposed much higher risk level for getting close contacts than in other urban activities. This observation shapes a sharp contrast to conventional epidemic models where the spread of diseases is only considered during

human activities in a particular zone or node while the risk of disease transmission during travel is totally ignored.

In conclusion, the mobility pattern in urban areas is very different and considerably more complicated than in other areas, but our understanding of its relationship with the spread of infectious diseases is still limited due to oversimplified assumptions in conventional epidemic models. The dissertation is therefore motivated to develop advanced models to investigate the role played by urban transportation systems in the spread of infectious diseases.

### 1.2.2 The era of big data

The compartment model considers the spread of infectious diseases at the macroscopic level. Such level of aggregation is valuable for decision making at the regional level, but it is also important to understand at the individual level on how disease may propagate from one to the other based on individual contact patterns. And the understanding of behavior changes at individual level is also a significant factor for accurate interpretation of people's reactions during disease outbreaks for developing individual models.

While real-time information of human mobility was barely accessible in the past, recent advances in location-based services, pervasive computing, and the dissemination of smart phones especially in urban areas provide us the opportunity to collect high resolution data of human mobility and activities at individual level. In particular, the intensive use of social network applications such as Facebook and Twitter enable us to construct virtual or even real-world contact networks. In addition, the adoption of on-board GPS devices, the use of physical or mobile travel passes, and the rise of on-demand mobility services provide the digital footprints of urban travelers in fine detail. With all of these, we are now able to trace detailed individual travel trajectories, restore daily activity sequences, and build contact networks among indi-

viduals. This turns impossible ideas in the past into possible and valuable topics at present.

The availability of big data provides us an unprecedented opportunity to model the disease contagion at individual level, however, it also introduces new challenge in modeling individual behavior during disease outbreaks. Specifically, the era of big data implies that people are more connected than ever before and are exposed to abundant information resources from social medias and news agencies. And people's behavior during disease outbreaks is unlikely to be independent from the information they have access to. That being said, human behavior is no longer the same in the era of big data: they are more likely to make rational decisions rather than greedy ones due to the improved level of knowledge of the whole system state. In this regard, it may no longer be reasonable to assume that contact networks and activity sequences may remain the same as the disease proceeds over time. This imposes an additional challenge for modeling disease contagion at individual level, and becomes the second motivation of the dissertation.

### 1.2.3 Gap in the literature

Based on previous discussions, it can be seen that the spread of infectious disease is closely related to urban mobility and urban transportation systems, and great opportunities and challenges coexist in the field for addressing the research problems from both macroscopic and microscopic levels. However, existing studies in understanding the dynamics of infectious diseases are mostly explored within the fields of biology and pathology, or through mathematical models without considering the crucial components of urban human mobility (detailed review of related mathematical models is conducted in the following chapter). And there is an emerging need to investigate this issue from transportation engineering perspective to build the connection between the spread of infectious diseases and urban transportation systems.

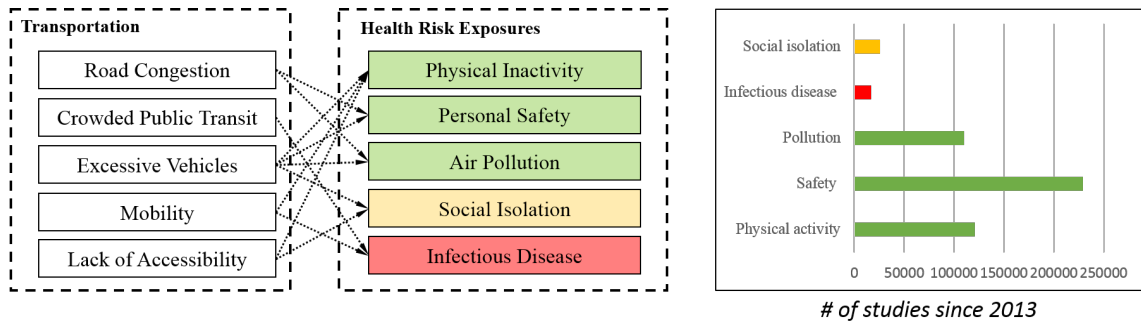


Figure 1.6.: Relationship between transportation engineering and public health, and the number of studies on each topic since 2013. Data were collected from Google Scholar.

In fact, the research idea on understanding the impact of transportation system on public health is not new, and has already drawn attentions from many scholars. But the studies almost exclusively focus on physical inactivity, personal safety, air pollution, and social isolation. There are only few studies exploring human mobility and the spread of infectious diseases, mainly from the global air travel perspective [19–21]. And this research gap is visualized by summarizing most popular research fields in transportation engineering, their relationship with public health, and the existing number of related studies (using keyword "transportation" with the corresponding health risk exposure keyword searching through Google Scholar search engine) since 2013 in Figure 1.6. While there are over 200,000 studies on safety related topics alone, and the number of studies on pollution and physical inactivity being well over 100,000, there are fewer than 20,000 studies associated with the key word "transportation + infectious disease", not mentioning that few of the 20,000 are indeed investigating this topic. Clearly, infectious disease within urban transportation system is an understudied yet significant research field, which motivates the dissertation to make one of the initial attempts to bridge this gap.

### 1.3 Objectives of the dissertation

With the background that infectious diseases become a major challenge for urban areas especially in developing countries, and that the spread of infectious diseases is closely related to the functionality and structure characteristics of urban transportation systems, the dissertation aims to investigate how urban mobility and urban transportation system may promote or impede the spread of infectious diseases, and devise control strategies and design directions in developing a more resilient and less vulnerable urban transportation system to mitigate the threats from disease outbreaks. To achieve this goal, four major objectives are proposed in this dissertation as follows.

First, the dissertation will build the connection between the spread of the infectious diseases and the overall structural of urban transportation system. Urban transportation system is a complex system consisting of multiple travel modes and it is not uncommon that the system serves tens of millions of daily passengers. In this regard, it is important to take the multi-modal nature of urban transportation system into consideration and treat the movement of such larger population size as passenger flow at the network level. And from the network level, mathematical models and computational tools will be developed to assess the functionality of the multi-modal transportation system during disease outbreaks.

Second, the dissertation will build a data-driven framework to further investigate the structure property of urban transportation system to gain insights in deriving control strategies and design policies. Based on large-scale travel data, the dissertation will examine the structure of physical transportation networks such as metro networks, and reconstruct the underlying contact networks to understand how individual travelers meet each other in urban transportation systems. While the first objective focuses more on the optimal coordination among different transportation modes, the second objective helps to identify how vulnerable each individual travel mode is to infectious diseases, and understand what measures can be taken to improve the vulnerability of the particular travel mode.

Third, the dissertation will study how individual travel behavior may change as the disease proceeds, and reveal underlying implications on how change of individual behavior may affect the dynamics of infectious diseases. The impacts of individual behavior are often neglected when modeling diseases to reduce model and computational complexity. However, this is likely to result in over or under estimations of the actual disease scales and false interpretation of disease dynamics. The dissertation will consider how individuals may adjust their behavior and protect themselves when observing the states of other travelers who they met during travel, and when exposed to various information resources such as news agencies and social medias.

Finally, and most importantly, the dissertation will bring into attention the relationship between urban transportation system and the spread of infectious diseases to the general public. The results and findings of the dissertation will help to understand how our urban transportation system will contribute to the spread of infectious diseases, and will improve our knowledge on possible control measures for transportation systems to address the challenges of infectious diseases in urban areas.

#### 1.4 Organization of the dissertation

The dissertation aims to develop mathematical models from both macroscopic and microscopic levels, help to understand the disease spreading process with the transportation system in urban areas, and assist future decision makings in identifying critical nodes in transportation systems and frame control strategies during disease outbreaks. The overall structure of the dissertation is shown in Figure 1.7.

The first part of the dissertation focuses on developing macroscopic models to model regional spread dynamics of communicable diseases, which corresponds to the regional and transportation system modeling branch in Figure 1.7. The main contributions of the first part can be summarized as:

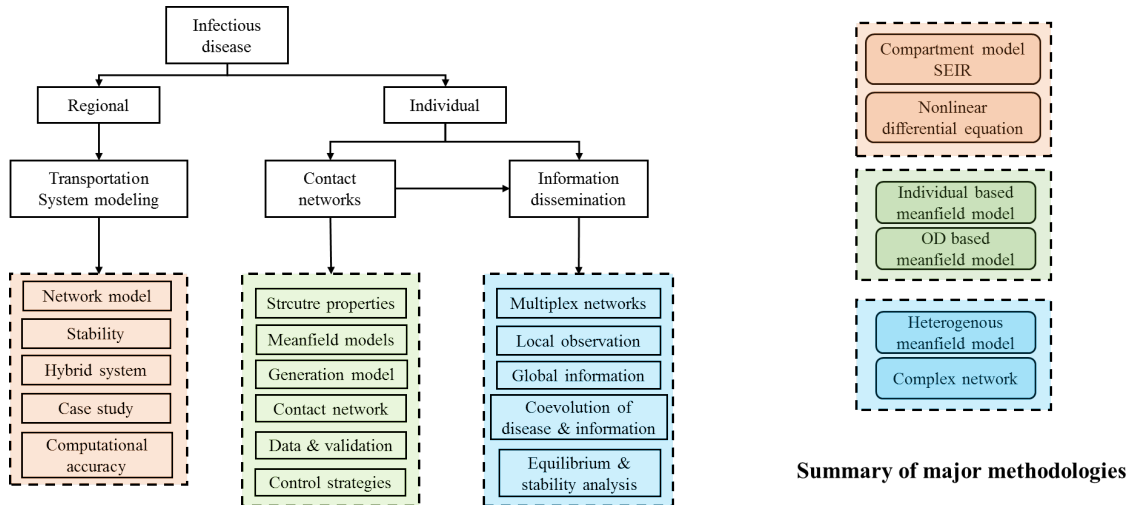


Figure 1.7.: Dissertation framework

1. The dissertation develops the mathematical framework to understand the population movement and the contagion pattern between healthy and infected people.
2. Various modes of urban transportation are explicitly modeled during the disease spreading process, and the effectiveness of entry-control strategies are evaluated based on different urban structures.
3. The selfish travel behavior of urban passengers are considered which result in the hybrid system modeling scheme of the urban disease transmission with transportation system.
4. The models not only focus on limiting behavior of the system, but also investigate the intermediate process of disease transmission. And over-approximation technique for the hybrid automata is developed which gives the upper-bound for the peak value of number of infected population during disease outbreaks.

The second part of the dissertation, including contact network and information dissemination models, focuses on developing microscopic tools to understand disease

dynamics among individuals. The contributions of the second part can be summarized as:

1. The dissertation develops a data-driven framework to construct the individual contact network within transportation systems.
2. The dissertation develops individual based models to understand the percolation of diseases in the constructed contact network.
3. The dissertation builds the connection between structure and functionality of contact networks during disease outbreaks.
4. The dissertation incorporates individuals' behavior change when being exposed to various information resources related to disease states.
5. The dissertation reveals various stable system states for the spread of infectious diseases in the contact network.

The dissertation is organized as follows. Chapter 2 reviews the basics of epidemic models for both compartment models and contact network epidemiology, and summarizes recent literature on both topics. Chapter 3 builds macroscopic models for the spread of infectious diseases in urban transportation systems at regional level. In particular, this chapter develops the spatial model of urban activities with various travel modes as the ODE system. Hybrid automata approach is also introduced to model control strategies. Chapter 5 and 6 discuss the development of models at individual level. Chapter 5 utilizes the smart card transaction data to reconstruct the contact network of metro travelers, which is the mass transit mode with highest usage as well as highest risk exposure. The data driven approach for building the network growth model is introduced, and the vulnerability of the constructed travel contact network is analyzed. Chapter 6 considers that individuals will change their behavior when exposed to various information sources, and models the co-evolution of disease and information dynamics in the multiplex networks setting. Three possible stable states

for disease and information co-evolution are discussed, and the synchronization between disease and information spreading is investigated under different stable states. Finally, chapter 7 concludes the dissertation and discusses future research directions.

## 2. EPIDEMIC MODELING

### 2.1 The basics

Epidemic modeling is the subject of developing mathematical models to understand the spreading process as well as the limiting state of infectious diseases. There are two main approaches to accomplish the goal. First, the compartment model where population are divided into independent compartments and the system dynamics is usually modeled as the set of ordinary differential equations (ODE). Second, the contact network epidemiology approach, which is based on complex network theories where individuals are treated as nodes and their contact pattern shapes the topology of the network. We next briefly introduce the classical models for each of the two approaches.

#### 2.1.1 The susceptible-infectious-recovery (SIR) model

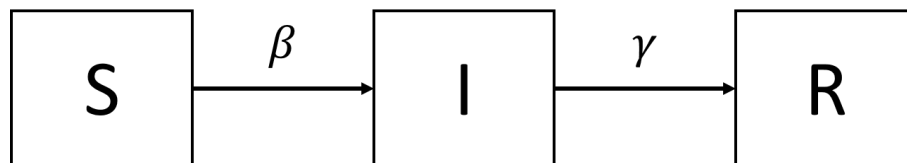


Figure 2.1.: Illustration of the SIR model with contagion rate  $\beta$  and recovery rate  $\gamma$ . (compartment model)

One of the simplest and mostly recognized compartment epidemic models is the SIR model, derived from early papers by Kermack and McKendrick [22, 23]. The key assumption of the SIR model as well as for other compartment models is that all members within the same compartment are homogeneous, having equal chance of

being infected. The main idea of the SIR model is that it separates population into susceptible (S), infectious (I), and recovered (R) states, as shown in Figure 2.1. The S population is also considered as the healthy population, and vulnerable to infections upon contact with I population at the rate of  $\beta$ . And once people get infected, they will be subtracted from the S population and added to the I population. The I population has a chance of *gamma* to get recovered from the disease. And once the person is recovered, he or she will be considered as gaining permanent immunity (or death) and will never return to other compartments. This dynamic process can be mathematically written as:

$$\frac{dS}{dt} = -\beta \frac{SI}{N} \quad (2.1.1)$$

$$\frac{dI}{dt} = \beta \frac{SI}{N} - \gamma I \quad (2.1.2)$$

$$\frac{dR}{dt} = \gamma I \quad (2.1.3)$$

where  $N = S + I + R$  is the total population and is usually considered as fixed, and the term  $\frac{I}{N}$  captures the chance that a susceptible individual may get in contact with infected people within population of size  $N$ . The initial condition of the SIR system is that  $S, I > 0$  and  $R = 0$  at time  $t = 0$ . The classical SIR model can be further extended to incorporate birth and death of population, include additional compartments such as the exposed (E) compartment where people are infected but not yet infectious, and introduce vertical transmissions in addition to the transmission between compartments.

One of the most important characteristics of the SIR model is its threshold phenomenon, where the threshold refers to the critical point determined by model parameters whether the disease is going to invade the whole population or eventually die out. That is, if we rewrite  $\frac{dI}{dt}$  as

$$\frac{dI}{dt} = I\left(\beta \frac{S}{N} - \gamma\right) \quad (2.1.4)$$

and if  $S < \frac{\gamma N}{\beta}$ , then  $\frac{dI}{dt} < 0$  and the disease will die out. Otherwise all population will become infected and eventually stay in the R compartment. In common practice, we usually omit the  $N$  term and represent  $S/N$  directly as the single term - the proportion of susceptible population. Then critical threshold  $\frac{\beta}{\gamma}$  is usually termed as the basic reproduction number, or  $R_0$ . If  $R_0 > 1$ , the disease will invade the population, and the physical interpretation of  $R_0$  is the number of secondary infections an infected individual may produce.

### 2.1.2 Disease over the network

The study of disease spreading over the network is a recent and innovative field of research [24] as compared to the compartment model approach which has over 90 years of history. Different from the compartment models where the population is assumed to be perfectly mixed, each individual is now treated as a single node in the network, and the focus of the network approach is to understand the impact of network topology on the disease diffusion process. Note that the SIR process or its other variants are still applied in the contact network. But instead of using the idea of compartments, each node in the network may have the state of S, I, and R respectively. Figure 2.2 shows an example of disease diffusion on networks under the SIR scheme.

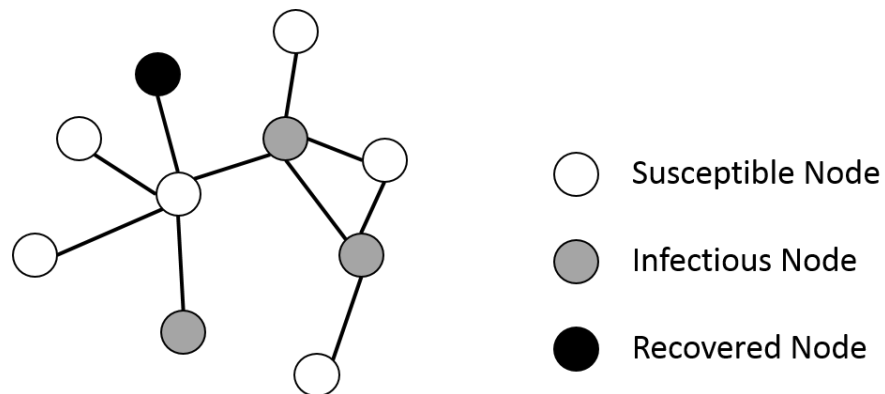


Figure 2.2.: Illustration of the SIR model over networks.

At each time step, each susceptible node has the probability  $\lambda$  of being infected if it is connected to one or more infected nodes. Similarly, each infected nodes has the probability of  $\mu$  for recovery. While the focus of the network approach is to understand the collective behaviors over the network, the disease transmission is modeled based on the degree distribution of the network. For instance,  $I_k(t)$  refers to the proportion of nodes of degree  $k$  that are in the infected states at time  $t$ , and we have the following differential equations for capturing the full system dynamics:

$$\frac{dS_k}{dt} = -\lambda k S_k(t) \Theta(t) \quad (2.1.5)$$

$$\frac{dI_k}{dt} = \lambda k S_k(t) \Theta(t) - \mu I_k(t) \quad (2.1.6)$$

$$\frac{dR_k}{dt} = \mu I_k(t) \quad (2.1.7)$$

where  $\Theta(t)$  is the probability that any link in the network is adjacent to an infected node. It can be seen that the network approach has a similar structure as compared to the compartment model, but it distinguishes nodes with different degrees thus allowing for individual heterogeneity and accounting for network structures.

The variable  $\Theta(t)$  can be approximated as:

$$\Theta(t) = \frac{\sum_k P(k) I_k(t)}{\langle k \rangle} \quad (2.1.8)$$

where  $\langle k \rangle$  is the average node degree. And the underlying assumption of this approximation is that all links are independent in the given network, for the sake of computational simplicity for the approximation, which therefore makes the differential equations integrable.

And the idea of reproduction number also exists for the network approach, where the interest lies in analyzing the critical threshold whether the disease is eliminated

or becomes permanent at time  $t \rightarrow \infty$ . And following above equations, the existing results [25] suggested that the critical transmission threshold  $\lambda_c$  can be expressed as:

$$\lambda_c = \frac{\langle k \rangle}{\langle k^2 \rangle} \quad (2.1.9)$$

so that whether the disease may invade or not depends not only on the value of  $\lambda$ , but also the topology of the network itself.

## 2.2 Literature review on compartment models for epidemic modeling

This section reviews the development of the compartment models for epidemic modeling from both theoretical and practical aspects, and we refer to [26, 27] for fundamentals and comprehensive review of this field.

As introduced in section 2.1.1, the compartment model of epidemic modeling is based on the key assumption of homogeneous mixing of population within the same compartment, and the sequences of studies are developed based on the pioneer works by Kermack and Mckendrick [22, 23]. Their studies developed a compartment model based on simple assumptions regarding the rate of transmission between different divisions of population, and the prediction from the model showed the disease pattern with intensive growth of infected population and eventually the disease disappeared. There were part of the population being unaffected, and these patterns have been observed in numerous epidemics in the history. Their results gave rise to the SIR model, which is mainly used for modeling diseases that confer immunity against infection, also the SIS model, which is mainly used for diseases where infected population are subject to reinfection and will return to susceptible population upon recovery. One concern related to the compartment model is the form of incident rate, which is usually used in regardless of the total community size (e.g.,  $\beta SI/N$  instead of  $\beta N^v SI/N$ ). Anderson and May [28] used data from five human diseases in communities, with various population size ranging from 1,000 to 400,000, to validate the correctness of this incidence form. They reported that by using the incidence form  $\beta N^v SI/N$ , the  $v$  lied

in between 0.03 and 0.07, which implies that it is more reasonable to use  $v = 0$  (where community size plays no role) instead of taking  $v$  as 1. And the results suggested that human beings are infected during their daily activities, which are barely affected by the size of their community.

Significant efforts have been made in deriving meaningful variants of compartment models for different kinds of diseases under different invasion conditions. There are compartment models for general types of diseases such as SIR, SIS, SEIR, and SEIS models. And there are also more specific models which consider the treatment state where a portion of infected population may get cured by vaccines and are moved to a different compartment [29], the models with latent period after which people may either turn into infected state or asymptomatic state with decreasing infectious rate over time [30], and also models with quarantine and isolation states where infected individual may be isolated from the mass population during the outbreaks of a new disease when no vaccine has been developed [31]. Besides the transmission of diseases between compartments of different states, the rate of infection and mortality usually vary with different age structures which give rise to the age-structured models [32,33]. The age-structured models use the partial differential equations (PDE) to capture the variation of disease related coefficients as a function of time in addition to the ODE system for compartment models. And Castillo-Chavez and Hethcote further extended the age-structured model by considering the cross-immunity effects when one strain of certain influenza may provide additional protection of other types of influenzas [34]. Moreover, seasonality was found to be another important factor that may have significant impact on the disease dynamics, which may result in the periodical outbreaks of infectious diseases and the existence of multiple equilibriums [35]. In addition to the regular transmission between the compartments which is horizontal, many diseases may also spread via vertical transmission by transplacental transferring of disease agents. And this can be captured by the compartment model by considering that a certain portion of infectious population's offspring are infected at birth,

where Busenberg and Cooke provided a comprehensive review of related disease and epidemic models of vertical transmission [36].

With the presence of infectious disease, the nature question to ask is what we can do to impede or even eliminate the invasion of the diseases. Pulse vaccine is among the most effective methods for controlling the diseases from spreading, by repeatedly vaccinating target groups of people at risk. This method has been reported to contribute to the eradication of measles at relatively low values of vaccination [37]. And Shulgin et al. developed the SIR model with pulse vaccination strategy [38] to capture the disease dynamics. They demonstrated that the effectiveness of pulse vaccination under seasonal variation, and compared the effectiveness of different vaccination policies. Alberto [39] further improved the study by modeling vertical transmission of diseases with pulse vaccination strategy. Finally, besides considering additional compartments and control strategies, the compartment models can be further improved by incorporating spatial aspects of human activities. Instead of having homogeneous behavior within the same compartment, people within the same disease state may have very different activity patterns. A typical example is that an infected individual goes to work during day time but returns to home at night, and the activity pattern and therefore the contagion rate will be totally different at these two locations. In light of this issue, Arino and Driessche proposed the multi-city epidemic model [40], where the population dynamics was first modeled among multiple cities and the disease dynamics was investigated at the equilibrium of population movement. And this study forms the basis for modeling the impact of urban transportation system during disease outbreaks in the dissertation.

With rich and comprehensive extensions of the basic epidemic models, efforts have also been made to understand important mathematical properties of these models and have contributed to better understanding of complex disease dynamics. One important property derived from the epidemic models is the herd immunity, which serves as the basis for deriving effective control strategies of mass immunization [41]. Such property suggests that immunization at individual level may map to the eradication

of diseases at the community level once a threshold portion of individuals are immunized. Another fundamental attribute of epidemic models is the basic reproduction numbers, or  $R_0$ , which serves as the indicator of disease free equilibrium or endemic equilibrium states of infectious diseases. In light of the significance of  $R_0$ , there exists many studies exploring efficient ways of calculating  $R_0$  for complicated compartment models. Diekmann et al. [42] introduced the guidelines on how to derive this number. And Diekmann et al. [43] further proposed the idea of next generation matrix (NGM), which becomes the state-of-the-art methods for calculating  $R_0$  analytically based on the largest eigenvalue of the NGM. As most of the interests of epidemic modeling lie at understanding the asymptotic behaviors of the developed models, the stability analysis of various equilibrium solutions has been comprehensively investigated in this field. This includes but are not limited to proving the stability of SEIR models [44], the global stability of SIR models with time delay [45], the stability when pulse vaccination strategy is considered [46], and the use of Lyapunov functions to prove global stability of equilibrium solutions for a collection of epidemic models [47]. While the bilinear incidence rate  $\beta SI$  is used in most of the studies, there are also discussions on understanding the disease dynamics of nonlinear incidence rate  $\beta S^a I^b$  based on different choices of  $a$  and  $b$  values [48, 49].

Finally, based on the theoretical developments of epidemic models, there are also a number of studies that validate the correctness of the developed models using historical disease data. Rvachev and Longini applied the SEIR models at the global level [50]. They considered that travelers can spread infection from city to city and these cities are distributed across several continents. The model was implemented to forecast the 1968-1969 influenza pandemic starting from Hong Kong, and the estimated results were found to be mostly consistent with the time-space spread of the actual data recorded by WHO. Arazoza et al. [14] applied the compartment models to estimate the size of Cuban HIV epidemic, and their results suggested that the model may well fit the historical data and the estimated values were close to the reported size of HIV population. Riley et al. [51] used the 2003 SARS data to estimate the

$R_0$  value of SARS, and implemented the stochastic metapopulation compartmental model to understand the disease dynamics and compare the future trajectories of diseases under various control policies. Fraser et al. [52] used the data collected from H1N1 influenza to fit the parameters for the age-structured disease transmission models, and the model was used for projecting future trajectories of the disease outbreak. Fisman et al. [15] fitted disease parameters from the data of 2014 West Africa Ebola outbreak, and introduced a simple two parameter mathematical models to estimate the fate of the Ebola outbreaks. Their findings suggested that a small reductions in the transmission rate may reduce tens of thousands of infected population and therefore intervention strategies are highly desired.

### 2.3 Literature review on disease over networks

While there has been a rich literature in the theoretical development of compartment epidemic models and such models have been shown to be accurate in predicting disease dynamics in several case studies, the biggest drawback of the model comes from its most fundamental assumption: the perfectly mixed population within each compartment. As pointed out by Meyers [53], such assumption may lead to estimations of disease outbreak being significantly biased: the  $R_0$  was estimated to be between 2.2 and 3.6 but the spread of the disease was actually limited based on the SARS record data. There also exists a huge discrepancy between estimated value from the model and the actual cases: it was estimated to have 30,000 to 10 million SARS cases in China while the actual number reported was only 782 cases [54]. And this sheds the light on accounting for individual differences while modeling disease dynamics, which gives rise to the study of disease dynamics over the networks.

This research field is still in its infancy as compared to the long history of compartment models for infectious diseases. Earliest works in this field were conducted by Moore and Newmann [55] in 2000 on the percolation of epidemics in small-world networks, and by Satorras and Vespignani in 2001 [24], where they studied the spread

of epidemics in the scale-free network whose nodes degree follows the power-law distribution. One of the most significant findings from their study was the absence of epidemic threshold, meaning that diseases may invade the scale-free network regardless of their infectious rate. On the other hand, the epidemic threshold still held for networks with exponentially bounded connectivity [56]. Newman [57] presented the first work on analytical solutions of epidemic modeling over the networks with arbitrary degree distribution based on percolation theory. Motivated by the idea of herd immunity, Satorras and Vespignani further investigated the immunization issue for complex networks [58]. And another surprising result was revealed that the scale-free network may not acquire global immunity even if an unrealistic number of agents in the network is immunized, which shapes a sharp contrast to the results of herd immunity obtained from compartment models. Instead, target immunization should be encouraged based on nodes' connectivity properties rather than randomization strategy, which was found to significantly improve networks' vulnerability to infectious diseases. One of the drawbacks of these studies is the homogeneous assumption for the nodes with the same degree, which is an effort made to simplify the analytical difficulties related to the complex network approach. Under such assumption, nodes with the same degree are considered independent from each other, which is unlikely to be case in many real world networks. To address this drawback, Bogun et al. [59] introduced degree correlation into the network approach, and they concluded that the nodes correlation does not change the fact of the absence of epidemic threshold in the highly vulnerable scale-free network. Due to the potential large network sizes, it is usually intractable to conduct individual level analyses to derive meaningful results. Instead, certain level of aggregation is needed to understand the collective behavior over the networks, and the efforts made so far can be categorized into three approaches [60]. The first approach follows the degree-based mean-field theory, where statistically equivalence is assumed for nodes with the same degree and the primary interests is on the disease dynamics over the given degree distribution. Examples of studies adopting this approach include [56, 58, 59]. The second approach follows the

individual-based mean-field theory, where the adjacency matrix of the network and therefore the concrete topology of the network plays an explicit role in determining the dynamics of disease spreading over the network. Representative works using this approach include [61–63]. The third approach is based on the generating functions that are motivated from the percolation theory. The philosophy of this approach is to represent the probability that a link is connected to infectious and susceptible individuals by derivatives of generating functions. Works by [53, 57, 64] fall into this category. We refer readers to a more comprehensive review of the fundamental works on the disease dynamics over the complex network in [60, 65].

While the results of these theoretical developments are mainly derived from a given network, which can be in the form of the adjacency matrix or through the degree distribution. But in reality, the network structure barely stays fixed and is likely to evolve over time. This gives rise to studies that focus on understanding how the change of network topology may affect the disease dynamics. Gross et al. [66] developed one of the early world on this topic by introducing the idea of adaptive networks. In their study, susceptible nodes were assumed to avoid contact with infected ones, and this process was realized through network rewiring. And a complete different picture of disease dynamics emerged such as the existence of bifurcation and state oscillation, which stressed the importance of studying disease spreading over dynamic rather than static networks. Karsai et al. [67] used mobile phone data to obtain the event contact duration between individuals, which resulted in different weight on each edges representing their contact duration, and they studied the SI process on the weighted network. Stehlé et al. [68] conducted a simulation of SEIR model over the contact network, which was constructed based on the contact pattern as well as contact duration data collected during a conference. Ren and Wang introduced a different approach to model the change of network topology, where they defined the behavior of individuals on their movements across different communities, and they modeled the SIS epidemic process on the time varying network [69].

## 2.4 Summary

In this section, we introduce mathematical basics of compartment epidemic models and disease modeling over networks. We also review the theoretical development of compartment epidemic models, including the variants of conventional SIR and SIS models and the mathematical properties related to the variants of the developed models. The application of the developed compartment models are also discussed. For the disease models on networks, we review pioneer works that constructed the theoretical foundations and the important findings that are in contrast to the results obtained from compartment models. We summarize three major approaches for analyzing disease dynamics over network, and review the literature which highlighted the importance of varying network topology on the accurate understanding of actual disease processes. While both compartment models as well as network approaches have their pros and cons, each of these two category still has their own significance in modeling and understanding the dynamics of infectious diseases. In particular, the network approach is not viable for large scale modeling at regional or global scale, due to lack of individual network data as well as the issues related to the scalability of the approach, where the compartment models are needed to understand the trajectories of the diseases and perform future estimations. On the other hand, the network approach accounts for individual heterogeneity and takes the network topology into consideration, which complements the critical drawback of the compartment models due to the unrealistic assumption of fully mixed population. And the results obtained from network approaches may help to better calibrate the compartment models' parameters at aggregate level to mitigate the issue due to unrealistic assumptions. As a consequence, both modeling approaches are powerful and useful tools for understanding disease dynamics and their usage will depend on different applications and the typical kind of research questions to be answered. And the dissertation will therefore develop macroscopic and microscopic models based on both kinds of approaches.

Based on the literature review, the drawbacks of existing studies are summarized as follows, which lead to the topics that will be studied in this dissertation:

1. The research field of compartment models almost focuses exclusively on devising new compartments for various diseases and analyzing the corresponding mathematical properties. But few efforts were made to account for the mixed population and their heterogeneous behaviors. While the issue is not vital when the population is better mixed and the activity patterns are more tractable in rural places, the existing models are not viable for modeling infectious diseases in urban areas.
2. Both compartment model approach and network approach focus on the dynamics of the disease itself, while the component of human's rational behavior is missing in existing studies. That is, one drawback of the existing studies is the implicit assumption that human's behavior during diseases is the same as of the daily patterns. But there is no doubt that people will behave differently if they are aware of the outbreaks of the disease, and their behavior may vary based on the level of information they access to related to the disease pattern.
3. Despite the recent development of theoretical literature on the network approach, there are very few studies that analyze how vulnerable is real world systems to the invade of infectious diseases. One possible reason is due to lack of data to reconstruct the network topology of real systems. But with recent advances in pervasive computing, location based services, and the popularity of smart phone and related applications, we have more information about individual activity patterns than ever before. And there is an emerging need to assess the how disease may spread in real systems and whether or not the system is controllable during the outbreak.

PART I: NETWORK MODEL FOR SPREADING OF INFECTIOUS DISEASES



### 3. MODELING DISEASE CONTAGION IN URBAN TRANSPORTATION SYSTEM

#### 3.1 Introduction

Urbanization in the past few decades has attracted billions of people into the urban areas. According to the United Nation, by the end of 2014, there were over 3.9 billion people living in urban areas, and the number is estimated to reach 6.3 billion (70% of total world population) in 2050 [70]. The increasing urban population gives rise to the growth of global economy, the development of urban infrastructures, and improved accessibility to service such as education and health care. But the rapid urbanization with unplanned urban development also lead to unprecedented challenges, among which WHO entitles the health risk as the most significant challenge for urban areas in the 21st Century. In order to meet the challenges, it is encouraged that urban areas should promote the urban planning for safety and healthy behavior, and facilities should be designed to make urban areas resilient to emergencies and disasters. In this study, we focus on one particular health challenge, the communicable infectious disease (CID) in urban areas, and investigate how urban transportation system is related to the spread and control of CIDs.

It is well-understood that urban traffic is the main contributor for road injuries, and traffic emission is also identified as one of the major sources for urban air pollution which lead to respiratory and chronic diseases [71, 72]. However, all these health exposures are related to noncommunicable diseases, and the connections between urban transportation and CIDs are often underrated. Despite the fact that we have access to piped water, better waste management, and medical treatment due to the urbanization, the infectious disease remains a major health threat and contributes to

approximately 19% of global death and 76% of deaths are associated with infectious diseases in Africa by the end of 2010 [73]. More importantly, while infectious diseases emerged in rural areas may only reach limited people and remain local in the past, increased mobility and activity intensity worldwide make it easier for infectious disease to affect a large population and results in global pandemic. Among all the possible factors, the development of transportation system and the amount of people traveling within the system undoubtedly lies in the heart for the spread of CIDs. On one hand, people are making more trips and traveling at longer distance at both local and global level. At local level, the average annual person-mile traveled in united states has increased by 169% from 1969 to 2009 [74]. And globally, the revenue passenger-kilometer has doubled every 15 years during 1974-2014, and is estimated to be doubled again in the next 15 years [75]. On the other hand, people are spending more time in the transportation system, especially in urban areas. As for New York City, the average commuting to work time exceeds 40 minutes for 69% of the city's neighborhoods, and 59% of New York commuters use mass transit as the tool for commuting. Note that the two deciding factors for CIDs to spread is the close contact and the contact duration. And the two aspects from the transportation system clearly imply the risk exposures while travel for urban population. This motivates us to model the process and understand how travel behavior may affect the spread of infectious diseases in urban areas.

There are two main approaches in the literature for characterizing the dynamics of the spread of infectious diseases. The first approach comprises of the compartment model, where the initial SIR model (also known as Kermack-McKendrick model) divides the population into compartments of susceptible, infected, and recovered, and non-linear ordinary differential equations (ODE) are used to model the dynamics among the compartments [22]. Based on the SIR model, a variety of models have been developed to account for more realistic disease nature, including models which consider the incubation period [44], the vertical transmission [76], the age structure [34], and the vaccine strategy [38,39]. And extensive efforts were made to understand the

property of the model and analyze the local and global stability of the non-linear ODEs, where surveys of related works can be found in [48, 77]. One major criticism for the compartment model is the unrealistic assumption, where the population in each compartment is assumed to be fully mixed and therefore each individual has the same behavior. Therefore, the model may fail to represent actual contact patterns for many real-world diseases. To address this shortcoming, the second approach is developed by modeling the disease propagation at individual level based on network topology, where each individual is represented by a vertex and their contact pattern is captured by the edge [53, 57]. The approach was developed based on the method of bond percolation model, and the generation function was used for deriving the important attributes of a certain contact network, including the average degree and excessive degree, which later used to calculate the size of disease outbreaks. Danon et al. [78] conducted a comprehensive review of the works in this approach. The contact network model helps to capture diverse interactions among individuals with given distribution, however, it is not applicable to understand the spread of disease at urban level: it is computationally intractable to construct the individual contact network for all urban populations and it is also impossible to obtain the necessary input for the contact network as evaluating the individual's contact pattern will be very expensive.

As a consequence, to model the spread of CIDs for the urban area, the compartment model is still the idea choice due to its simple math nature and the scalability when it comes to model the mass urban population. However, the simplistic assumption of homogeneous mixed population needs to be corrected as the population dynamics is highly complex both spatially and temporally in large cities. In particular, human mobility is the decisive factor for the spread of infectious disease, and the model needs to account for the nature of how population circulate around the city. On one hand, the diverse land use pattern suggests that the spatial movement is an essential aspect to be considered since people move from places to places to participate in activities. On the other hand, the contagion during travel is another

significant contributing factor to the spread of CIDs, which accounts for the cross-infection between people to-and-from different directions. More importantly, people have the highest chance of close contact with others during travel, especially when using public transit.

In this study, we develop the epidemic model which models the traffic contagion at urban level. The contributions of our paper are mainly two-fold. The first contribution from our paper is from the modeling approach. The model is formulated based on the conventional SEIR model, and the spatial population movement and the contagion of people during travel are introduced to address the oversimplified assumption of the basic model. We model the spread of CIDs in urban areas as a system ODEs, and introduces two sub-models to capture the system dynamics. The first sub-model is the mobility model, which determines the population in each area and the amount of people moving between places. The second model is developed upon the mobility dynamics, which captures the movement of susceptible, exposed, infected, and recovered population. In particular, the disease dynamics involves two parts: (1) the contagion that takes place at the destination areas and (2) the contagion that takes place during travel. We further discuss the properties of both mobility and disease models, and show the stability of the disease-free equilibrium (DFE) for the ODE system. The second contribution of our paper that we investigate the safety verification problem using the model developed.

## 3.2 Modeling preliminaries

### 3.2.1 Notation

We summarize the list of variables used in this section as follows:

Table 3.1.: Table of notation

Notation	Description
<b>Variables</b>	
$S$	Susceptible population.
$E$	Exposed (latent) population.
$I$	Infected population.
$R$	The population who recovered from disease and got immunity.
$N_i^p$	Total amount of people who are current present at patch $i$ .
$N_i^r$	Resident population at patch $i$ .
$N_{ij}$	The amount of people who are residents of patch $i$ and currently present at patch $j$ .
<b>Fixed parameters</b>	
$\beta$	Contagion rate between $S$ and $I$ .
$1/\sigma$	Length of latent period for population $E$ .
$1/\gamma$	Length of infectious period for population $I$ .
$\mu$	Death and birth rate.
$P$	Total number of patches in the area.
$\alpha_i$	Arrival (departure) rate of external population for patch $i$ .
$g_i$	Total departure rate of patch $i$ .
$m_{ij}$	The rate of movement from patch $i$ to patch $j$ , where $\sum_j m_{ij} = 1$ .
$r_{ij}$	The rate of return from patch $j$ to patch $i$
$d^M$	Control rate of travel mode $M$ .

### 3.2.2 Epidemic modeling

The well-known compartment model for capturing the dynamics of infectious diseases was proposed by W.O.Kermack and A.G.McKendrick [22], where they consider that the population may experience three states over time:

- Susceptible class or  $S(t)$  is used to represent the number of individuals not yet infected with the disease at time  $t$ , or those susceptible to the disease.
- Infected class or  $I(t)$  denotes the number of individuals who have been infected with the disease and are capable of spreading the disease to those in the susceptible category.
- Removed class or  $R(t)$  is the compartment used for those individuals who have been infected and then removed from the disease, either due to immunization or due to death. Those in this category are not able to be infected again or to transmit the infection to others.

And the compartment model has several key assumptions: (1) each individual in the population has an equal probability of contracting the disease with a rate of  $\beta$ , (2) the population leaving the susceptible class is equal to the number of people entering the infected class, (3) people recovered from the disease with a mean recovery of  $1/\gamma$  gain permanent immunity to the disease, and (4) the death rate is the same as the birth rate so that the total population is fixed.

In reality, people who are infected by certain diseases may not present any symptoms until the end of the incubation period, and it is important to take this latent period into consideration for more accurate representation of disease dynamics. Consequently, the SEIR model was introduced with an additional compartment which is known as the latent class ( $E(t)$ ) [79]. The population of  $E$  are considered as exposed

but not infectious, and will proceed into the infectious state with an average length of latent period of  $\frac{1}{\sigma}$ . Such disease dynamics can be mathematically represented as:

$$\frac{dS}{dt} = -\beta SI + \mu(N - S) \quad (3.2.1)$$

$$\frac{dE}{dt} = \beta SI - \mu E - \sigma E \quad (3.2.2)$$

$$\frac{dI}{dt} = \sigma E - \gamma I - \mu I \quad (3.2.3)$$

$$\frac{dR}{dt} = \gamma I - \mu R \quad (3.2.4)$$

### 3.2.3 Mobility model

The spread of infectious disease is closely interacted with the mobility pattern of urban population. Before discussing the mathematical model for capturing disease dynamics, we first present the mobility model that is followed by urban population.

The mobility model used in this study is developed from the intra-city mobility model proposed by Sattenspiel and Dietz [80], where we explicitly captures the arrival and departure of people from external areas. This is especially important considering that infectious diseases are usually introduced into a certain area by external visitors. For simplicity, we assume that the arrival and departure rate are equivalent for each patch. We model the urban area as a collection of  $P$  patches, where people are divided into two groups: residents and visitors. Let  $N_{ij}$  be the population at patch  $j$  who are residents of patch  $i$ , we have the following two equations to capture the total residents and visitors for a given patch:

$$N_i^r = \sum_{j=1}^P N_{ij}, \forall i \quad (3.2.5)$$

$$N_i^p = \sum_{j=1}^P N_{ji}, \forall i \quad (3.2.6)$$

Equation 3.2.5 suggests that the amount of residents at patch  $i$  can be calculated as the summation of population who are residents of patch  $i$  and currently at patch  $j$ . Similarly, equation 3.2.6 states that visitor population at patch  $i$  consist of the residents of patch  $i$  who remain in  $i$ , as well as the population who reach patch  $i$  from other patches.

People who are considered as residents are assumed to have a permanent residing location at patch  $i$ . Additionally, external population are assumed to arrive at patch  $i$  with a ratio of total residents of patch  $i$ . They are also modeled as the residents of patch  $i$ , and they may leave the city from a different patch  $j$ . For residents at patch  $i$ , they may visit patch  $j$  for various reasons (e.g., for work or entertainment) with the rate of  $\rho_{ij}$ , and will return to their home at the rate of  $r_{ij}$ . Denote the time derivative  $\frac{dX}{dt}$  as  $\dot{X}$ , we have the following two ordinary differential equations (ODE) for computing the mobility dynamics within a urban area:

$$\dot{N}_{ij} = -r_{ij}N_{ij} + g_i m_{ij} N_{ii} - \alpha_i N_{ij} \quad (3.2.7)$$

$$\dot{N}_{ii} = \sum_{j=1}^P r_{ij} N_{ij} - g_i N_{ii} + \alpha_i N_i^r - \alpha_i N_{ii} \quad (3.2.8)$$

Equation 3.2.7 captures the change rate of residents of patch  $i$  who are visitors in patch  $j$ , which is measured by the population difference between residents who leave  $i$  for  $j$  and the return of residents from  $j$  to  $i$ . Note that people leave  $i$  for  $j$  may also depart the city with the rate of  $\alpha_i$ . And equation 3.2.8 characterizes the change of residents remaining in patch  $i$ , which involves two component. The first component captures the departing and returning of original residents of patch  $i$ , and the second component refers to the population to and from external areas.

Based on equation 3.2.7 and 3.2.8, we develop the rate of change formulations for resident and visitor population as:

$$\begin{aligned}
\dot{N}_i^r &= \sum_{j=1}^P \dot{N}_{ij} \\
&= \sum_{j=1, j \neq i}^P r_{ij} N_{ij} - g_i N_{ii} + \alpha_i N_i^r - \alpha_i N_{ii} + \sum_{j=1, j \neq i}^P [-r_{ij} N_{ij} + g_i m_{ij} N_{ii} - \alpha_i N_{ij}]
\end{aligned} \tag{3.2.9}$$

$$\begin{aligned}
\dot{N}_i^p &= \sum_{j=1}^P \dot{N}_{ji} \\
&= \sum_{j=1}^P r_{ij} N_{ij} - g_i N_{ii} + \alpha_i N_i^r - \alpha_i N_{ii} + \sum_{j=1, j \neq i}^P [g_j m_{ij} N_{jj} - r_{ji} N_{ji} - \alpha_j N_{ji}] \\
&= \sum_{j=1, j \neq i}^P (r_{ij} N_{ij} - r_{ji} N_{ji}) + \sum_{j=1, j \neq i}^P g_j m_{ij} N_{jj} - g_i N_{ii}
\end{aligned} \tag{3.2.10}$$

Moreover, for equation 3.2.9, we have:

$$\begin{aligned}
\dot{N}_i^r &= \sum_{j=1, j \neq i}^P r_{ij} N_{ij} + \sum_{j=1, j \neq i}^P -r_{ij} N_{ij} - g_i N_{ii} + \sum_{j=1, j \neq i}^P g_i m_{ij} N_{ii} + \alpha_i N_i^r - \alpha_i N_{ii} - \sum_{j=1, j \neq i}^P \alpha_i N_{ij} = 0
\end{aligned} \tag{3.2.11}$$

which implies that total residents patch  $i$  is fixed.

**Proposition 3.2.1** *The system described by equation 4.1-4.9 has a unique equilibrium solution, and the solution is globally asymptotically stable (G.A.S). In particular, at equilibrium, we have*

$$N_{ii}^* + \sum_{j=1, j \neq i}^P K_{ij} N_{ij}^* = N_i^r \tag{3.2.12}$$

$$N_{ii}^* = \frac{1}{1 + \sum_{j=1, j \neq i}^P K_{ij}} N_i^r \tag{3.2.13}$$

where  $K_{ij} = \frac{g_i m_{ij}}{r_{ij} + \alpha_i}$ .

**Proof** The equilibrium solution of the system can be calculated by setting equation 3.2.7 and 3.2.8 to zero. From 3.2.7, we have:

$$N_{ij}^* = \frac{g_i m_{ij}}{r_{ij} + \alpha_i} N_{ii}^* \quad (3.2.14)$$

Let  $K_{ij} = \frac{g_i m_{ij}}{r_{ij} + \alpha_i}$ . Based on equation 3.2.5 and the fact that  $N_i^r$  is fixed, we have:

$$N_{ii}^* + \sum_{j=1, j \neq i}^P K_{ij} N_{ii}^* = N_i^r \quad (3.2.15)$$

We therefore have

$$N_{ii}^* = \frac{1}{1 + \sum_{j=1, j \neq i}^P K_{ij}} N_i^r \quad (3.2.16)$$

which gives equation 3.2.12. And by combining the above equation equation 3.2.14 we arrive at equation 3.2.13.

To prove that the equilibrium solution is G.A.S, one can write the whole matrix  $M$  for system  $dN/dt = MN$ , and it can be easily shown that the matrix  $M$  has all negative real eigenvalues, which implies that the equilibrium point is G.A.S. ■

In the following sections, we will write  $N_{ij}$  to denote equilibrium population flow  $N_{ij}^*$  for notation simplicity.

### 3.3 Modeling disease spreading with travel contagion

#### 3.3.1 The basic model

##### 1. Notation

We summarize the list of variables used in this section as follows

Table 3.2.: Table of notation

Notation	Description
<b>Variables</b>	
$S_{ij}$	Susceptible population who are residents of patch $i$ and currently in patch $j$ .
$E_{ij}$	Exposed (latent) population who are residents of patch $i$ and currently in patch $j$ .
$I_{ij}$	Infected population who are residents of patch $i$ and currently in patch $j$ .
$R_{ij}$	Recovered population who are residents of patch $i$ and currently in patch $j$ .
$t_{ij}^m$	Induced travel time for moving from patch $i$ to patch $j$ using mode $m$ .
$N_i^p$	Population at patch $i$ .
$N_{ij}$	The amount of people currently at patch $j$ who are the residents of patch $i$ .
<b>Fixed parameters</b>	
$M$	Total number of travel modes available.
$m$	Travel mode $m$ , where $m = 1, 2, \dots, M$ .
$\beta_{inn}$	Within zone disease transmission rate.
$\beta_{tra}^m$	Disease transmission rate for travel mode $m$ .
$c_{ij}^m$	The ratio of people who choose travel mode $m$ between patch $i$ and patch $j$ .
$d_l^m$	Rate of remaining infected people for travel mode $m$ at control level $l$ .

## 2. System dynamics

An important component missing from the previously discussed SEIR model is the spatial interaction. The model only considers local dynamics, but it is essential for urban areas to model explicitly how population flow moving around the city. In particular, these flows are driven by various activities, such as work, school, or entertainment. And people get in contact with others by taking different activities through various transportation tools. As long as some individuals are infected, their activities and the urban transportation mobility will take the disease to every corner of the city. This motivates us to understand the the spread of infectious disease in urban area by modeling the system with the following 6 dynamics:

1. The mobility dynamics of urban population follows the model as discussed in section 3.2.
2. Similar to the SEIR model, we consider  $S_{ij}$  being affected by  $i_{ij}$  with the inner-patch contagion rate  $\beta_{inn}$ .
3. In addition to the spread due to within patch activities, we also consider people get infected during travel. That is,  $S_{ij}$  may be infected by contacting with  $I_{ij}$  if they use the same travel mode  $m$ , with the contagion rate of  $\beta_{tra}^m$ .
4. Once people in  $S_{ij}$  are infected, they become  $E_{ij}$ . They are not infectious until the end of the latent period, and the length of latent period is characterized by  $1/\sigma$ .
5. People in  $E_{ij}$  become  $I_{ij}$  at the end of the latent period. And the length of the infectious period is characterized by  $1/\gamma$ .
6. At the end of their infectious period, people in  $I_{ij}$  become  $R_{ij}$ . For simplicity, we consider that they gain permanent immunity to the disease and will be no longer infected.

In particular, the contagion process between susceptible and infected population can be illustrated by the example of a 3-patch network as shown in Figure 3.1 There

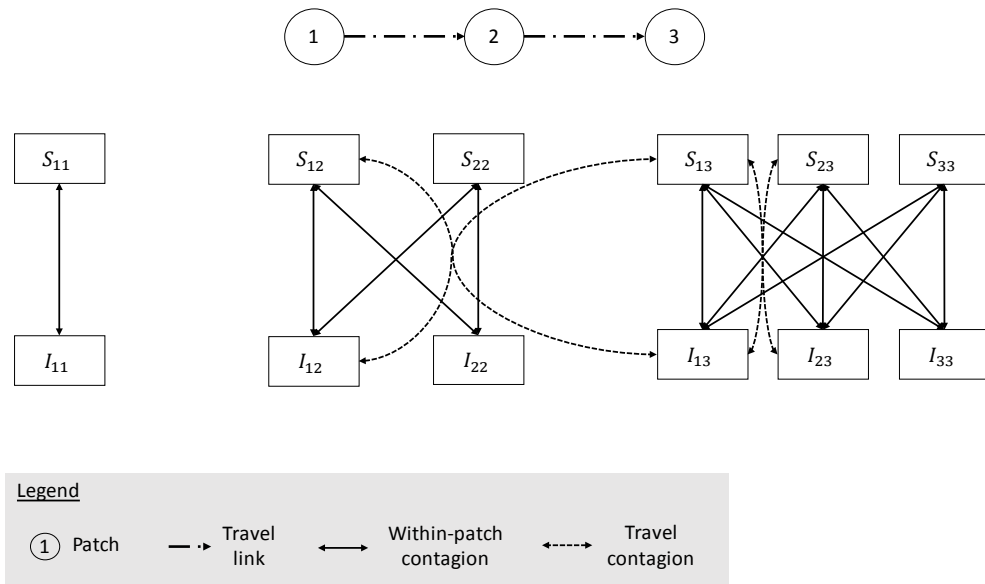


Figure 3.1.: Illustration of the disease contagion process in a 3-patch network

are 3 patches in the network, with two travel links 1-2 and 2-3 and three possible routes: from patch 1 to patch 2, from patch 1 to patch 3, and from patch 2 to patch 3. And we have two different contagions in this network. One is the inner-patch contagion which takes place between  $S$  and  $I$  population in the same patch. Additionally, there is travel contagion (shown in dashed line), which may happen if two population share overlay segments in their travel routes. Consequently, we have two possible travel contagions: between people travel from 1 to 2 and 1 to 3, and

between people travel from 1 to 3 and 2 to 3. While this is only an illustration, the overlay segment will be later differentiated based on the travel modes as well.

### 3. Formulation

Now we present the mathematical formulations which capture the dynamics of disease spreading in urban area:

$$\begin{aligned} \dot{S}_{ii} = & -g_i S_{ii} + \sum_{j=1, j \neq i}^P r_{ij} S_{ij} + \alpha_i^S N_i^r - \alpha_i S_{ii} - \beta_{inn} \frac{S_{ii} \sum_{j=1}^P I_{ji}}{N_i^p} \\ & - \sum_{j=1, j \neq i}^P \sum_{m=1}^M c_{ji}^m \beta_{tra}^m r_{ij} S_{ij} \frac{\sum_{k=1, k \neq i}^P c_{ki}^m \delta_{ki, ji}^m (r_{ik} I_{ik} + g_k m_{ki} I_{kk})}{\sum_{k=1, k \neq i}^P c_{ki}^m \delta_{ki, ji}^m (r_{ik} N_{ik} + g_k m_{ki} N_{kk})} \end{aligned} \quad (3.3.1)$$

$$\begin{aligned} \dot{S}_{ij} = & -r_{ij} S_{ij} + g_i m_{ij} S_{ii} - \alpha_i S_{ij} - \beta_{inn} \frac{S_{ij} \sum_{k=1}^P I_{kj}}{N_j^p} \\ & - \sum_{m=1}^M c_{ij}^m \beta_{tra}^m g_i m_{ij} S_{ii} \frac{\sum_{k=1, k \neq j}^P c_{kj}^m \delta_{kj, ij}^m (g_k m_{kj} I_{kk} + r_{jk} I_{jk})}{\sum_{k=1, k \neq j}^P c_{kj}^m \delta_{kj, ij}^m (g_k m_{kj} N_{kk} + r_{jk} N_{jk})} \end{aligned} \quad (3.3.2)$$

$$\begin{aligned} \dot{E}_{ii} = & -g_i E_{ii} + \sum_{j=1, j \neq i}^P r_{ij} E_{ij} + \alpha_i^E N_i^r - \alpha_i E_{ii} - \sigma E_{ii} + \beta_{inn} \frac{S_{ii} \sum_{j=1}^P I_{ji}}{N_i^p} \\ & + \sum_{j=1, j \neq i}^P \sum_{m=1}^M c_{ji}^m \beta_{tra}^m r_{ij} S_{ij} \frac{\sum_{k=1, k \neq i}^P c_{ki}^m \delta_{ki, ji}^m (r_{ik} I_{ik} + g_k m_{ki} I_{kk})}{\sum_{k=1, k \neq i}^P c_{ki}^m \delta_{ki, ji}^m (r_{ik} N_{ik} + g_k m_{ki} N_{kk})} \end{aligned} \quad (3.3.3)$$

$$\begin{aligned} \dot{E}_{ij} = & -r_{ij} E_{ij} + g_i m_{ij} E_{ii} - \alpha_i E_{ij} - \sigma E_{ij} + \beta_{inn} \frac{S_{ij} \sum_{k=1}^P I_{kj}}{N_j^p} \\ & + \sum_{m=1}^M c_{ij}^m \beta_{tra}^m g_i m_{ij} S_{ii} \frac{\sum_{k=1, k \neq j}^P c_{kj}^m \delta_{kj, ij}^m (g_k m_{kj} I_{kk} + r_{jk} I_{jk})}{\sum_{k=1, k \neq j}^P c_{kj}^m \delta_{kj, ij}^m (g_k m_{kj} N_{kk} + r_{jk} N_{jk})} \end{aligned} \quad (3.3.4)$$

$$\dot{I}_{ii} = -g_i I_{ii} + \sum_{j=1, j \neq i}^P r_{ij} I_{ij} + \alpha_i^I N_i^r - \alpha_i I_{ii} + \sigma E_{ii} - \gamma I_{ii} \quad (3.3.5)$$

$$\dot{I}_{ij} = -r_{ij}I_{ij} + g_i m_{ij} I_{ii} - \alpha_i I_{ij} + \sigma E_{ij} - \gamma I_{ij} \quad (3.3.6)$$

$$\dot{R}_{ii} = -g_i R_{ii} + \sum_{j=1, j \neq i}^P r_{ij} R_{ij} + \alpha_i^R N_i^R - \alpha_i S_{ii} + \gamma I_{ii} \quad (3.3.7)$$

$$\dot{R}_{ij} = -r_{ij} R_{ij} + g_i m_{ij} R_{ii} - \alpha_i R_{ij} + \gamma I_{ij} \quad (3.3.8)$$

While the system described by equations 3.3.1-3.3.8 may look complicated, it can be easily understood by decomposing each equation into the part of mobility dynamics and the part of disease dynamics. In particular, for equations characterizing the dynamics of  $S_{ii}, E_{ii}, I_{ii}, R_{ii}$ , the first four terms on the right-hand-side (RHS) capture the mobility dynamics, which are consistent with equation 3.2.8. Similarly, the first three terms on the RHS of equations for  $S_{ij}, E_{ij}, I_{ij}, R_{ij}$  can be analogous to equation 3.2.7.

The disease dynamics of equation 3.3.1 has two components. The first component with the coefficient  $\beta_{inn}$  characterizes the within patch spread of diseases, where  $\sum_j I_{ji}$  refers to total infected population in patch  $i$  and the contagion has the bilinear incident form which is consistent with the SEIR model. The second component which is associated with the coefficient  $\beta_{tra}$  denote the spread of diseases during travel. Specifically, this term describes how susceptible people who return from  $j$  to  $i$  get in contact with infectious population. For the contagion to take place,  $S$  and  $I$  must be in the same travel mode and share trip segment(s) in common. And the indicator variable  $\delta_{ki,ji}^m$  is introduced to indicate if trips made from  $k$  to  $i$  and from  $j$  to  $i$  using travel mode  $m$  have overlapping parts. And the infected  $S_{ii}$  are added to  $E_{ii}$  as shown in equation 3.3.3. Moreover,  $E_{ii}$  and  $I_{ii}$  (or equation 3.3.3 and 3.3.5) are connected by the term  $\sigma E_{ii}$ , which implies the end of latent period. Similarly,  $I_{ii}$  and  $R_{ii}$  (or equation 3.3.5 and 3.3.7) are correlated by the term  $\gamma I_{ii}$ .

On the other hand, the disease dynamics for equation 3.3.2 also involves two components. The first component with the coefficient  $\beta_{inn}$  captures how  $S_{ij}$  gets

infected during the contagion with other infected population. The second component with the coefficient  $\beta_{tra}$  describes the spread of diseases while people are traveling from  $i$  to  $j$ . That is, only departed population  $g_j m_{ij} S_{ii}$  may have the chance of being infected during their travel to  $j$ . And the contagion may happen when they get in contact with departed infectious population who have the same destination using the same mode, which is captured by  $\sum_{k=1, k \neq j}^P c_{kj}^m \delta_{kj, ij}^m g_k m_{kj} I_{kk}$ . And both parts of infected  $S_{ij}$  are added to  $E_{ij}$  as shown in equation 3.3.4. Finally, we have the same correlations between  $E_{ij}$  and  $I_{ij}$ , and between  $I_{ij}$  and  $R_{ij}$ , as discussed in the previous paragraph. This concludes the basic model for characterizing disease dynamics with travel contagion.

### 3.3.2 Stability of the transportation system

Considering that an infectious disease has been introduced, and people are aware of the disease patterns in the city. An essential question to answer is that if the disease will eventually invade the population. This requires the understanding of the stability of disease free equilibrium (DFE). In other words, if the DFE is stable, then the disease will be absent from the population, otherwise it is always possible for disease outbreak.

**Definition 3.3.1** *The disease dynamic system characterized by equation 5.1-5.8 has two equilibrium points. The first equilibrium point is the disease free equilibrium (DFE):*

$$S_{ij} = N_{ij}, E_{ij} = I_{ij} = R_{ij} = 0 \quad (3.3.9)$$

*The second equilibrium point is the endemic equilibrium:*

$$\sum_{ij} S_{ij} = 0 \quad (3.3.10)$$

*such that no susceptible population available and all people are eventually infected.*

In this section we analyze the properties of the epidemic model with travel contagion, and discuss the condition under which the DFE will be stable. Due to the existence of bilinear terms, there are more than one equilibrium point in the system, and the equilibrium points are unlikely to be G.A.S due to the nonlinearity of the system. We first introduce the definition of reproduction rate  $R_0$ , which is arguably the most important quantity in infectious disease modeling.

**Definition 3.3.2 (Basic Reproduction Number)** *The basic reproduction rate is the the number of cases one case generates on average over the course of its infectious period, in an otherwise uninfected population.*

If  $R_0 < 1$ , it indicates that on average each new infected person will affect less than one uninfected person during his or her infection. Therefore, the disease will die out in the long run, and reach the DFE point asymptotically. Consequently, in order to show that the transportation system is stable at DFE, it is equivalent to show that the  $R_0$  of the system is smaller than 1.

According to [43,81], the reproduction ratio  $R_0$  can be measured by the dominant eigenvalue of the next generation matrix (NGM) [42], which is denoted by  $K$ . In particular, the NGM can be calculated as:

$$K = -T\Sigma^{-1} \tag{3.3.11}$$

where  $T$  is called the transmission matrix and  $\Sigma$  is the transition matrix [43]. Note that for both  $T$  and  $\Sigma$ , only states associated with infections are taken into consideration. As for our study, the states that will affect the NGM are  $E_{11}, E_{12}, \dots, E_{ij}, I_{11}, I_{12}, \dots, I_{ij}$ . If there are  $P$  patches, the NGM takes the dimension  $2P^2 \times 2P^2$ . For the transmission matrix, it captures all the dynamics related to newly infected population, while the rest of the dynamics of the system are included in the transition matrix  $\Sigma$ .

If we linearize the transportation model at the DFE point (considering that all  $S_{ij}$ s are constant), the matrix  $T$  can be written as four blocks:

$$\mathbf{T} = \begin{array}{ccc} \mathbf{E} & \mathbf{I} & N^r \\ \left[ \begin{array}{ccc} 0 & E \rightarrow I & 0 \\ 0 & I \rightarrow I & N^r \rightarrow I \\ 0 & 0 & 0 \end{array} \right] & \begin{array}{l} \mathbf{E} \\ \mathbf{I} \\ N^r \end{array} \end{array} \quad (3.3.12)$$

where  $E \rightarrow I$  and  $I \rightarrow I$  are  $P^2 \times P^2$  matrices, whose entry denotes the coefficient values that matches an element of  $E$  or  $I$  to an element in  $I$ . Considering two variables  $E_{i,j}$  and  $I_{k,l}$ , then the matrix  $E \rightarrow I$  can be formally expressed by distinguishing the following 4 scenarios:

1.  $i \neq j, k \neq l$ .
2.  $i \neq j, k = l$ .
3.  $i = j, k \neq l$ .
4.  $i = j, k = l$

and

$$E \rightarrow I(ij, kl) = \begin{cases} \beta_{inn} \frac{N_{ij}}{N_j^P} + \frac{\sum_{m=1}^M c_{ij}^m \beta_{tra}^m g_i m_{ij} N_{ii} c_{lk}^m \delta_{lk,ij}^m r_{kl}}{\sum_{k=1, k \neq j}^P c_{kj}^m \delta_{kj,ij}^m (g_k m_{kj} N_{kk} + r_{jk} N_{jk})}, \text{ case 1} \\ \beta_{inn} \frac{N_{ij}}{N_j^P} + \frac{\sum_{m=1}^M c_{ij}^m \beta_{tra}^m g_i m_{ij} N_{ii} c_{lk}^m \delta_{lk,ij}^m g_k m_{kj}}{\sum_{k=1, k \neq j}^P c_{kj}^m \delta_{kj,ij}^m (g_k m_{kj} N_{kk} + r_{jk} N_{jk})}, \text{ case 2} \\ \beta_{inn} \frac{N_{ij}}{N_j^P} + \frac{\sum_{j=1, j \neq i}^P \sum_{m=1}^M c_{ji}^m \beta_{tra}^m r_{ij} S_{ij} c_{lk}^m \delta_{lk,ji}^m r_{kl}}{\sum_{k=1, k \neq i}^P c_{ki}^m \delta_{ki,ji}^m (r_{ik} N_{ik} + g_k m_{ki} N_{kk})}, \text{ case 3} \\ \beta_{inn} \frac{N_{ij}}{N_j^P} + \frac{\sum_{j=1, j \neq i}^P \sum_{m=1}^M c_{ji}^m \beta_{tra}^m r_{ij} S_{ij} c_{lk}^m \delta_{lk,ji}^m g_k m_{ki}}{\sum_{k=1, k \neq i}^P c_{ki}^m \delta_{ki,ji}^m (r_{ik} N_{ik} + g_k m_{ki} N_{kk})}, \text{ case 4} \end{cases} \quad (3.3.13)$$

Similarly, we can express the entries of  $I \rightarrow I$  by distinguishing the following scenarios:

1.  $i \neq j, k = l = i$ .
2.  $i = j, k \neq l, k = i$ .

and

$$I \rightarrow I(ij, kl) = \begin{cases} g_i m_{ij}, \text{ case 1} \\ r_{kl}, \text{ case 2} \\ 0, \text{ otherwise} \end{cases} \quad (3.3.14)$$

Finally, for the matrix  $N^r \rightarrow I$ , we have:

$$N^r \rightarrow I(k, ij) = \begin{cases} \alpha_i^I, \text{ if } i = j \text{ and } k = i \\ 0, \text{ otherwise} \end{cases} \quad (3.3.15)$$

This concludes the transmission matrix. And we next discuss the structure of the transition matrix, as follows.

For the transition matrix  $\Sigma$ , it is more complicated and can be written as the following block form:

$$\Sigma = \begin{array}{ccc} \mathbf{E} & \mathbf{I} & N^r \\ \left[ \begin{array}{ccc} E \rightarrow E & 0 & N^r \rightarrow E \\ E \rightarrow I & I \rightarrow I & 0 \\ \delta_E & \delta_I & 0 \end{array} \right] & \begin{array}{l} \mathbf{E} \\ \mathbf{I} \\ N^r \end{array} \end{array} \quad (3.3.16)$$

And each block matrices take the following form:

$$E \rightarrow E(ij, kl) = \begin{cases} -g_i - \sigma - \alpha_i, \text{ if } i = j \text{ and } kl = ij \\ r_{kl}, \text{ if } i = j \text{ and } k = i \\ -r_{ij} - \sigma - \alpha_i, \text{ if } i \neq j \text{ and } ij = kl \\ g_i m_{ij}, \text{ if } i \neq j \text{ and } k = l = i \\ 0, \text{ otherwise} \end{cases} \quad (3.3.17)$$

$$N^r \rightarrow E(k, ij) = \begin{cases} \alpha_i^E, & \text{if } i = j \text{ and } k = i \\ 0, & \text{otherwise} \end{cases} \quad (3.3.18)$$

$$E \rightarrow I(ij, kl) = \begin{cases} \sigma, & \text{if } ij = kl \\ 0, & \text{otherwise} \end{cases} \quad (3.3.19)$$

$$I \rightarrow I(ij, kl) = \begin{cases} -g_i - \alpha_i - \gamma, & \text{if } i = j \text{ and } ij = kl \\ -r_{ij} - \alpha_i - \gamma, & \text{if } i \neq j \text{ and } ij = kl \\ 0, & \text{otherwise} \end{cases} \quad (3.3.20)$$

**Proposition 3.3.1** *If  $\rho(K) < 1$ , then the DFE is stable. If  $\rho(K) > 1$ , the DFE is unstable.  $\rho$  refers to the spectrum radius of a matrix.*

**Proof** The proof comes naturally from the definition of  $R_0$ . ■

### 3.3.3 Control the spread of disease within transportation system

Since we have developed the model for infectious disease within transportation system, the next question to ask is that if we can control the spread of disease by placing entrance screening for transportation system. In particular, we have seen the implementation of radiation thermometers during the 2003 SARS outbreak for subway and bus systems, which aimed to screen out risky passengers with high body temperature. And additional measures such as distributing masks and random inspection by medical workers may also be efficient to reduce the risk exposure during travel. Meanwhile, placing entrance screening will also decrease system efficiency by introducing entry delays, which in return affecting the travel behavior of passengers in mode selection. This relationship is illustrated in Figure 3.2. Specifically, we assume that the efforts (e.g., time and resource) required grows faster than the increments in control effectiveness, so that a high detection rate of infected people will result in a much higher entry delay.

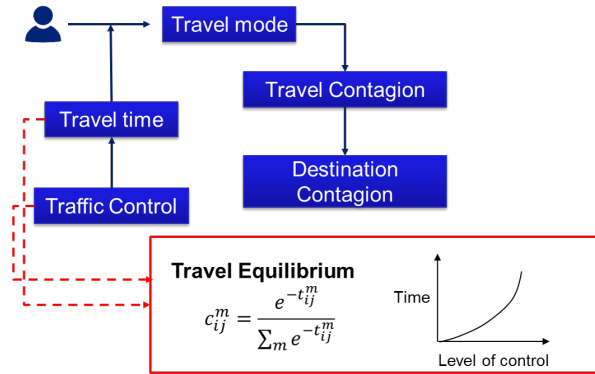


Figure 3.2.: Illustration of the passenger dynamics

While deriving the optimal control strategy will be intrinsically complicated for the proposed model, we make the first attempt to understand if it is possible to avoid the outbreaks of disease by placing controls on transportation system. In other words, our objective is to assess if a given control strategy may eventually lead to DFE state, and the problem falls into the field of safety verification. In the realistic transportation system, it is hardly possible to place the entry control for all travel modes. Instead, it is only viable to conduct such control over the medium and high capacity travel modes, such as buses and metros. As a consequence, in our study, we consider that passengers may choose from one or the following three travel modes:

1. **Low capacity mode** such as private vehicles and taxis
2. **Medium capacity mode** such as vans and buses
3. **High capacity mode** such as metro system

And passengers will choose the mode which maximize their utility (or the one with the least travel time). We consider rational behavior of passengers, and introduce the logistic function to quantify the model split ratio as:

$$S_{ij}^m = m_{ij} S_i \frac{e^{t_{ij}^m}}{\sum_{i=1}^M e^{t_{ij}^i}} \quad (3.3.21)$$

$$I_{ij}^m = m_{ij} I_i \frac{e^{t_{ij}^m}}{\sum_{i=1}^M e^{t_{ij}^i}} \quad (3.3.22)$$

We assume that the low capacity mode is not controllable, but typically having fewer passengers per vehicle and passengers having less chance of getting infected. On the contrary, passengers using medium or high capacity mode are usually exposed to much more people in a small compartment for a longer time, and are therefore having much higher chances of being infected. This assumption leads to the following requirement for the effective contact rate:

$$\beta_{tra}^{large} > \beta_{tra}^{med} > \beta_{tra}^{small} \quad (3.3.23)$$

Based on the discussion above, we arrive at the model which explicitly incorporates control over transportation system:

$$\begin{aligned} \dot{S}_{ii} = & -g_i S_{ii} + \sum_{j=1, j \neq i}^P r_{ij} S_{ij} + \alpha_i^S N_i^r - \alpha_i S_{ii} - \beta_{inn} \frac{S_{ii} \sum_{j=1}^P I_{ji}}{N_i^p} \\ & - \sum_{j=1, j \neq i}^P \sum_{m=1}^M c_{ji}^m \beta_{tra}^m r_{ij} S_{ij} \frac{\sum_{k=1, k \neq i}^P c_{ki}^m \delta_{ki, ji}^m d_l^m (r_{ik} I_{ik} + g_k m_{ki} I_{kk})}{\sum_{k=1, k \neq i}^P c_{ki}^m \delta_{ki, ji}^m (r_{ik} N_{ik} + g_k m_{ki} N_{kk})} \end{aligned} \quad (3.3.24)$$

$$\begin{aligned} \dot{S}_{ij} = & -r_{ij} S_{ij} + g_i m_{ij} S_{ii} - \alpha_i S_{ij} - \beta_{inn} \frac{S_{ij} \sum_{k=1}^P I_{kj}}{N_j^p} \\ & - \sum_{m=1}^M c_{ij}^m \beta_{tra}^m g_i m_{ij} S_{ii} \frac{\sum_{k=1, k \neq j}^P c_{kj}^m \delta_{kj, ij}^m d_l^m (g_k m_{kj} I_{kk} + r_{jk} I_{jk})}{\sum_{k=1, k \neq j}^P c_{kj}^m \delta_{kj, ij}^m (g_k m_{kj} N_{kk} + r_{jk} N_{jk})} \end{aligned} \quad (3.3.25)$$

$$\begin{aligned} \dot{E}_{ii} = & -g_i E_{ii} + \sum_{j=1, j \neq i}^P r_{ij} E_{ij} + \alpha_i^E N_i^r - \alpha_i E_{ii} - \sigma E_{ii} + \beta_{inn} \frac{S_{ii} \sum_{j=1}^P I_{ji}}{N_i^p} \\ & + \sum_{j=1, j \neq i}^P \sum_{m=1}^M c_{ji}^m \beta_{tra}^m r_{ij} S_{ij} \frac{\sum_{k=1, k \neq i}^P c_{ki}^m \delta_{ki, ji}^m d_l^m (r_{ik} I_{ik} + g_k m_{ki} I_{kk})}{\sum_{k=1, k \neq i}^P c_{ki}^m \delta_{ki, ji}^m (r_{ik} N_{ik} + g_k m_{ki} N_{kk})} \end{aligned} \quad (3.3.26)$$

$$\begin{aligned} \dot{E}_{ij} = & -r_{ij}E_{ij} + g_i m_{ij} E_{ii} - \alpha_i E_{ij} - \sigma E_{ij} + \beta_{inn} \frac{S_{ij} \sum_{k=1}^P I_{kj}}{N_j^P} \\ & + \sum_{m=1}^M c_{ij}^m \beta_{tra}^m g_i m_{ij} S_{ii} \frac{\sum_{k=1, k \neq j}^P c_{kj}^m \delta_{kj, ij}^m d_l^m (g_k m_{kj} I_{kk} + r_{jk} I_{jk})}{\sum_{k=1, k \neq j}^P c_{kj}^m \delta_{kj, ij}^m (g_k m_{kj} N_{kk} + r_{jk} N_{jk})} \end{aligned} \quad (3.3.27)$$

$$\dot{I}_{ii} = -g_i I_{ii} + \alpha_i^I N_i^r - \alpha_i I_{ii} + \sum_{j=1, j \neq i}^P \sum_m r_{ij} d_l^m c_{ij}^m I_{ij} + \sigma E_{ii} - \gamma I_{ii} \quad (3.3.28)$$

$$\dot{I}_{ij} = -r_{ij} I_{ij} - \alpha_i I_{ij} + \sum_m g_i m_{ij} c_{ij}^m d_l^m I_{ii} + \sigma E_{ij} - \gamma I_{ij} \quad (3.3.29)$$

$$\dot{R}_{ii} = -g_i R_{ii} + \alpha_i^R N_i^r - \alpha_i S_{ii} + \sum_{j=1, j \neq i}^P r_{ij} R_{ij} + \gamma I_{ii} + \sum_{j=1, j \neq i}^P \sum_m r_{ij} c_{ij}^m (1 - d_l^m) I_{ij} \quad (3.3.30)$$

$$\dot{R}_{ij} = -r_{ij} R_{ij} + g_i m_{ij} R_{ii} - \alpha_i R_{ij} + \gamma I_{ij} + \sum_m g_i m_{ij} c_{ij}^m (1 - d_l^m) I_{ii} \quad (3.3.31)$$

### 3.4 Verification for the control strategies

In this section, we present two control strategies for preventing the spread of disease, and then prove the correctness of them. We start with a simple strategy, the controlled transportation system can be modeled by a diagram shown in Figure 3.3.

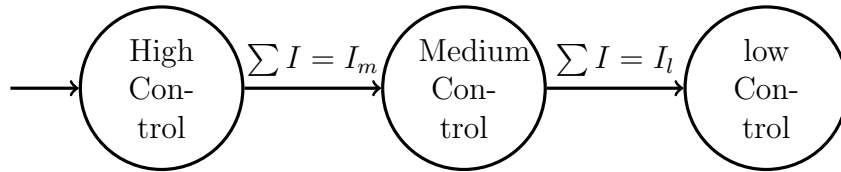


Figure 3.3.: Controlled transportation system

We briefly explain the behavior of the above system, the formal definition will be given later. The system consists of 3 modes each of which corresponds to a control level. Initially, the system is in the high control mode which means the total infected population i.e.,  $\sum I$  is higher than  $I_m$  which is a threshold for activating the medium control mode. When the infected population reaches  $I_m$ , the system switches immediately to the medium control mode to perform a less restrictive control. Similarly, when a lower threshold  $I_l$  is reached, the system switches immediately to the low control mode in which  $\sum I$  is expected to degenerate to a safe level in a specified amount of time.

As we will introduce later that the system in Figure 3.3 can be formalized by a hybrid automaton which is also called hybrid system in the paper. The correctness of the controlled system can be specified as that there is no unsafe state reachable. To prove this, we compute the reachable state set of the system in a bounded time horizon and show that no unsafe state is included.

### 3.4.1 Hybrid automata

Hybrid automata [82] are formal models for the systems composed of a discrete controller interacting with a physical environment. The definition of a hybrid automaton is given as below where we denote the set of reals by  $\mathbb{R}$ , and the cardinality of a set  $S$  is denoted by  $|S|$ .

**Definition 3.4.1** *A hybrid automaton is defined by a tuple  $\mathcal{A} = \langle Loc, Var, Flow, Trans, Inv, Init \rangle$  such that*

- *Loc is a finite set which consists of all discrete locations (or modes) of the system,*
- *Var is a finite set which contains all continuous variables of the system,*
- *Flow is a function associating each location a continuous dynamics which is defined by an ODE,*

- *Trans* consists of finitely many discrete jumps among the locations. A jump from  $\ell$  to  $\ell'$  is defined by a tuple  $\langle \ell, G, R, \ell' \rangle$  such that  $G \subseteq \mathbb{R}^{|\text{Var}|}$ ,  $R : \mathbb{R}^{|\text{Var}|} \rightarrow \mathbb{R}^{|\text{Var}|}$  are called the guard and reset respectively. The jump is enabled, i.e., allowed to take place, only if the guard  $G$  is satisfied by the variable values. After the jump is made, the variable values are reassigned according to the reset  $R$ .
- *Inv* is a function that defines an invariant, i.e., a valid variable value range,  $\text{Inv}(\ell) \subseteq \mathbb{R}^{|\text{Var}|}$  for each location  $\ell \in \text{Loc}$ ,
- *Init* is a set which contains all initial states of the system.

A *state* of a hybrid automaton  $\mathcal{A}$  is denoted by a pair  $(\ell, v)$  wherein  $\ell$  is the current mode and  $v$  is a constant vector whose components denote the current values of the state variables. A state  $(\ell, v)$  can evolve to  $(\ell', v')$  in the following two ways:

- *Continuous evolution*, i.e.,  $\ell = \ell'$  and there is a solution  $\varphi(t)$  of the ODE of  $\ell$  such that  $v = \varphi(t_1)$ ,  $v' = \varphi(t_2)$  for some  $0 \leq t_1 \leq t_2$ , and  $\varphi(t) \in \text{Inv}(\ell)$  for all  $t \in [0, t_2]$ . In other words,  $v'$  can be reached from  $v$  in the vector field defined by the ODE.
- *Discrete evolution*, i.e., there is a jump  $\langle \ell, G, R, \ell' \rangle$  such that  $v \in G$  and  $v$  is updated to  $v'$  according to  $R$ .

An *execution* of a hybrid automaton is a sequence of states such that for each successive states, the former one can evolve to the latter one. The time duration of an execution is the total amount of time spent in the continuous evolution, since jumps are considered to take no time. We call a state *reachable* if it occurs in at least one execution of the system. For succinctness, we collectively denote  $(\ell, V)$  for the state set  $\{(\ell, v) \mid v \in V\}$ .

**Example 3.4.1** *We consider a 2-dimensional hybrid automaton, i.e., a hybrid automaton with 2 variables, shown in Figure 3.4. Initially, the system is in mode  $\ell_1$  with the variable value set  $x \in [2, 2.2]$ ,  $t = 0$ . The continuous dynamics there is given*

by the ODE  $\dot{x} = x, \dot{t} = 1$  which governs the change of the variables in the invariant  $x \leq 5$ . When  $x \in [4.8, 5]$ , the system may take a jump to switch to mode  $\ell_2$  such that  $x, t$  still keep their values unchanged, i.e., the reset is an identity mapping. In mode  $\ell_2$ , the variables still evolves in the invariant  $x \leq 5$  according to another ODE  $\dot{x} = -x, \dot{t} = 1$ .

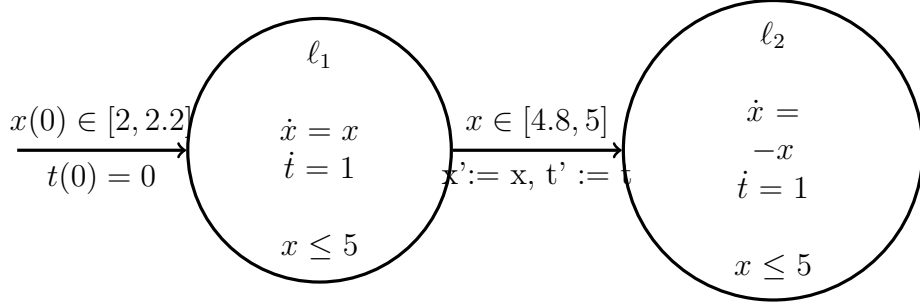


Figure 3.4.: A 2-dimensional hybrid automaton

To prove the safety of a hybrid automaton according to an unsafe state set, we need to explore all reachable states and prove that no unsafe state is reachable. However, reachable set computation is a notoriously difficult task on hybrid automata, since the *reachability problem*, i.e., to check whether a state is reachable or not, on hybrid automata is not decidable (see [82]). Hence, we resort to approximation methods.

One popular way to prove the safety is to compute an overapproximation of the reachable set, if the result has no intersection with the unsafe set then the system is safe. In this paper, we use the tool named FLOW\* [83] to generate overapproximations (flowpipes) for reachable set segments in a bounded time horizon. If there is no unsafe state contained in the flowpipes, then the system is safe.

### 3.4.2 Reachability analysis using Taylor model flowpipe construction

We give an introduction of the high-level techniques for computing Taylor model flowpipes for nonlinear hybrid automata. Since hybrid automata have two types of evolutions, we first introduce the method on continuous dynamics which are consid-

ered harder to handle, and then turn to jumps. In the remaining content, we call the set of reals between some  $a, b \in \mathbb{R}$  and  $a \leq b$  an *interval*, and denote it by  $[a, b]$ . The arithmetic on intervals are defined in [84].

**Taylor models.** Taylor models are proposed by Berz and Makino as a replacement of intervals in rigorous computation (see [85]). A Taylor Model (TM) is defined by a pair  $(p, I)$  such that  $p$  is a polynomial over a finite set of variables whose ranges are intervals, and  $I$  is an interval. A continuous function  $f(x)$  over an interval domain  $D$ , i.e.,  $x \in D$ , can be overapproximated by a TM  $(p(x), I)$ , i.e.,  $\forall x \in D. (f(x) \in p(x) + I)$ . Figure 3.5 shows an example such that for all  $x \in D$ , there is  $f(x) \in p(x) + [a, b]$ . Usually,  $p$  can be computed as a Taylor expansion of  $f$ , and  $I$  is an interval enclosure of the remainder term. If  $f$  is an analytical function then  $I$  can be arbitrarily reduced. Vector-valued functions, such as ODE solutions, can be overapproximated by a vector of single TMs, i.e., TMs whose range dimensions are 1. In this paper, we call TM matrices and vectors also TMs. TMs are closed under many operations such as addition, multiplication and integration, one may refer to [86] for more details.

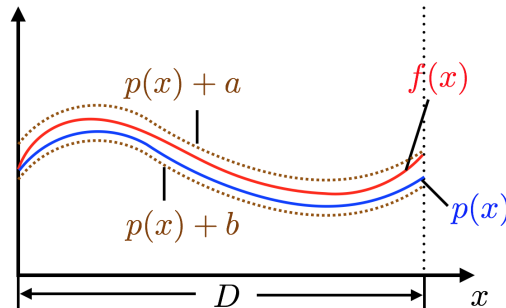


Figure 3.5.: Example of a Taylor model  $(p(x), [a, b])$

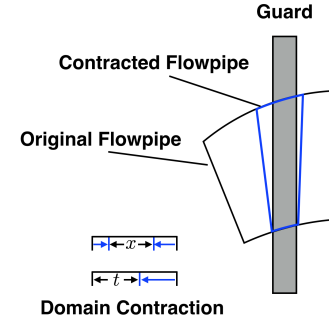


Figure 3.6.: Example of domain contraction

**Motivation of using TM flowpipes.** One of the most important applications of TMs is to perform validated integration for nonlinear ODEs. That is, given an ODE  $\dot{x} = f(x)$ , an initial condition  $x(0) \in X_0$ , and a time horizon  $[0, T]$ , the exact solution  $\varphi_f(x_0, t)$  from a state  $x_0 \in X_0$  at some time  $t \in [0, T]$  can be overapproximated by a TM using the technique called *TM integration* [87]. More precisely, the TM integration method consecutively computes a TM flowpipe  $(p(x_0, t), I)$  for

the forward flowmap  $\varphi_f(x_0, t)$  with  $x_0 \in X_0$  over a time step interval in  $[0, T]$  until the whole time horizon is covered. For example, the method computes  $N$  TMs  $(p_1(x_0, t), I_1), \dots, (p_N(x_0, t), I_N)$  such that  $(p_i(x_0, t), I_i)$  overapproximates  $\varphi_f(x_0, (i-1)\frac{T}{N} + t)$  for  $x_0 \in X_0$  and  $t \in [0, \frac{T}{N}]$  for all  $i = 1, \dots, N$ . Then a state which is not contained in any TM flowpipe is not reachable. TM integration usually has much better accuracy than the interval-based methods on nonlinear ODEs (see [88]). Therefore, we can use TM integration to produce high quality flowpipes in the reachability analysis under continuous dynamics. However, it leaves us a difficulty to deal with mode invariants and jumps.

**Flowpipe/guard and flowpipe/invariant intersections.** We need to intersect a TM flowpipe with a set in the following two situations. (1) When computing the flowpipes in a mode, we need to intersect the flowpipes with the mode invariant in order to eliminate the overestimation as much as possible, since any state outside the invariant is not reachable. (2) We need to intersect a flowpipe with a jump guard to obtain a tighter overapproximation for the reachable set on which the jump is enabled. In the paper, both invariants and guards are defined by constraints of the form  $p \leq c$  wherein  $p$  is a polynomial over the state and time variables, and  $c$  is a constant. Therefore, an intersection can be viewed as applying the constraints defining the set to refine the TM flowpipe. Since the intersections are generally not TMs, we use the *domain contraction* technique to derive a contracted TM for the intersection. Figure 3.6 illustrates an example. The domain of the original TM flowpipe is contracted according to the guard, so that the contracted flowpipe forms an overapproximation of the intersection. Moreover, we may further overapproximate the result and intersect it with the guard again to eliminate the part outside the guard. One may refer to [88, 89] for more details.

Now we turn to the main framework of the reachability analysis for nonlinear hybrid automata. The abstract algorithm is presented by Algorithm 1. Each main iteration alternates between the flowpipe computation for continuous and discrete dynamics. The whole procedure terminates when the time horizon  $[0, T]$  is covered or

the maximum jump depth is reached. For each jump, we aggregate the intersections to avoid state explosion. Figure 3.7 illustrates an example of intersecting a set of flowpipes with a guard. We also give a running example as follows.

---

**Algorithm 1:** Flowpipe construction for hybrid automata

---

**Input:**  $\mathcal{A} = \langle Loc, Var, Flow, Trans, Inv, Init \rangle$  wherein  $Init = (\ell_0, V_0), T, k$ .

**Output:** Overapproximation of the state set which are reachable in the time  $[0, T]$  by at most  $k$  jumps.

```

1: Add  $(\ell_0, V_0, 0, 0)$  to Queue;           # the queue keeping new initial sets
2:  $\mathcal{R} \leftarrow \emptyset$ ;                 # resulting flowpipes
3: while Queue is not empty do
4:   Dequeue the first state set in Queue and keep it as  $(\ell, V, t_0, n)$ ;
5:   Compute the TM flowpipes  $\mathcal{F}_1, \dots, \mathcal{F}_m$  from  $V$  under the continuous
     dynamics of mode  $\ell$  for the time horizon  $[t_0, T]$ ;
6:    $\mathcal{R} \leftarrow \mathcal{R} \cup \{\mathcal{F}_1, \dots, \mathcal{F}_m\}$ ;
7:   for all  $\langle \ell, G, R, \ell' \rangle \in Trans$  do
8:      $C \leftarrow \emptyset$ ;                 # aggregation set
9:     for all  $i = 1, \dots, m$  do
10:      if  $\mathcal{F}_i \cap G \neq \emptyset$  then
11:        Contract  $\mathcal{F}_i$  to  $\mathcal{F}'_i$  w.r.t.  $G$ ;           # domain contraction
12:         $C \leftarrow C \cup \{\mathcal{F}'_i\}$ ;
13:      end if
14:    end for
15:    if  $C \neq \emptyset$  then
16:      Overapproximate  $C$  by a TM  $C'$  which covers the time interval  $[t'_0, t_e]$ 
        such that  $t_0 \leq t'_0 \leq t_e \leq T$ ;
17:      if  $t'_0 < T$  and  $n < k$  then
18:        Compute  $C_R$  as the image of  $C'$  under the mapping defined by  $R$ ;
19:        Add  $(\ell', C_R, t'_0, n + 1)$  to Queue;
20:      end if
21:    end if
22:  end for
23: end while
24: return  $\mathcal{R}$ ;

```

---

**Theorem 3.4.2** ([88]) *Algorithm 1 returns an overapproximation of the set of states which are reachable in the time  $[0, T]$  via at most  $k$  jumps.*

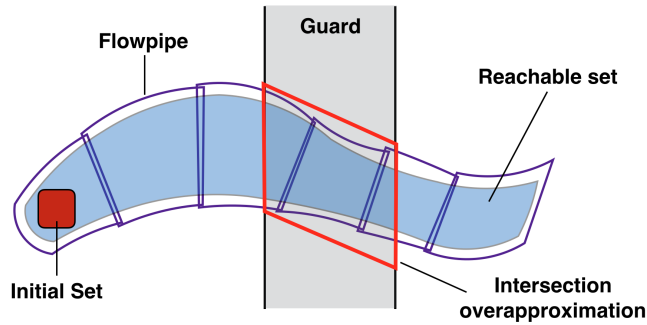


Figure 3.7.: An overapproximation for flowpipe/guard intersections

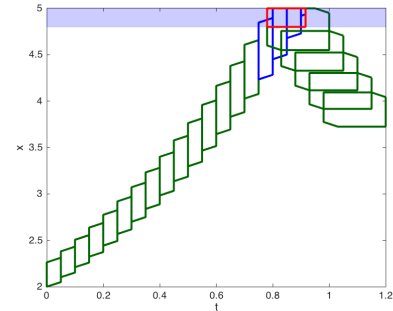


Figure 3.8.: Flowpipes for the 2-D hybrid automaton

**Example 3.4.3** *We consider the previous example. Figure 3.8 shows some computed TM flowpipes which are guaranteed to contain all executions which are impossible to compute exactly in the time horizon  $[0, 1]$ . Since TMs are hard to be plotted exactly, we show their octagon overapproximations. The four blue flowpipes are detected to intersect the guard, and the red box is a TM overapproximation for their intersections with the guard.*

**Complexity of a TM.** The size of a TM is mainly determined by the polynomial part, since the remainder only needs to be represented by its bounds. For a single TM over  $n$  variables of order  $k$ , the polynomial part can have  $\binom{n+k}{k}$  many terms in the worst case. Although this fact shows the inscalability of TMs, we still obtain relatively low time cost on our large examples in the paper.

## 3.5 Results

### 3.5.1 Experiment setting

The numerical experiments are conducted on a desktop with @3.5 GHz CPU and 32GB RAM. The codes are written in C++ and compiled with gcc in Linux system. The MPFR library is used for interval arithmetic and the Flow\* library is used for doing TM flowpipe construction. The numerical experiments have three

major parts. The first part is to compare the results on disease dynamics with and without modeling urban transportation system, including the difference in disease equilibrium patterns and the impact on  $R_0$  values. The second part focuses on the performance of the reachability analysis, where the computational performances as well as the tightness of the overapproximation is discussed. Finally, we investigate how disease outbreaks evolution may vary based on different urban structures. For the first two parts, we mainly focus on the test network as shown in Figure 3.9. The network has 3 nodes and 9 OD pairs, meaning that each node is accessible from the other. As each OD pair may have four states (S,E,I,R), the ODE system of this test network therefore has 36 state variables and 36 system equations. We consider the invasion of H1N1 influenza in 2009 as the case study for the test networks. According to the literature [90], the disease has the contact rate  $\beta$  of 0.585,  $\gamma$  being 0.09, and  $\sigma$  being 0.47, which suggests that H1N1 has an average latent period of 2 days and recovery time of 10 days. And based on the epidemic parameters, our objective is to compare how disease dynamics may vary in three different systems: the SEIR system without travel contagion, the SEIR system with travel contagion but no intervention strategies, and the SEIR system with travel contagion and entry control strategies. In particular, for the control strategies, we consider three different level of controls, namely the high level of control that may possibly eliminate 50% of suspicious travelers from entering the system, the medium level of control that may eliminate 30% of infected travelers, and the low control level where only 10% of infectious population may be identified. And different control strategies may have different impact on the travel time for the corresponding travel modes. The third part of the experiment setting will focus on a different set of networks, as shown in Figure 3.10. For this part, we consider networks that represent three different urban structures: the stripe-shaped network such as Shenzhen, China, the single-centered network including Paris and New York City, and the multi-centered networks (in this study we consider dual centers for simplicity) such as Beijing and Shanghai,

China. And we analyze how effective are various control strategies in controlling these networks.

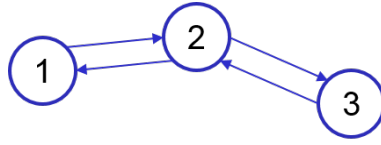


Figure 3.9.: Test network with 3 nodes

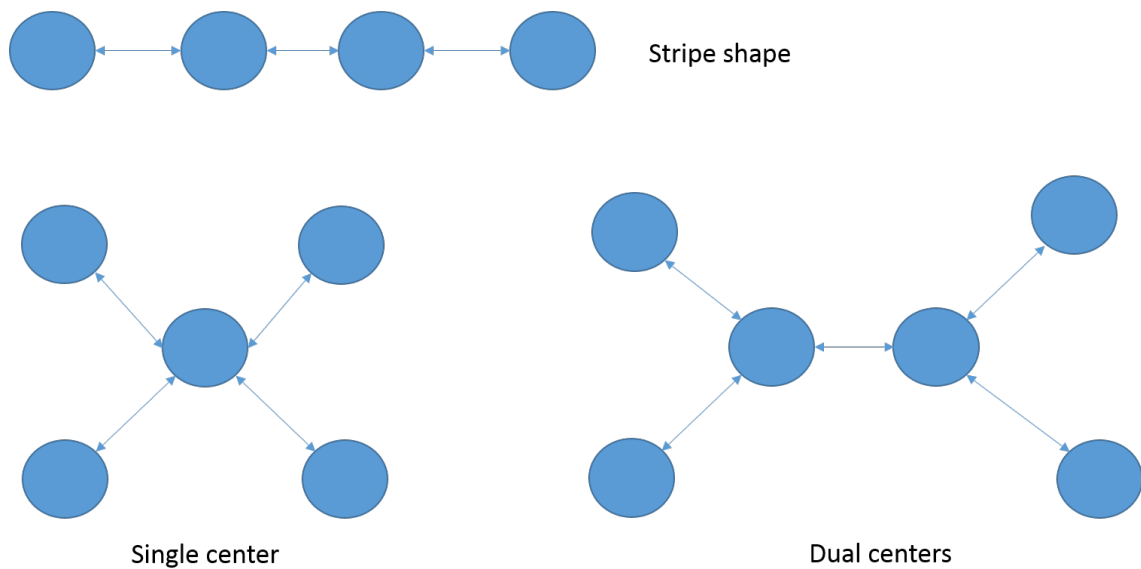


Figure 3.10.: Networks with three different urban structures

### 3.5.2 Case study: 2003 SARS outbreak in Beijing

One major difficulty related to mathematical modeling of infectious diseases is the validity of the developed models. In general, it is not possible yet ethical to validate the fidelity of the model with field experiments. And in this study, we investigate the validity of our model by measuring the alignment of its predicted results with the real-world ground data during the 2003 Severe Acute Respiratory Syndrome (SARS) outbreak in Beijing, China.

The 2003 Beijing SARS outbreak is one of the few disease outbreaks within urban areas that has documented the daily progress of the disease pattern. There were 2523 probable cases of SARS reported from March 5, 2003 to May 29, 2003 [91]. Multiple control measures had been implemented during the outbreak, including the set up of dedicated SARS hospital, information dissemination of real-time SARS pattern, and the closing of public facilities. As for the transit system, surveillance sites had been set at the airport, major train stations, and 71 roads that connect Beijing to peripheral areas. The metro system improved its ventilation system, and more frequent and thorough disinfections were conducted for both metro compartments and buses. In addition, staffs of bus and metro systems had been trained to identify and take immediate actions against probable patients during travel.



(a) Disinfection of metro compartment taking place on April 21, 2003 (b) Body temperature screening at the train station

Figure 3.11.: Measures were taken in mass transit systems to identify probable cases of SARS in Beijing

To model the SARS outbreak, we first divide Beijing into 5 areas as shown in Figure 3.12. Among the 14 million population in Beijing by the end of 2003, 40% of them reside inside the third ring road of Beijing (which corresponds to center area 3 in Figure 3.12). And we consider the rest 4 areas have similar population size, with each accounts for 15% of total population of Beijing. Due to lack of daily commuting data in 2003, we assume that the 70% of the activities for people living in area 3 are within area 3, and 40% of the activities are within the same area for the other 4 areas.

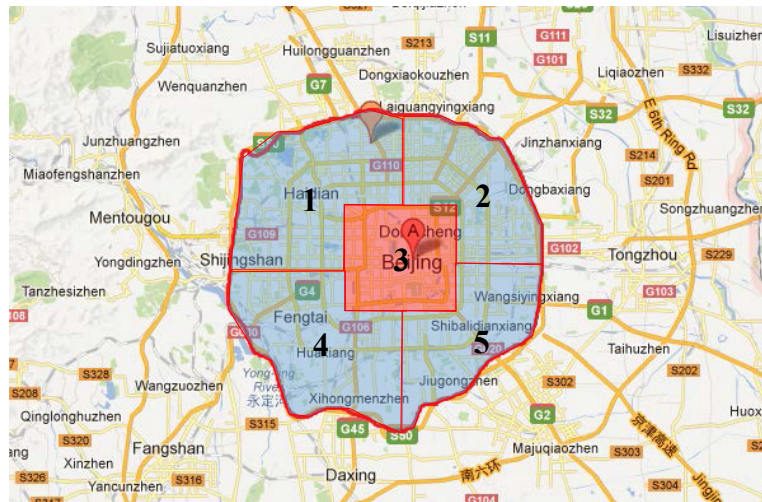


Figure 3.12.: The Beijing network with 5 nodes

This gives the vector of departure rate  $g = [0.6, 0.6, 0.3, 0.6, 0.6]$ . For each OD pair, we consider the return rate being 0.9. For residents of area 3 who leave the area for daily activities, we assume that they have equal chances to reach all other 4 areas. And for residents of area 1,2,4, and 5, we consider that they have 40% of chance to visit area 3, and 20% for other three places. Three transit modes are considered with capacity ranging from high to low, and the ratio of travel time for the same OD pair are set to 5:8:6. Considering various efforts made in mitigating disease spreading within transit system, we assume that the high capacity and medium capacity modes have 20% probability for identifying the probable case during travel. For the disease parameters, the typical incubation time for SARS is reported to be within 2-7 days, with 3-5 days being most common [92]. Consequently, we set  $\sigma = 1/3$  for the case study. Different from the its typical definition, the recovery state R in this case study should refer to the state where an infectious individual or probable case of SARS is identified and isolated from the mass population. Due to the effectiveness of information dissemination and increasing alertness of people to SARS, it is reasonable to consider that any people with symptoms may get easily identified as long as they take part in any social activities. This value along with the infectious rate  $\beta$  are usually identified through curve fitting from real-world data. The recovery rate is set to 0.6 in our study, meaning that in 60% of the cases the infectious individual will be identified and hospitalized. The infectious rate  $\beta$  was reported to take values between 0.57 to 1 in various cases [93,94]. But this value is temporally varying and is sensitive to the control measures being taken. In our study, we consider the infectious rate being 0.71 for the entire population, and therefore the effective transmission rate per contact being  $5.07e-8$ . Based on the parameter setting, we constructed the epidemic model of 100 dimensions for 25 OD pairs and the results are simulated using ODE45 simulator in MATLAB, as shown in Figure 3.13 and Figure 3.14.

We use the official data from Chinese Ministry of Health as the baseline observations, which gives the daily number of probable SARS cases starting from April 20, 2003 to June 12, 2003. While the number of infectious and latent population were

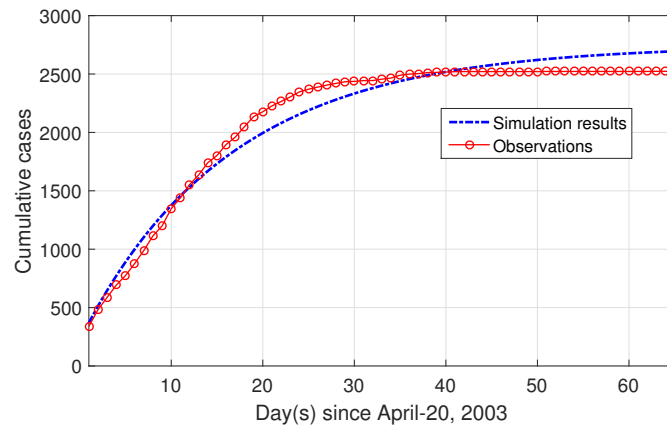


Figure 3.13.: Cumulative SARS cases since April-20, 2013, Beijing, China

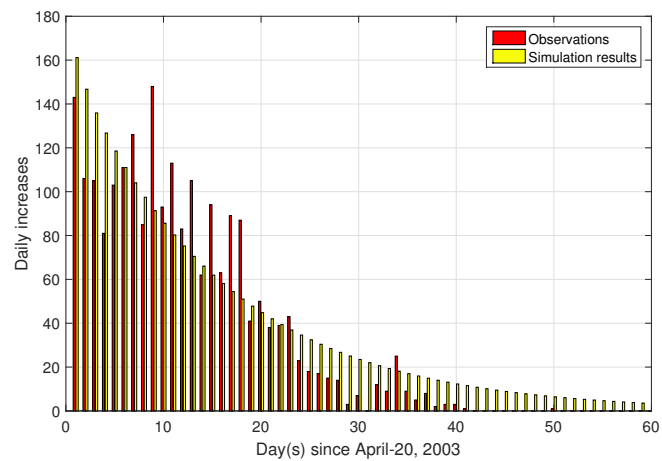


Figure 3.14.: Daily increases of SARS cases since April-20, 2013, Beijing, China

unknown, we assume  $E(0) = 420$ ,  $I(0) = 223$ , and  $R(0) = 210$ , and these people are evenly distributed in all 5 areas, where the simulated results well match the statistics reported in the first day (April-20, 2003). It can be verified from the results that the simulated curve for the number of cumulative cases may well approximate the actual observations reported, especially within the first 15 days. Moreover, the total number of cases based on the simulation is 2745, which is only 8.8% higher than the actual total cases. As for the daily number of cases, though the deterministic model may not be able to capture the stochasticity that takes place in the real-world, the simulated results still follow the trend similar to the actual observations. It provides a very good sense on how the disease may propagate over days with limited inputs, and the differences between simulation results and observations for daily increases is smaller than 15 cases in 47 out of the 65 days. In addition, if we only apply the conventional SEIR model in this case, the corresponding  $R_0$  value is  $0.71/0.6 = 1.183$ , which implies that the disease will invade the entire population which is entirely different from the actual observations. On the other hand, if we match the the  $R_0$  value of SEIR model with our proposed model ( $R_0 = 0.836$  in this case), the limiting number of cases will become 3774 cases, which is significantly higher than the observed value. And the SEIR model may be able to give a closer estimation of 2472 cases only if we set  $\gamma = 0.97$ , which implies that we are able to hospitalize the patients as soon as they get infected and such scenario is barely possible for any real-world disease outbreaks. Consequently, these results may well support the fidelity of our developed approach and reveal the potential of our model for predicting the propagation of disease outbreaks that take place in urban areas.

### 3.5.3 The role of contagion within transportation system

We next assess the importance of modeling travel contagion during urban disease outbreaks. We mainly focus on comparing the results from three different models: the disease model without modeling travel contagion (MWOTC), the disease model that

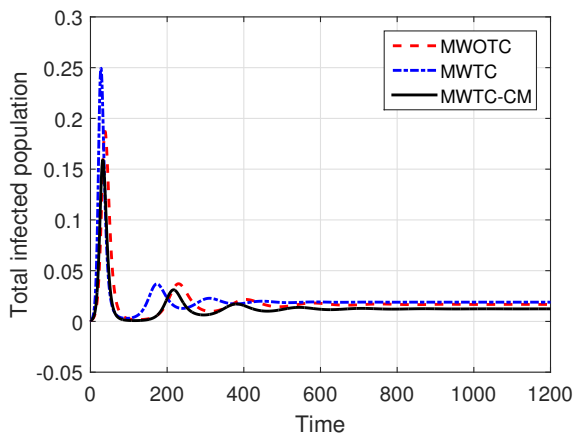
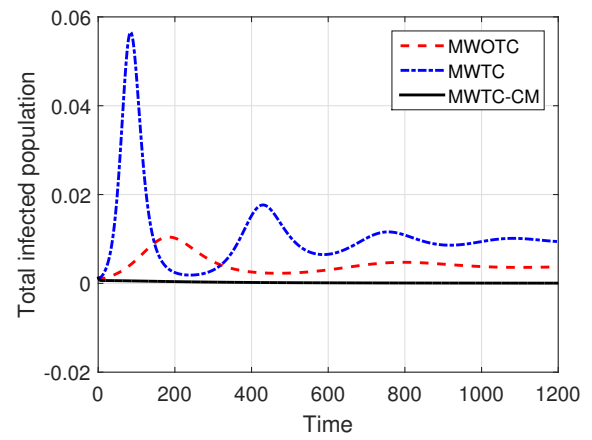
(a) Disease A with  $\beta = 0.7$ (b) Disease B with  $\beta = 0.25$ 

Figure 3.15.: Total infected population over time

models travel contagion but no interventions introduced (MWTC), and the disease model that model travel contagion and considers control measures over traffic modes (MWTC-CM). Note that MWOTC and MWTC are special cases of MWTC-CM, where MWTC-CM reduces to MWTC when the vector  $d$  is set to unity, and the MWTC can be reduced to MWOTC by let  $\beta_{tra} = 0$ . We investigate the differences in the disease dynamics among the three models from two aspects: the disease dynamics of different infectious diseases and the change of  $R_0$  with respect to different diseases. The same network as in the 2003 Beijing SARS case study is used in this section. For simplicity, we set total population to be 1 instead of 4, and assume that at the beginning only patch 1 has infectious people that account for 1% of the population, and all remaining people are in the susceptible state.

We first present the propagation dynamics associated with highly infectious and lowly infectious diseases. We assume that the incubation period is 4 days, and the average time of recovery is 5 days. The highly infectious disease A has  $\beta = 0.7$  and the  $\beta$  for lowly infectious disease B is 0.25. In addition, we consider 20% of travel control effectiveness for both diseases. The results of total infected population of the entire urban area are presented in Figure 3.15. For disease A, the corresponding  $R_0$  values for MWOTC, MWTC and MWTC-CM are 1.639, 2.013, and 1.834 respectively. And those of disease B are 1.051, 1.172, and 0.998. These two cases prove the correctness of our derivation of  $R_0$ , where the disease is endemic and persists in the population when  $R_0 > 1$ , and the system converges to the DFE state when  $R_0 < 1$  (MWTC-CM for disease B). And in both cases, we observe that the equilibrium points are stable.

As can be seen in both cases, without considering travel contagion, it is likely that we will underestimate the peak number of infected population and obtain a delayed prediction of the peak time. And such gaps are more obvious during the outbreak of the less infectious disease B. It is not difficult to interpret the higher peak of infected population, since by modeling travel contagion we are considering an additional layer of interactions between susceptible and infected people during their travels. And for the early arrival of the disease peak, it is due to the faster synchronization of

disease pattern over the urban area with the help of travel contagion. This effect is illustrated in Figure 3.16, where the total number of infected people in each patch of the network is presented. At time step 0, the patch one start with 1% of infected people and all other patches are free of disease. As time progresses, we observe the infected population of patch 1 first drops and then starts to increase. But the point where the change of gradient takes place is quite different in the two cases. Without travel contagion, the infected population in patch 1 starts to increase around time step 30, while the corresponding time step is around time step 15 if the travel contagion is modeled. In addition, since patch 1,2,4,and 5 have similar population size and travel pattern, we observe that their disease dynamics start to converge after the initial several steps. And model with travel contagion reaches this convergence earlier than without modeling travel contagion. All of these suggest the faster synchronization of disease pattern due to the existence of travel contagion. On the other hand, if we place control measures to our transit system to make it more invulnerable to infectious diseases, we are able to effectively reduce the peak size of the diseases, as well as the total number of infected people over the entire disease outbreak. But more importantly, it can be verified that by controlling the transit system through moderate efforts, it is possible to change the state of the disease from endemic to DFE, which results in the elimination of the disease overtime. This is especially meaningful for diseases such as influenza where people are paying less attention to due to comparatively insignificant consequences and we barely have effective measures for its eradication besides mass annual vaccination.

We next evaluate how the two key parameters  $R_0$  and  $R_\infty$  may differ in the three models with respect to different disease infectious rates, as shown in Figure 3.17. It is known that  $R_0 = 1$  is the threshold of disease invasion, and by modeling travel contagions, it is likely that the disease tends to be endemic while the result reported without travel contagion is disease free. And the gap between with and without travel contagion in  $R_0$  tends to increase as  $\beta$  increase, meaning that it is even more crucial to consider the travel contagion for diseases with higher transmission rate. Moreover,

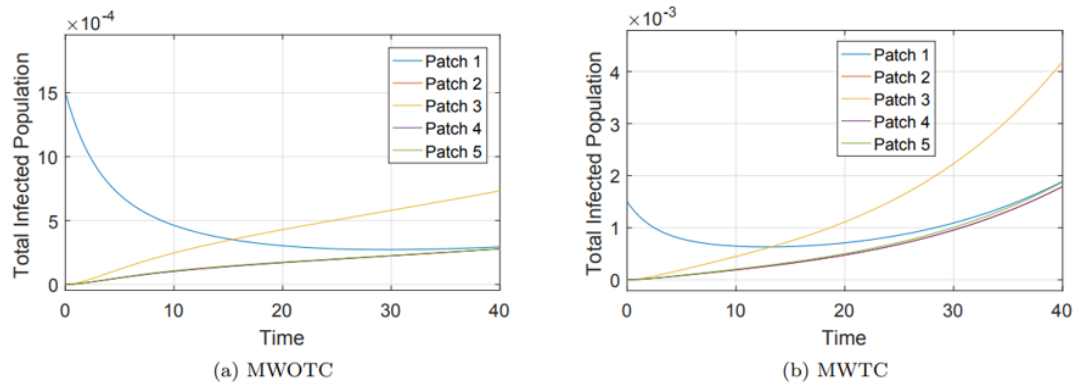


Figure 3.16.: Total number of infected people in each patch

while disease pattern may change from DFE to equilibrium by considering travel contagion, a moderate control intervention (eliminating 20% of infected population) may driver bring the disease back to the DFE state, as shown in Figure 3.17(b). And the control strategy is increasingly effective as  $\beta$  changes from 0.1 to 0.4, where we may reduce the total infected population during endemic by over 50%.

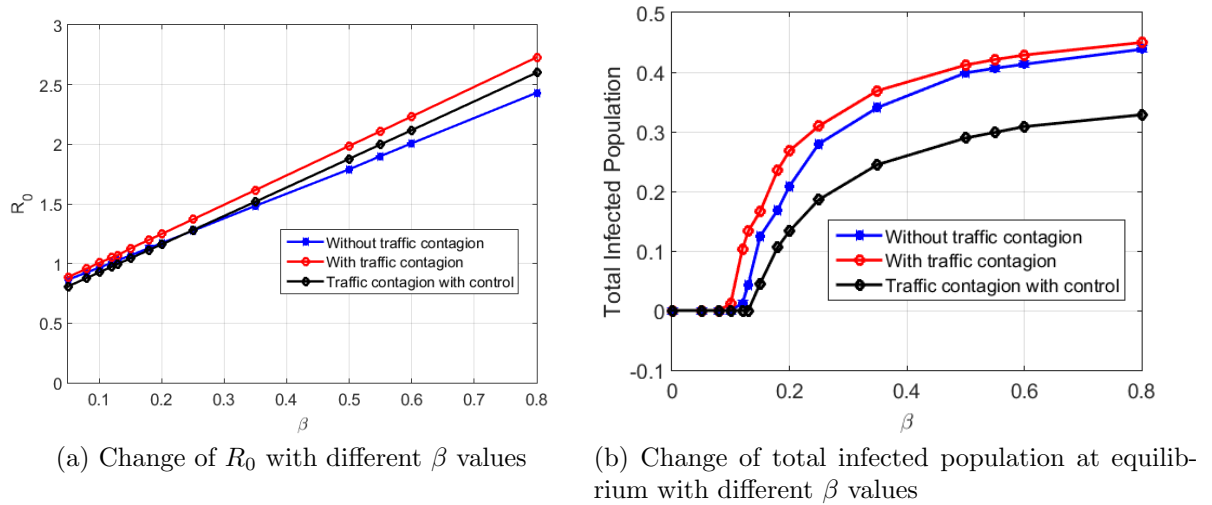
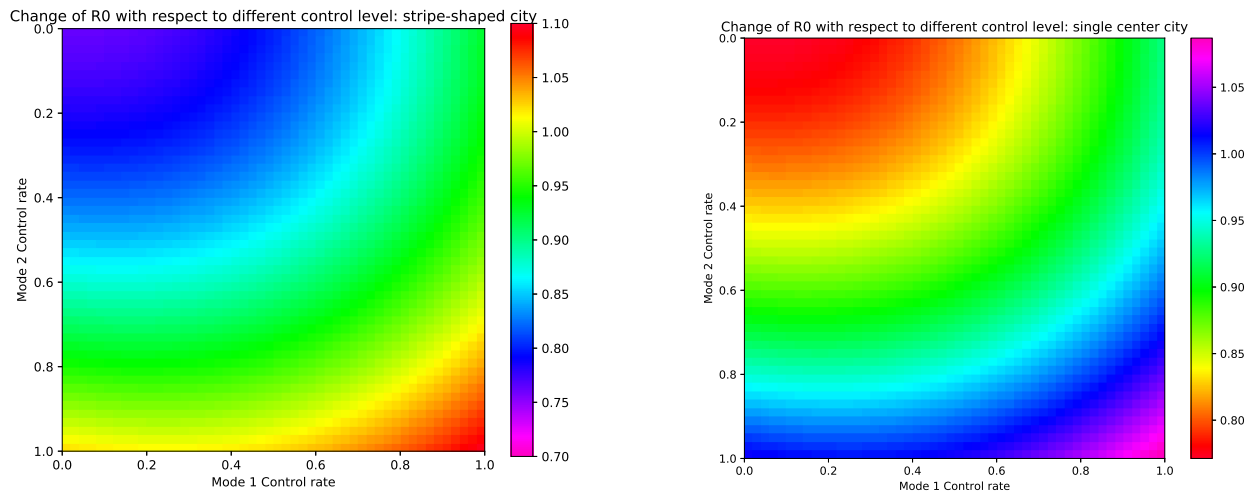


Figure 3.17.: The change of  $R_0$  by modeling urban travel

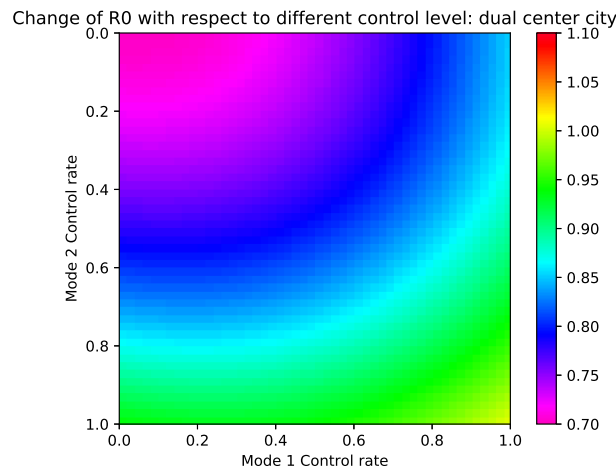
Finally, we would like to evaluate how different control strategies may be effective under different urban structures. That is, the way people travel and get in contact may be different with different urban structures. We consider the three networks as introduced before, and vary control effectiveness for medium and high capacity modes, from 0% to 100% effective, and the results are shown in Figure 3.18. There are clearly boundaries on the effectiveness of the controlling strategies, as increasing the effectiveness will add extra travel times thus driving travelers to other modes. Therefore, for the particular disease, we see that the least  $R_0$  achieved is approximately 0.7 in Figure 3.18(c). And we can further see the decreasing marginal effectiveness of the control strategies, e.g. with 80% control for mode 2 in single center network, the effectiveness does not change at all if we increase the level of control for mode 1 from 40% to 0%. But most importantly, given the same level of control, there are

clear differences of  $R_0$  value if the urban structure is different. In general, the city with single center is more vulnerable to the invade of infectious diseases due to most activities are centered in the middle of the city, which is reflected by both highest  $R_0$  and lowest  $R_0$  possible in the figure. And without any intervention, the urban structure with multiple nodes tend to have the lowest  $R_0$  of 1.0, while the value is 1.1 for stripe-shaped and single center networks.



(a) Control over stripe-shaped city

(b) Control over cities with single center



(c) Control over cities with dual centers

Figure 3.18.: Comparison of no-control scheme versus hybrid system setting

### 3.5.4 Reachability analysis

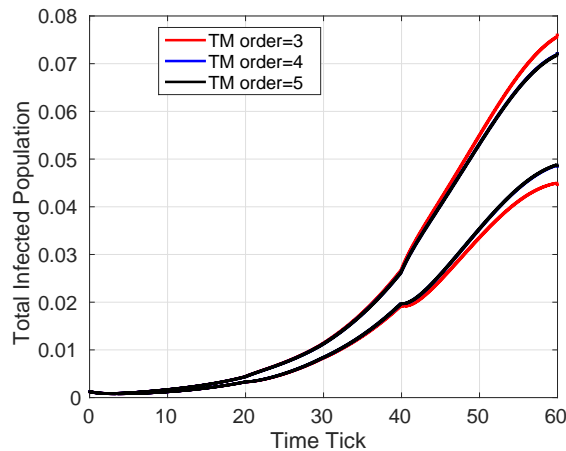
We next discuss the impact of modeling parameters and their impacts on the accuracy and computation time of the constructed flowpipe over-approximation. In particular, we focus on the order of TMs and the precision of cut-off threshold, which are the two major factors that may affect the tightness of the estimation.

Table 3.3.: Computational efficiency of the Taylor model approach with different parameter settings

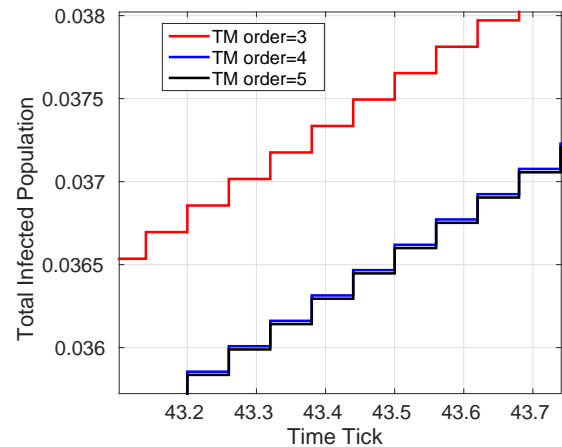
Case	Network nodes	Dimension	Cut-off	Taylor_Order	Time per step(s)
1	4	64	1.00E-06	5	812.73
2	4	64	1.00E-06	4	577.25
3	4	64	1.00E-06	3	515.25
4	4	64	1.00E-08	5	604.42
5	4	64	1.00E-08	4	533.53
6	4	64	1.00E-08	3	515.08
7	4	64	1.00E-10	5	1939.09
8	4	64	1.00E-10	4	493.98
9	4	64	1.00E-10	3	481.27

Table 3.3 presents the computational time spent for the four-network which has 64 dimensions and state variables, and we vary the parameter setting to compare the resulting level of accuracy of the constructed flowpipes and the corresponding CPU time in seconds. In all cases, the symbolic remainder approach [95] is adopted with the queue length equals to one-third of the total number of estimation steps, for the sake of reducing numerical errors due to wrapping effects. The 64-dimensional non-linear ODE system is in general a huge system and often computational expensive to evaluate numerically, but our results suggest that the TM approach complete the over-approximation in an efficient manner, where the time required for computing each time step (corresponding to one day in our case) ranges from 480 to 813 seconds depending on the system parameter setting. That is, we may analyze the disease outbreaks and predict the flowpipe of the disease trend for upcoming 100 days in approximately 14 hours, which is a reasonable amount of time for any practical imple-

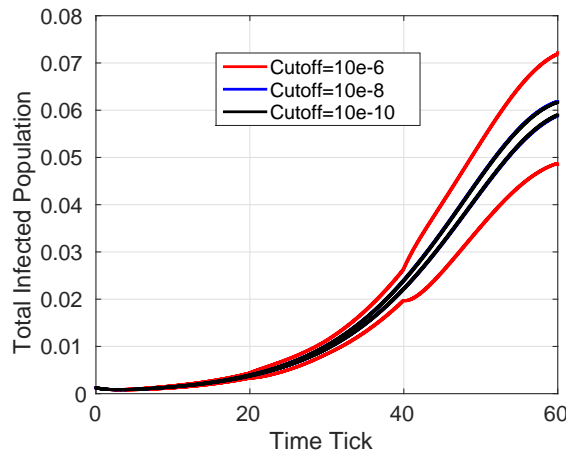
mentation considering its property of guaranteed safety. And this computation time may be significantly improved if the current sequential construction of TM model is extended to allow for parallelization to make more sufficient use of the computing power available.



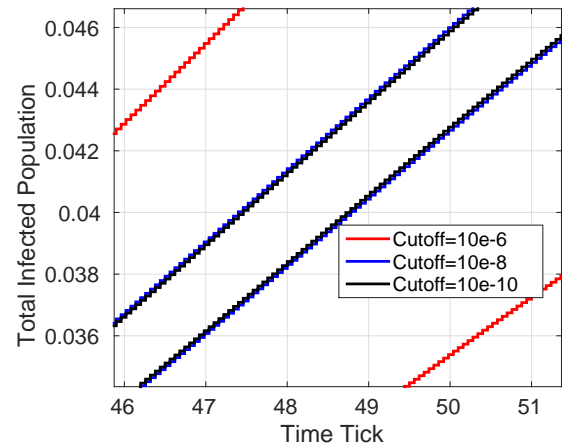
(a) Cutoff threshold= $10e-6$ , and vary TM from 3 to 5



(b) Cutoff threshold= $10e-6$ , and vary TM from 3 to 5 (zoom)



(c) TM=4, and vary cutoff threshold from  $10e-6$  to  $10e-10$



(d) TM=4, and vary cutoff threshold from  $10e-6$  to  $10e-10$ (zoom)

Figure 3.19.: Accuracy with different cutoff thresholds and Taylor model orders

Figure 3.19 illustrates the impact of different TM orders and cutoff sizes on the tightness of the over-approximation results. Since the ODE system involves mostly

bilinear terms, we start with TM order of 3 and cutoff size being  $1e-6$ , and then increase the TM order and reduce the cutoff threshold to compare the gain over the level of accuracy versus the additional computation time spent. It is observed that by increasing TM order from 3 to 4, there is a notable improvement on the tightness of the over-approximation as shown in Figure 3.19(a)-(b). This suggests that TM order 3 may produce overly conservative results and a higher order is expected. If we further increase the TM order from 4 to 5, the gain is only minimal as compared to over 40% increase in the computation time. These imply that TM order 4 is sufficient to obtain accurate results for the ODE system that we study. On the other hand, we fix TM order to 4 and investigate how the overapproximation results change with respect to the cutoff threshold. As shown in Figure 3.19(c)-(d), a large cutoff threshold (e.g.,  $10e-6$ ) will lead to significantly overestimated upper and lower bounds. But if we reduce the cutoff threshold by 2 orders, we may obtain a very tight over-approximation, and the difference is hardly distinguishable if we use a even smaller cutoff threshold. These results suggest higher TM orders and smaller cutoff threshold will improve the tightness of the over-approximation, but the marginal gain may be diminishing rapidly. Consequently, TM order of 4 and cutoff threshold being  $10e-8$  would be one of the optimal parameter settings for the flowpipe construction of our ODE system. And similar evaluation approach may be adopted if the different ODE systems are investigated.

For Figure 3.18 (a)-(d), they show the reachable set when starting from the infected states, where the infected population  $\in [0.18, 0.2]$ . It can be verified that the traffic control does help to eliminate the disease and reduce the spread of the disease. In particular, for  $I_{11}$ , it can be seen that at the end of the time interval the infected population is reduced to  $[0.07, 0.09]$ , while for the no control case there is a clear sign of disease outbreak since there are 50% more infected people. Similarly, for  $I_{12}$ , the control helps to reduce the infected population to less than 0.02, and the overall trend is monotonically decreasing, but the no control case has a larger population of infectious people and the amount of infected people increases towards the end. As for

$I_{33}$ , it starts from the DFE state, and the no control case clearly shows the pattern of disease outbreak, while for the controlled system there are much fewer infected population. Also, the amount of infected people tends to decrease if we enlarge the time interval.

One key concern related to interval arithmetic approaches for over-approximating ODE systems is the wrapping effect. And it is practically inevitable that the TM may produce extra residuals due to overly wrapping the original system of equations at each time step, unless the ODE system itself is exactly the TM. Since the numerical residue may carry over to the calculations in following steps, a small wrapping residual may have bull-whip effect on the constructed over-approximating flowpipe. Since we have shown only the first 60 steps of the ODE system, readers may be curious to see if the over-approximation flowpipe may eventually explode as the time progresses. We investigate this issue numerically by comparing the constructed flowpipe with the results from the ODE simulator and evaluating the residual error  $\bar{e}_t$  at each time step which is measured as:

$$\bar{e}_t = \frac{v_t^m - v_t'}{v_t'} \quad (3.5.1)$$

where  $v_t^m$  is the estimated upper bound of the ODE system from model  $m$  (e.g., model with TM order 3 and cutoff threshold  $10e - 6$ ) at time  $t$ , and  $v_t'$  is the estimated upper bound of the ODE system from the benchmark model. Since we shall never know the exact upper bound of the flowpipe, we need to specify the benchmark model which may produce highly tight estimation of the actually upper bound. In our numerical experiments, we set the benchmark model to the one with TM order 5 and cutoff threshold being  $10e - 10$ , and compare all other models listed in in Table 3.3. The results are shown in Figure 3.20. There are two important observations related to the results. First, as compared to the benchmark model, it can be seen that the error  $\bar{e}$  increases rapidly in the first few time steps, but has a concave shape which eventually gets stabilized overtime. That is, while the rate of error is increasing initially, the error is shown to converge to a certain value as time progresses. The second observation is related to the value of such error. Since we consider a unit of population in our

experiment, even an error of  $1e-3$  may lead to a difference of 10,000 infected people to an urban area with over 10 million population, which may render the plausibility of the over-approximation. From these experiments, it can be seen that for lower TM order and larger cutoff size, such error may be as high as 0.1 as compared to the base model, which is equivalent to around 7000 difference of infected population at the disease peak for 10 million population. By improving the order of TM and cutoff threshold, this error may be significantly reduced and may be as small as  $e^{-8}$  in our case as compared to the base model, so that the difference is around 20 people at the disease peak. These imply that the residual errors due to wrapping effects are very well addressed with the TM approach and the resulting over-approximating flowpipe has high fidelity when it is applied to estimate the upper and lower bound of infected population size.

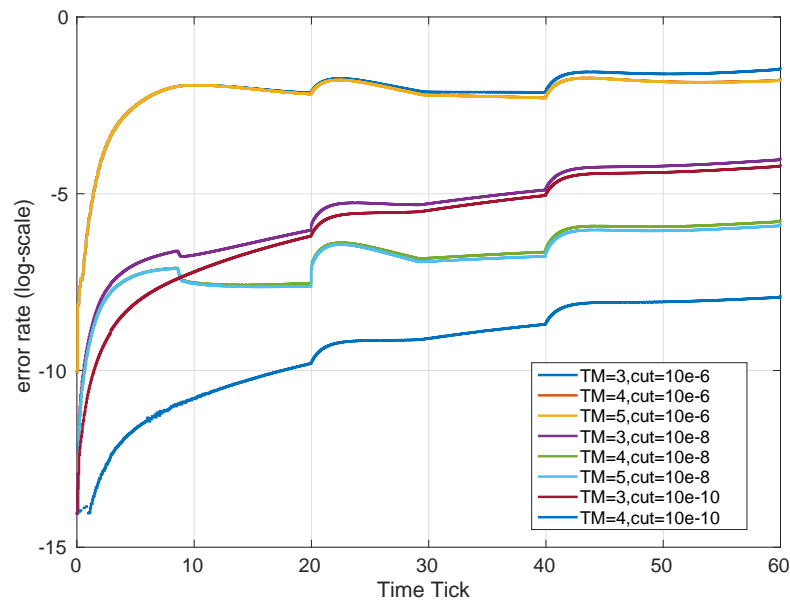
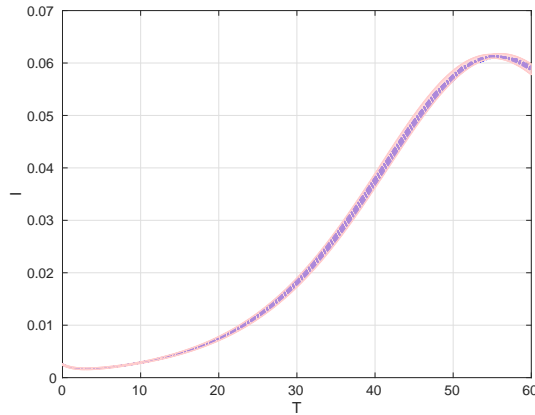


Figure 3.20.: Evaluation of successive errors (in log scale) due to wrapping effect at each time step

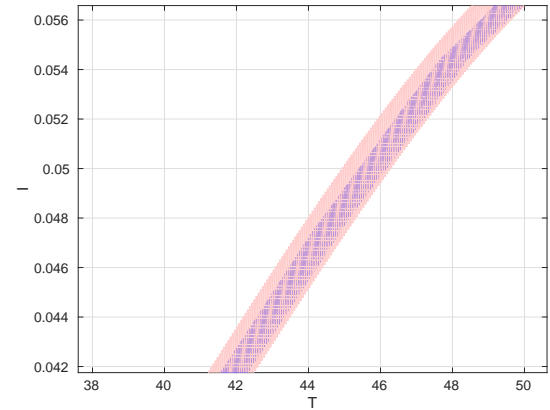
Finally, we compare the resulted over-approximation flowpipes with that generated from the ODE solvers in MATLAB. In particular, we choose the ode15s con-

sidering the stiff nature of the disease models, where a small change in parameter settings and initial conditions may result in very different system dynamics [96]. A typical misconception regarding the numerical evaluation of the SEIR system is that the constructed trajectory via numerical solver may accurately represent the disease dynamics. However, in reality, we will never have the exact information on the initial condition of the disease pattern. Instead, the decision maker may only have a rough estimate of the total infected population at current time step, e.g., 100-200 people, and this initial interval will be projected into a wide range regarding the number of infected people at the disease peak. Under such circumstances, it may require infinite number of trajectories to be constructed by originating from the initial set. And the numerical solver also suffers from the remainder errors at each time step which will be accumulated towards the target value of estimation. As stated before, a small prediction error may result in a huge gap between the actual number of infected people versus the predicted value, not mentioning that there is no guarantee on the correctness of the solution from the numerical solver. On the contrary, the TM overapproximation ensures that the eventual state of disease is within the constructed flowpipe, thus the decision maker may clearly tell if the scale of the disease will be under control at certain time steps. We show the comparison of trajectories constructed by the ode15s with the TM flowpipe in Figure 3.21. The initial set for the reachability analysis is a box, where we consider the total initial infected population is within the range  $[0.002375, 0.002625]$  and the initial set is box so that the total population still sums to one. And we simulated 100 and 500 trajectories using ode15s by starting from randomly selected points from the initial set. The computation time for each trajectory is 20.6 seconds for the 60 time steps, so that the flowpipe construction takes the time of approximately simulating 1450 trajectories. However, even simulating such many trajectories may only result in a biased understanding of the disease pattern, as we can see from the gap between the trajectories and the shaded area, and that some trajectories are lied outside of the boundary of the constructed flowpipe. Therefore, we may falsely interpret the disease peak as well the time of

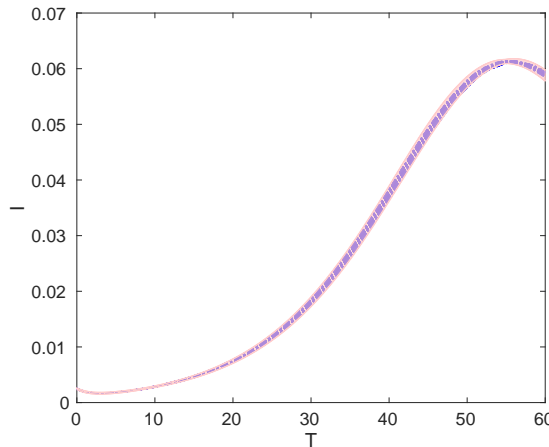
the peak by simply using the numerical ode solvers. And this comparison clearly illustrates the necessary of flowpipe overapproximation for real-world applications of disease modeling in populated urban areas.



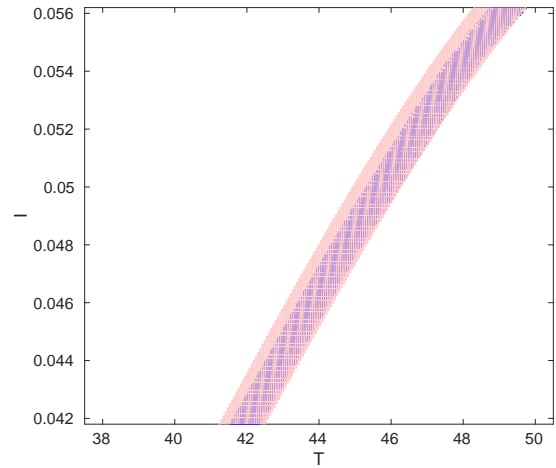
(a) 100 Trajectories from ODE15s and the shaded area of TM flowpipe



(b) 100 Trajectories from ODE15s and the shaded area of TM flowpipe (zoom)



(c) 500 Trajectories from ODE15s and the shaded area of TM flowpipe



(d) 500 Trajectories from ODE15s and the shaded area of TM flowpipe (zoom)

Figure 3.21.: Accuracy with different cutoff thresholds and Taylor model orders

### 3.6 Conclusion

In this chapter, a comprehensive mathematical model is presented for understanding the spread of infectious disease in urban areas considering the inter-dependencies among different transportation modes and the selfish behavior of urban travelers. The model starts with the dynamic system to capture the population movement among different patches, and derives the equilibrium flow pattern from the system. Based on the stable commuting pattern, the spread of disease is formulated as a bilinear S-E-I-R system, and different levels of controls on the urban transportation system are modeled as a hybrid system. The main objective of the model is to understand whether controlling an urban transportation system helps to eliminate or reduce the speed of disease spreading by properly designing the hybrid system.

The 2003 Beijing SARS data and census data were used to calibrate the commuting and disease patterns, which contributes to the case study for validating the effectiveness of the modeling approach. The model is shown to be able to predict the terminal disease size as well as the ongoing daily dynamics of the disease accurately. Further numerical experiments of the model suggest that failing to capture the travel contagion while modeling the spread of infectious diseases tends to underestimate the size of the disease outbreaks, and may false interpret the terminal states of certain infectious diseases. Moreover, it is shown that by placing moderate control to regulate the entrance of the urban transportation system, it is possible to turn into a possibly endemic disease into the DFE state, and may contribute to significantly lower the size of the disease outbreak when the disease is endemic. In addition, the urban form is also found to have significant impact on the outcomes of infectious diseases, where more decentralized urban structure with multiple commercial centers tend to be more resilient to the invasion of infectious diseases. Finally, the constructed flow-pipes of the disease system is found to be able to accurately over-approximate the set of possible trajectories in an efficient manner. These results provide valuable insights in understanding the role of urban transportation system in facilitating the pace of disease transmission and its contribution to increase the size of the disease outbreaks.

However, this chapter also shows the possibility for mitigating the risk of infectious diseases if control strategies are properly designed. And the model developed in this chapter will help to devise such strategies efficiently.

## PART II: DISEASE SPREADING IN CONTACT NETWORK

## 4. METRO CONTACT MODELING

### 4.1 Introduction

There are three key factors that lie at the heart of the design philosophy for urban transportation system: affordable, accessible, and efficient. In order to improve the mobility of mass urban population and provide affordable and accessible tools for urban commuters, it is inevitable that a large number of people should be transported at the same time. However, without carefully inspecting the structure of urban transportation systems, such design philosophy is likely to turn the benefits of urban transportation system into critical risk exposures that favor the spread of infectious diseases from almost every aspect.

First, purely pursuing efficiency and seeking to transport as many people as possible at the same time can be translated into high population density within transportation systems. This significantly increases the chance of close contact between individuals and offer an ideal environment that facilitates the disease spreading process. Second, accessibility and affordability also come with the issue of travelers being exposed to highly heterogeneous population during travel. Meanwhile, they have to spend more time in transportation system as transit routes are likely to deviate from their shortest paths. These suggest that the chance that an individual may get infected will be much higher considering the diversity of potential contacts and exposure duration during travel. Finally, the mass transit system mainly consists of buses and metro trains where the ventilation may be poor and the potential airborne diseases may float around in the closed compartments. The combination of these factors naturally leads to the concern where an individual is susceptible to high risk exposure while traveling in the transit system.

Unfortunately, the compartment model discussed in the first part of the dissertation is not able to capture these risk factors. That is, heterogeneous individual travelers will have very different travel time and origin and destination pairs, which eventually affect their contact patterns during travel. This clearly violates the homogeneous population assumption within the same compartment for the compartment model. And we have seen that increasing the number of compartments will be extremely computational expensive. This motivates to introduce new modeling approach to account for the heterogeneity of travel patterns at individual level.

The other difficulty for modeling individual contact pattern arises from the availability of data to reconstruct the travel activities within urban areas. It will be intrinsically difficult to recover the complete trip chain for each individual at the urban level, however, the availability of smart card transaction data provides us the opportunity to at least rebuild individual's trajectory within each travel mode. In this chapter, smart card transaction data from three major cities in China are introduced. The data capture passengers' entry and exit information within the metro system, and cover over 10 million daily passengers in all three cities. Web crawlers are further developed to extract the metro network structures and timetables, which in combination with the smart card transaction data reconstruct the contact networks within metro system at individual level. Based on the reconstructed contact networks, two mean-field approaches are proposed to evaluate real-time risk levels of metro systems, and reveal the underlying generation mechanism to explain how two individuals may get in contact with each other and infer their contagion time.

The chapter is organized as follows. The second section introduces the smart card transaction data and summary statistics of the metro networks of the three major cities in China. The third section presents the algorithm for constructing metro contact network (MCN) and the results and analyses of constructed MCNs. Section four and five discuss the mathematical models and analyses for individual based mean-field approach and OD based mean field approach. Section six presents the generation model for the contact patterns of MCN. Finally, section seven delivers

the results and insights of the models and section eight concludes the chapter with the summary of contributions and findings.

## 4.2 Data

We introduce the metro card transaction data to build the contagion matrix from travelers' daily commuting patterns. The metro card transaction data cover three major cities in China: Shanghai, Guangzhou, and Shenzhen. These data have similar structure, with each piece of record in the data containing the information of smart card ID, transaction ID, transaction time, station ID, and transaction type. The transaction type indicates if the transaction is entry or exit at the transaction station. Since each smart card is associated with a unique ID, we can therefore construct the trip sequences for each individual (each card) based on the transaction time and transaction type. A sample of smart card transaction data can be seen as follows:

- ....
- 326244087,22,22:40:07,1
- 660355429,22,23:13:11,1
- 684235395,21,22:35:47,0
- 880025090,22,22:21:20,1
- 667942666,22,22:40:17,1
- 880025090,21,21:58:40,0
- ...

For the data, the first column corresponds to smart card ID, the second column represents the station ID, the third column is the time when the transaction took place, and the last column refers to the transaction type, where 1 indicates exit and 0 is entry.

For each city, we extract the data of five work days for further analysis. The detailed statistics of the data is shown in Table 4.2.

Table 4.1.: Summary of metro card transaction data from three major cities in China

City	Start date	End date	# metro lines	# stations	Average daily records
Guangzhou	2017.04.13	2017.04.17	8	166	1.6 million
Shanghai	2015.04.13	2015.04.17	13	288	4.16 million
Shenzhen	2016.04.14	2016.04.18	5	118	2.13 million

The metro networks in these cities have quite different structures, which are primarily tailored to the urban landscape of each particular city. Shanghai metro network is the one with the longest mileage and most stations. It also has the highest number of daily passenger volume. Guangzhou and Shenzhen are similar in terms of the scale of their metro networks, however, the shape of the metro network differs from each other. In particular, Shenzhen is a stripe-shaped city where commercial areas are located in the middle and residential places are distributed at east and west sides of the city. The shapes of metro networks, half-hourly passenger demand, and distributions of passenger trip time of the three cities are presented in Figure 4.1.

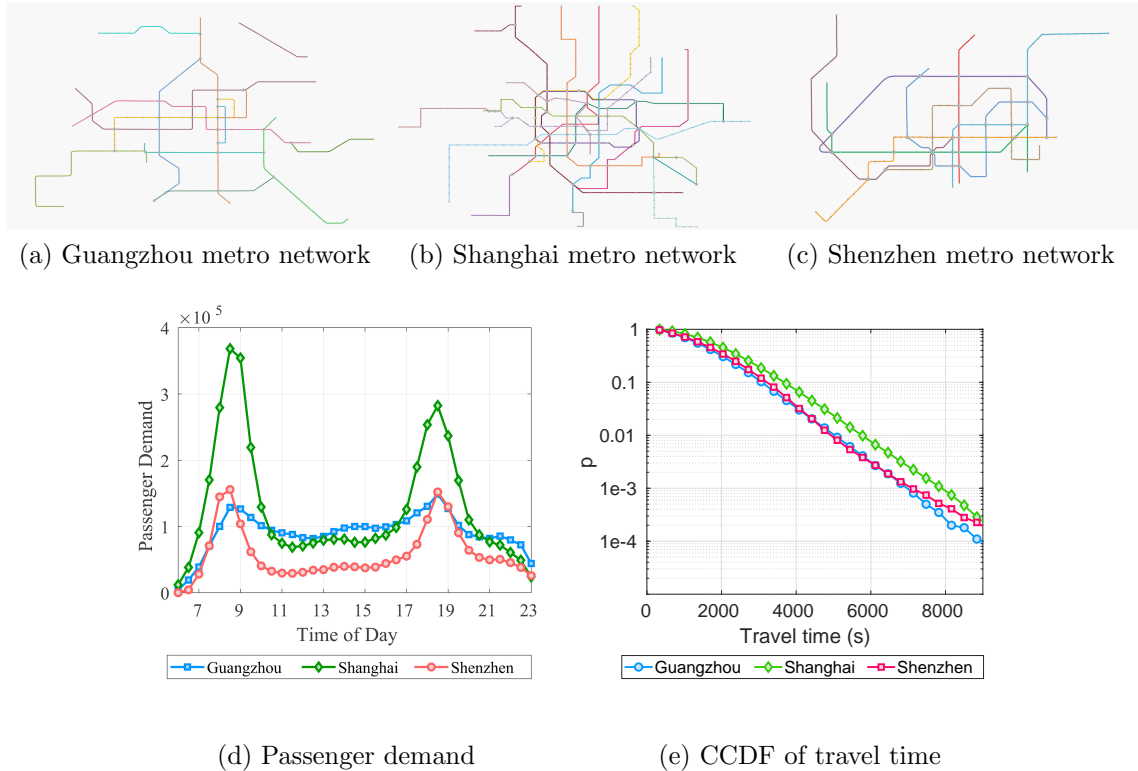


Figure 4.1.: Metro network structures, passenger demand distributions, and passenger travel time distributions of the three cities

### 4.3 Metro contact network

Smart card transaction data only provide information on entry and exit of passengers in the metro system. Based on the smart card transaction data for metro networks, we next develop the algorithm for constructing metro contact network (MCN). The contact network is constructed at individual level, where **we define contact as two individuals having positive probability that they will come in contact within effective transmission range**. By effective transmission range, we refer to that two individuals are close enough so that the airborne transmission of an infectious disease is feasible.

To construct the metro contact network, the following information is required:

1. Weighted adjacency matrix of the metro network.
2. Schedule of metro trains.

The weighted adjacency matrix captures the travel time between two adjacent stations. For two stations where a transfer is required, the time of transfer is also added to reflect the actual travel time between the two stations. As for the schedule of metro trains, it provides valuable information on the likelihood that two individuals will get in contact if their time of arrival at a particular station is  $k$  minutes apart, which we denote as  $p_{i,j}(k)$ . This can be understood as the probability that two passengers will get on the same train given their arrival time at the station.

To obtain these two data sources, we develop a set of web crawlers and extract the metro network adjacency matrix from GaoDe Map API [97]. In addition, the time tables of the three metro systems are extracted from their official websites [98], which contain the travel time between two stations as well as the frequency of the metro trains during different time periods. Finally, the transfer time required between a pair of adjacency stations is calculated by first quoting the travel time between the two stations using Google API and then subtracting the travel time between the two stations based on the values obtained from the timetable.

We define the transmission rate between two passengers  $i$  and  $j$  as  $\beta_{i,j}$ , and

$$\beta_{i,j} = \beta \frac{\bar{L}_{i,j} p_{i,j}(|t_i, t_j|)}{C} \quad (4.3.1)$$

where  $\beta$  is the transmission strength of a particular disease per unit time if two individuals are within effective transmission range,  $\bar{L}_{i,j}$  represents the expected travel time of the overlapping trip segment between the two passengers, and  $p_{i,j}(|t_i, t_j|)$  represents the probability that two individuals will be on the same train, and  $C$  is a scaling constant which accounts for the capacity of the metro train. For simplicity, we consider  $C$  to be the same for all metro lines, but it can be easily extended to account for the varying train capacity of different lines. As a result, we denote  $\beta_{i,j}$  as the expected contagion risk between two individuals  $i$  and  $j$ .

To evaluate  $p_{i,j}(t_i, t_j)$ , we conducted simulation experiments to understand how the probability may change as a function of the gap of arrival, and the result is shown in Figure 4.2. This suggests that the chance of being on the same train decreases linearly with increasing arrival gap, and the chance is bounded by the frequency of the metro train, where any gap beyond the arrival interval of the metro train will result in zero chance of contact.

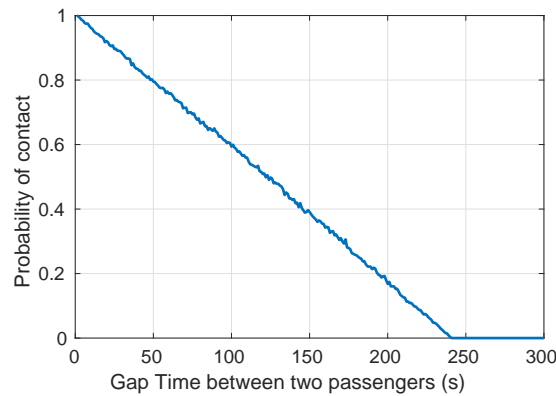


Figure 4.2.: Probability that two passengers will be on the same train as a function of their gap of arrival time at the station

Given this information, we now introduce the algorithm for generating metro contact network from the smart card transaction data. The algorithm takes the demand distribution at each station, the trip split ratio among the stations, the weighted adjacency matrix, and the number of passengers  $N$  as inputs. The output of the algorithm is a  $N$  by  $N$  weighted adjacency matrix  $G$  for the individual contact network, where each entry  $G_{i,j}$  equals  $\beta_{i,j}$ , the expected risk exposure between two individuals  $i$  and  $j$ . We consider that the contagion process between any two individuals is symmetric. As a consequence, the resulting matrix  $G$  is symmetric with all positive values.

The process for generating MCN is described as follows:

1. Generate the origin, destination, and departure time for  $N$  passengers.
2. Find the shortest travel path for each individual.

3. For each pair of passenger  $i$  and  $j$ , determine if they have overlapping travel segments  $L$ .
4. If  $L > 0$ , determine their first meeting location, station  $m$ , the duration of  $L$ , and calculate their arrival time at the meeting station  $t_{i,m}, t_{j,m}$  respectively.
5. Compute the expected exposure risk  $\beta_{i,j}$ , set  $G_{i,j} \leftarrow \beta_{i,j}$ .
6. Repeat this process until all pairs of passengers are processed. Output  $G$ .

There are two computationally expensive steps in this algorithm. First, calculating the shortest path between a pair of individuals. Since there is no congestion effect when traveling in metro system (unlike road networks), the shortest path between any pair of metro stations will not vary over time. We use Dijkstra algorithm to calculate all pair shortest paths between all metro stations beforehand, and store the shortest path matrix in memory to speed up this process. Second, determining the length of overlapping travel segment  $L$  of two passengers and the corresponding first meeting station  $m$  can be viewed as identifying the longest common subsequence (LCS) of two strings, where the string corresponds to individual's trip trajectory (in term of stations) within the metro system. Finding LCS has the worst complexity of  $O(l_1 * l_2)$ , where  $l_1$  and  $l_2$  are the lengths of two paths respectively. And in worst case, LCS will be executed  $O(N^2)$  times. This becomes the bottleneck of the contact network generation algorithm if we deal with millions of passengers, since the algorithm scales quadratically with increasing number of passengers as well as the size of the metro network.

Based on the MCN generation algorithm, we simulate the structure of MCNs using the data from three cities. The results are shown in Figure 4.3.

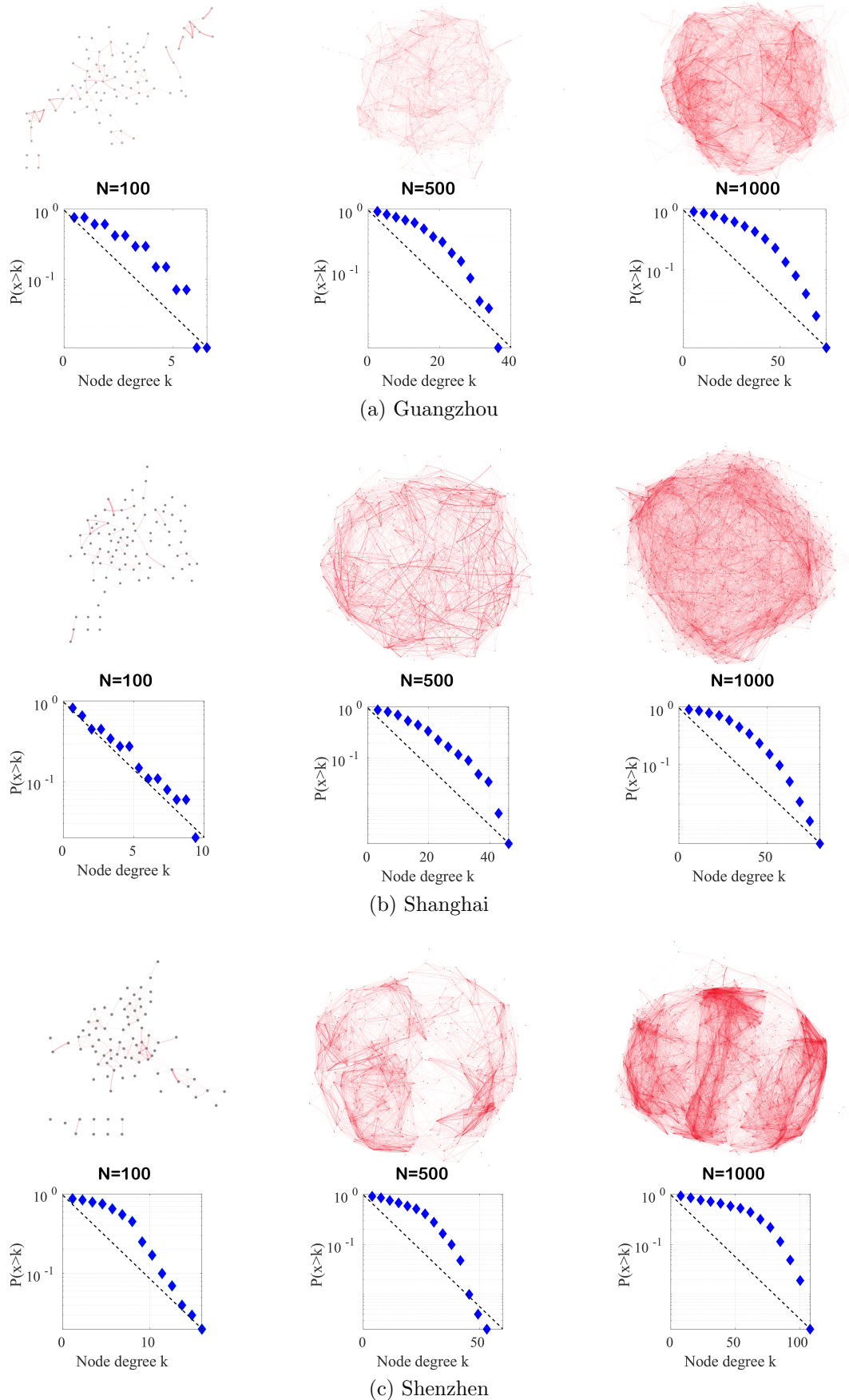


Figure 4.3.: Visualization of sample MCNs from the three cities, with 100, 500, and 1000 passengers from left to right, followed by their degree distributions

Table 4.2.: Summary statistics of the generated contact networks

	Hetero- geneity	Clustering coefficient	Centralization	Diameter	Radius	Characteristic path length
Guangzhou	0.53	0.49	0.052	7	4	2.797
Shanghai	0.48	0.40	0.052	5	3	2.62
Shenzhen	0.53	0.56	0.057	7	4	2.829

The MCNs of the three cities have different network structures at first glance. We see that with the same number of nodes in MCNs, the density of edges and the weight on the edge are different among the three cities. In particular, edges with higher weight are plotted with higher width and transparency. Shenzhen metro has the highest edge density as compared to the other two cities, and the passengers are observed to be more connected locally. Moreover, based on the edge distribution, Shenzhen metro network also has a greater number of nodes with higher degree, and the highest degree is also higher than other cities. This clearly suggests that the shape of metro network structure as well as the urban shape may have significant impacts on the contact patterns of passengers within metro network.

However, despite the differences, the three cities have many similarities which indicate the existence of a possibly universal generation pattern that governs the mechanism on how people get into contact while travel. First, as shown in Figure 4.1(e), the travel time distributions have exponentially decayed tails across the three cities, suggesting that the energy of human mobility is bounded by the size of the metro network. Second, we observe that, though being different in scale, the degree distributions are very similar in terms of the overall shape. Majority of the nodes are observed to have relatively low degrees, and there are a few nodes with higher degree. And the probability of high degree nodes drops rapidly with increasing degree values. Finally, the similarities are also evaluated statistically with the results shown in Table 4.2. MCNs of all three cities tend to have high clustering coefficients, heterogeneity statistics, but also have low centralization, diameter, radius, and characteristic path length (CPL) statistics. From these statistics, we can easily tell that

all MCNs appear small-world alike network structure. This means that, in real world, it may require little efforts for an infectious individual to reach the passenger that are farthest from him in the metro system, and each passenger are connected to a large number of other travelers during the trip. This implies that an initial infectious person may quickly spread the disease across the network considering the small-world property, and MCNs are therefore highly vulnerable to the risk of infectious diseases. These observations propose the needs of in-depth investigations between the structure of the MCNs and the functionality of disease dynamics. And such relationship is established in the next section.

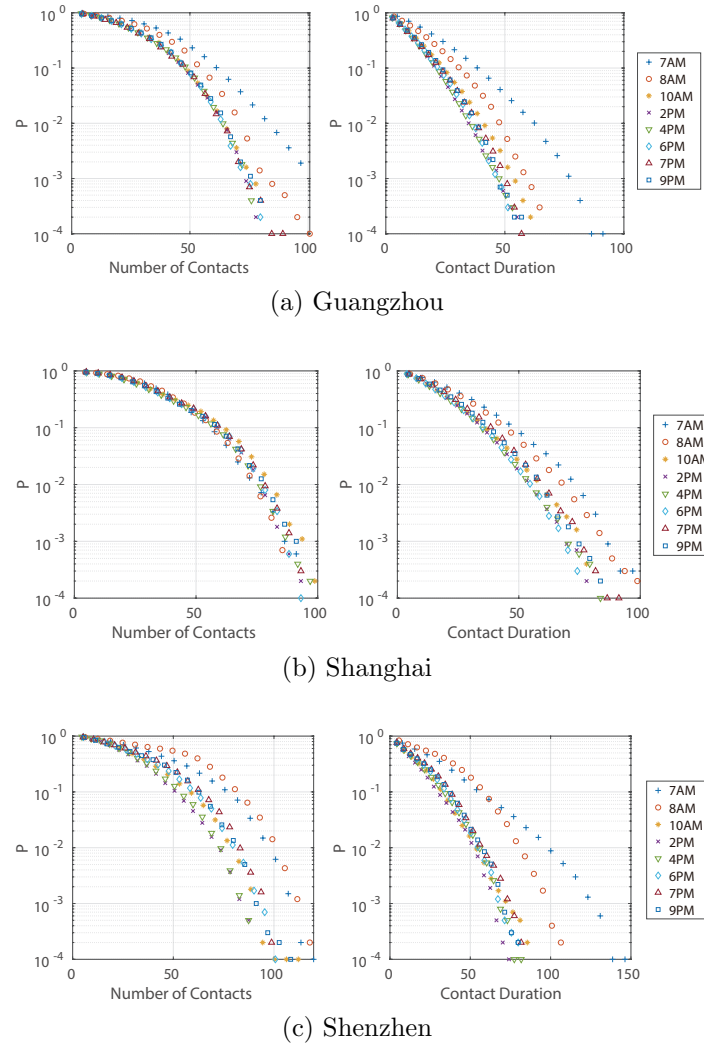


Figure 4.4.: CCDF of unweighted and weighted degree distributions for MCNs of the three cities.

The MCNs are generated by setting train frequency=5 minutes and  $N=1,000$  passengers. 7 different time periods are plotted: 7AM, 8AM, 10AM, 2PM, 4PM, 6PM, and 9PM. For each time period, the results are generated by combination the results of 20 MCN samples.

#### 4.4 Individual based transmission model

The study focuses on investigating the vulnerability of metro network to the invade of infectious disease. Based on the constructed MCNs, we next explore the risk level

of the metro system by developing the individual based disease transmission model. The individual based transmission model is derived from the individual-based mean field approach (IBMF) [61]. In the model, each individual is considered as a node, and the transmission will only take place between individuals who are connected ( $G_{i,j} > 0$ ). We introduce the classical susceptible-infectious-susceptible (SIS) model to represent disease dynamics within the contact network in the metro system.

The IBMF model takes the following items as model input:

1. The weighted adjacency matrix of the MCN  $G$ .
2. The disease characteristics. In this study, the characteristics include the transmission rate  $\beta$  and recovery rate  $\gamma$ .

One particular assumption of the IBMF model is that the transmission process from each neighbors of  $i$  to  $i$  is independent from the other.

#### 4.4.1 Disease transmission rate

In almost all literature, the transmission rate of a certain disease between two individuals is simply captured by a constant parameter  $\beta$ . However, for communicable diseases that spread upon contact, it is well understood that the exposure duration and contact distance between two individuals are two contributing factors to a successful transmission. And these factors become non-negligible if the transmission is modeled at individual level, and are accounted for in our study with the weighted entries of the MCN matrix  $G$ . It measures the expected contact duration of two individuals based on their travel profile, and scales the probability of contact by considering the chance if two individuals are within effective transmission distance when they travel. As a consequence, we are able to measure the heterogeneous transmis-

sion rate between each pair of individual  $i$  and  $j$  as  $G_{i,j}$ . And the recovery rate is considered to have the same meaning as in other disease modeling literature.

#### 4.4.2 Individual based transmission model

Now we introduce the IBMF for the contagion process giving the contact network  $G(V, E, W)$ . We first introduce notation used:

Table 4.3.: Table of notation

Variables	Descriptions
$p_{i,t}$	The probability that node $i$ is infected at time $t$ .
$\rho_{i,j}$	The chance that node $i$ will get in contact with node $j$ .
$d_{i,j}$	The duration that node $i$ and node $j$ will get in contact.
$q_{i,t}$	The probability that the neighbors of node $i$ do not transmit disease to node $i$ .
$\mathcal{N}(i)$	The set of neighbor nodes of node $i$ .
$r$	Recovery rate of the given disease, $r < 1$ .
$\beta_{i,j}$	The transmission rate between $i$ and $j$ per unit time.

When an individual  $i$  travels, the probability that  $i$  stays healthy at time  $t$  can be written as:

$$1 - p_{i,t} = (1 - p_{i,t-1})q_{i,t} + p_{i,t-1}r \quad (4.4.1)$$

where the first term on right hand side of the equation implies the node was healthy at time  $t - 1$  and is not infected at time  $t$ , and the second term suggests that the node was infected but gets recovered at time  $t$ .

The probability that all neighbors of  $i$  failed to transmit the disease can be written as:

$$q_{i,t} = \prod_{j \in \mathcal{N}(i)} (1 - p_{j,t} + (1 - \beta_{i,j})p_{j,t}) \quad (4.4.2)$$

The right hand side also contains two parts: either the neighbor  $j$  is not infected at current time  $t$  ( $1 - p_{j,t}$ ), or if  $j$  was infected but fails to transmit the diseases.

By rearranging equation 4.4.1, we can express the probability that node  $i$  is infected at time  $t$  as

$$p_{i,t} = 1 - p_{i,t-1}(q_{i,t} - r) - q_{i,t}, \forall i \in V \quad (4.4.3)$$

And the entire system dynamics over the MCN can be expressed in the matrix form as

$$\mathbf{P}_t = \mathcal{G}(\mathbf{P}_{t-1}) \quad (4.4.4)$$

So that the disease spreading on MCN is characterized as a non-linear dynamic system.

The disease transmission system on MCN has two equilibrium states. One is the disease free equilibrium (DFE), where each individual is in susceptible (healthy) state and the disease is completely eliminated. On the contrary is the endemic equilibrium, where there will always be a positive portion of individuals that are in infectious state. Formally, the DFE can be defined as

**Definition 4.4.1 (Disease free equilibrium (DFE))** *The system reaches the disease free equilibrium if  $p_{i,t} = 0$  for all nodes.*

The vulnerability of a metro system can therefore be analyzed by establishing the stability condition for the IBMF of the MCN to be DFE. The basic idea of the stability analysis is to start from the equilibrium point and introduce small perturbation. If this perturbation diminishes and the system goes back to the equilibrium point, the DFE point is said to be asymptotically stable, otherwise the MCN will reach the endemic state. Before we establish the condition for DFE to be stable, we first introduce the Gershgorin circle theorem [99] as follows

**Theorem 4.4.1 (Gershgorin circle theorem)** *Every eigenvalue of a complete matrix  $A$  lies within at least one of the Gershgorin discs  $D(a_{i,i}, R_i)$ :*

$$|\lambda - a_{i,i}| = \left| \sum_{j \neq i} a_{i,j} x_j \right| \leq \sum_{j \neq i} |a_{i,j}| |x_j| \leq \sum_{j \neq i} |a_{i,j}| = R_i. \quad (4.4.5)$$

where  $\lambda$  is the eigenvalue of  $A$ .

Based on Gershgorin circle theorem, we develop the following proposition for the stability of the DFE:

**Proposition 1** *The DFE is asymptotically stable if  $\max_i(\sum_j(\beta_{i,j})) \leq r$ .*

**Proof** We proof the proposition by linearizing the non-linear dynamic system at the DFE and measuring the partial derivatives  $K$ :

$$K = \frac{\partial \mathbf{P}_t(0)}{\partial \mathbf{p}_{t-1}} \quad (4.4.6)$$

where we have

$$K_{i,j} = -r + 1, \quad \text{if } i = j \quad (4.4.7)$$

$$K_{i,j} = \beta_{i,j}, \quad \text{if } i \neq j \text{ and } i, j \text{ are adjacent} \quad (4.4.8)$$

$$K_{i,j} = 0, \quad \text{o.w.} \quad (4.4.9)$$

Therefore we have

$$K = (1 - r)I + B \quad (4.4.10)$$

And  $K$  is also known as the next-generation matrix (NGM), where the dominant eigenvalue represents the reproduction number  $R_0$  of the disease system. For the DFE to be stable, we should have

$$\rho(K) = R_0 \leq 1 \quad (4.4.11)$$

So that the spectrum radius (largest eigenvalue) of  $K$  is smaller than 1, or each new infected individual may produce smaller than one unit of secondary infection so that the disease will eventually die out. Since all diagonal entries of  $K$  are identical, by applying Theorem 4.4.1, we have

$$\rho(K) \leq \max_i(R_i(K)) + K_{i,i} = \max_i(\sum_j(\beta_{i,j})) + 1 - r \quad (4.4.12)$$

This gives that  $\max_i(\sum_j(\beta_{i,j})) \leq r$  and completes the proof. ■

Note that the analysis establishes the upper-bound  $\bar{R}_0$  for  $R_0$  of the MCN network. We can guarantee that the system will reach DFE as long as  $\bar{R}_0 \leq 1$ , and the system is more vulnerable with increasing  $\bar{R}_0$  value.

Proposition 1 has several important implications. The risk level of the MCN is shown to be dictated by the individual who has the highest risk exposure. As long as the exposure rate of this particular individual is smaller than the recovery speed, the system will reach DFE. Otherwise the system may be either DFE or endemic. However, in practice, if we would like to control the spread of infectious diseases, it is unlikely that we may identify who exact the person is. Even if this person is identified, vaccine/quarantine of the individual does not necessarily reduce the risk level of the overall system, since the second riskiest person may have similar level of risk exposure. This implies that we would also need to examine the structure of the contact network to devise feasible control strategies. In addition, the model provides the solution to monitor the vulnerability of metro systems at very fine scale and identify the periods of time that are of particularly high risk level. But one significant drawback of the IBMF model comes from its computational bottleneck. It will be difficult to generate large-scale MCN that copes with the passenger demand level in many real-world scenarios, where the MCN serves as the key input for the analysis of the IBMF model. This motivates us to develop a more efficient solution based on IBMF model for monitoring the risk level of our metro systems using passenger travel data.

#### 4.5 OD-level model

The individual model has one appealing insight: the vulnerability of the metro contact network is determined by the individual of the highest risk exposure. And by identifying the individual, we can assess if a certain disease may invade or eventually be eliminated. However, the individual approach also has two major drawbacks. The

first drawback is the scalability of the approach. As for real-world metro contact network, millions of passengers will be included and therefore simulated. It is extremely expensive to construct a contact network of this scale and therefore difficult to assess the impact for real-world scenarios. Second, even if we have the computational power to construct the contact network of such details, it is difficult to provide measures for improving the vulnerability of the metro network from the results at individual level. These drawbacks motivate us to develop a scalable approach that is associated with the physical structure of the metro network but also retains the high fidelity of the individual level model. This gives rise to the origin-destination (OD) level contagion model as described in the following.

The OD-level approach is developed at network level. Instead of considering each individual as the node, the contact network at OD-level treats OD pairs as the set of nodes and the contagion pattern between OD pairs as the set of edges. It can be readily seen that the total number of OD pairs in a given metro network is simply the square of number of stations, which is much more scalable as compared to constructing contact networks for millions of passengers. Denote  $S_i$  and  $I_i$  as the susceptible population and infected population of OD pair  $i$ , and let  $\mathcal{P}$  be the set of OD pairs in the network, we have the following equations

$$E_{i,j} = \beta \bar{d}_{j,i} S_i I_j \quad (4.5.1)$$

where  $E_{i,j}$  represents the proportion of susceptible population of  $i$  being infected by the infectious population of  $j$ .  $\bar{d}_{j,i}$  is the expected contact duration between OD pairs  $i$  and  $j$ . The disease dynamics at the OD level can therefore be written as:

$$\frac{dI_i}{dt} = -\gamma I_i + \sum_{j \in \mathcal{P}} E_{i,j}, \forall i \in \mathcal{P} \quad (4.5.2)$$

Moreover, since  $I_i + S_i = N_i$ , where  $N_i$  is the total number of passengers for OD pair  $i$ , equation 4.5.3 can be further rewritten as:

$$\frac{dI_i}{dt} = -\gamma I_i + \sum_{j \in \mathcal{P}} \beta \bar{d}_{j,i} N_i I_j - \sum_{j \in \mathcal{P}} \beta \bar{d}_{j,i} I_i I_j, \forall i \in \mathcal{P} \quad (4.5.3)$$

And the matrix form is therefore

$$\frac{dI}{dt} = AI + b(I) \quad (4.5.4)$$

where  $A$  is a  $V$  by  $V$  matrix with its entry:  $a_{ii} = \beta \bar{d}_{i,i} N_i I_i - \gamma$  and  $a_{ij} = \beta \bar{d}_{j,i} N_i I_j$ .  $b(I)$  is a column vector with its entry being  $b(I)_i = -\sum_{j \in \mathcal{P}} \beta \bar{d}_{j,i} I_i I_j$ . Equation 4.5.4 gives the disease dynamics at the OD level, and we have the following theorem for the OD level model.

**Theorem 4.5.1** *Let  $A$  be an irreducible square matrix, and assume that  $a_{ij} \geq 0$  for every  $i \neq j$ . Then there exists an eigenvector  $\omega$  of  $A$  such that  $\omega > 0$ , and the corresponding eigenvalue is  $s(A)$ .*

**Theorem 4.5.2 (Theorem 3.1 in [100])** *The DFE is asymptotically stable if  $s(A) \leq 0$ .*

#### 4.5.1 Equivalence between individual model and the OD level model

We now show that, by applying Gershgorin circle theorem, the estimated disease threshold of the OD level model is equivalent to that of the expected disease threshold of the individual level model. Note that for individual level model, we have the disease threshold being estimated as:

$$\max_m \left( \sum_n (\beta_{m,n}) \right) \leq r \quad (4.5.5)$$

and

$$\mathbb{E} \max_m \left( \sum_n (\beta_{m,n}) \right) = \max_m \mathbb{E} \left( \sum_n (\beta_{m,n}) \right) \quad (4.5.6)$$

With each infection being independent from the other, we further have

$$\max_m \mathbb{E} \left( \sum_n (\beta_{m,n}) \right) = \max_m \left( \sum_n (\mathbb{E}(\beta_{m,n})) \right) \quad (4.5.7)$$

and

$$\mathbb{E} \beta_{m,n} = \beta \mathbb{E} \rho_{m,n} d_{m,n} = \beta \bar{d}_{m_p, n_p} \quad (4.5.8)$$

where  $m_p$  denotes the OD pair of passenger  $m$  and  $n_p$  denotes the OD pair of passenger  $n$ . Therefore, the expected contact time for any pair of individual in the metro contact network is equivalent to the expected contact time between their trip OD pairs.

For  $|N| \rightarrow \infty$ , for each passenger  $m$ , we have

$$\sum_n \mathbb{E} \beta_{m,n} = \sum_n \beta \bar{d}_{m_p, n_p} = \sum_j \beta \bar{d}_{m_p, j} N_j \quad (4.5.9)$$

and that  $\max_m (\sum_n (\beta_{m,n}))$  is equivalent to  $\max_i (\sum_j \beta \bar{d}_{i,j} N_j)$ .

Now applying Theorem 4.4.1 to  $A$ , we have

$$|s(A) - a_{ii}| \leq \sum_{j \neq i} |a_{ij}| = \max_i \sum_{j \neq i} \beta \bar{d}_{i,j} N_j \quad (4.5.10)$$

$$s(A) \leq \max_i a_{ii} + \sum_{j \neq i} \beta \bar{d}_{i,j} N_j = -\gamma + \max_i \sum_j \beta \bar{d}_{i,j} N_j \quad (4.5.11)$$

Combined with Theorem 4.5.2, we have the following result:

**Corollary 1** *The DFE of the OD-level model is asymptotically stable if  $\max_i \sum_j \beta \bar{d}_{i,j} N_j \leq \gamma$ .*

Moreover, based on equation 4.5.9 and Corollary 1, we now establish the following proposition for the equivalence between OD level model and the individual level model

**Proposition 2** *When  $|N| \rightarrow \infty$ , the upper-bound of the disease threshold of the OD level model is equivalent to that of the individual model.*

The proof of the proposition comes naturally from the above discussions in this section.

#### 4.6 Generation model

By observing that multiple metro networks in different cities share very similar degree distributions, and that the structure of the metro network will large affect the vulnerability of the system to infectious diseases, we need to establish the connection on how metro network structure will affect the resulting vulnerability. We develop the following criteria for the growth of the MCN, which contributes to abstracting the impact of physical metro network structure and constructing the MCN purely based on travel profile of each passenger. For the input of the generation model, the number of passengers and their corresponding travel distances are required. The number of passengers provides the number of nodes in this network, and the set of travel distances can be regarded as the weight of each node, which will be later used to infer the number of edges as well as the edge weights.

The growth of MCN consists of determining if two individuals will get into contact and then the duration of their contact. We consider that the number of contacts each individual may have is proportional to his/her time of travel, trip duration, metro operation schedules, and the physical metro network structure. If one spends more time in the metro system, he/she is more likely to have a greater number of contacts and therefore higher node degree. In addition, depending on the time of travel, the potential set of destinations of all travelers will be either more smaller (such as during morning peak hours) or larger (during off-peak time), which consequently affects the chance of contact. Moreover, the operation schedule and physical metro network structure should have significant impacts on the likelihood of contacts being formed. If metro trains are of high frequency, the chance of two individuals getting

into close contact should decrease. And this chance will be improved in smaller metro networks (less total mileage and fewer number of lines and stations), since the potential destinations of passengers are limited. Finally, if two people are within contagious distance, the duration of their contagion time should be affected by all these factors but operation schedule. And we consider that the contact duration is proportional to smaller trip duration of the two passengers.

#### 4.6.1 Generation rule

Based on these factors, we describe the generation model as follows:

**Model input: number of nodes  $N$ , node weight vector  $W_n$ , metro network structure coefficient  $\alpha$ , temporal adjust coefficient  $\gamma$ , and frequency parameter  $f$**

**Model output: a weighted contact duration network  $G$**

1. Scale the node weight vector to obtain adjusted travel time  $W_\alpha \leftarrow W^\alpha$ .
2. Scale  $W_\alpha$  to obtain the temporal adjusted weight vector  $W_{\alpha,\gamma} \leftarrow W_\alpha^\gamma$ .
3. Initialize an empty network  $G$  with  $N$  nodes.
4. Calculate the number of edges  $M$ , where  $M \propto fN \sum_i w_{\alpha,\gamma,i}$ .
5. Calculate the probability that a node will be selected  $p_i \leftarrow \frac{w_{\alpha,\gamma,i}}{\sum_j w_{\alpha,\gamma,j}}$ .
6. Select two nodes  $i$  and  $j$  based on their probability  $p_i$  and  $p_j$ . Connect  $i$  and  $j$  with an edge, and assign edge weight  $G_{i,j} \propto \min(w_{\alpha,\gamma,i}, w_{\alpha,\gamma,j})$ .
7. Repeat Step 3 until all  $M$  edges are added. Output network  $G$ .

The idea behind the generation model is that the node attaching process is governed by the weight of the node. If a node has higher weight, which corresponds to that a passenger will traverse through more stations in the metro network, it is

expected to have higher degree. This generation model is motivated by two observations. On one hand, the degree distribution of random network follows exponential distribution, and it implies that the node attaching behavior is unlikely to be the well-known preferential attachment behavior found in many real-world networks. On the other hand, we observe that the degree distribution of real-world metro contact network follows an exponential power-law distribution in the form of  $p(k) \propto e^{-k^\gamma}$ . The presence of the power-law term within the exponential function suggests that there may have certain preferential attachment alike behavior, which is most likely driven by some endogenous factors. And this term is the travel distance (number of stations as in metro network), as the distance itself follows a power-law distribution  $p(d) \propto d^{-\gamma}$ .

#### 4.6.2 Analytical expression

Based on the generation rule of the MCN, we can derive the analytical form of the generation model for the unweighted MCN. Note there will be one edge added to the network at each time step, so the probability of a node having degree  $k$  is the same as the number of times the node is selected out of the  $M$  edge additions. For node  $i$  of weight  $w_i$ , the probability that node  $i$  has degree  $k$  is given by:

$$p(k|w_i) = \binom{M}{k} p(w_i)^k (1 - p(w_i))^{M-k} \quad (4.6.1)$$

which follows the binomial distribution. For large  $M$  and small  $p(w_i)$ , the binomial distribution is known to be well approximated by Poisson distribution, with mean and variance  $\lambda_i = Mp(w_i)$ . Then equation 4.6.1 can be rewritten as:

$$p(k|w_i) = \frac{\lambda_i^k}{k!} e^{-\lambda_i} \quad (4.6.2)$$

and

$$p(k) = \sum_i p(k|w_i) p(w_i) = \frac{M^k}{k!} \sum_i p(w_i)^{k+1} e^{-Mp(w_i)} \quad (4.6.3)$$

Since  $M \propto fN \sum_i w_{\alpha,\gamma,i}$  and  $p(w_i) \propto w_i^\alpha$ , we should therefore have

$$p(k) \propto \frac{(fN \sum_j w_j^{\alpha\gamma})^k}{k!} \sum_i w_i^{\alpha k + \alpha} \exp(-fN \sum_j w_j^{\alpha\gamma} w_i^\alpha) \quad (4.6.4)$$

With Stirling's approximation, denote  $C = fN \sum_j w_j^{\alpha\gamma}$ , this can be further rewritten as:

$$p(k) \propto \left(\frac{eC}{k}\right)^k \sum_i w_i^{\alpha k + \alpha} \exp(-C w_i^\alpha) \quad (4.6.5)$$

Based on equation 4.4.4, we observe that the degree distribution is related to the metro frequency  $f$ , the number of passengers  $N$ , the travel time  $W$ , and the scaling parameters  $\alpha$  and  $\gamma$  which accounts for the metro network structure and temporal impacts. This analytic expression is consistent with our above analysis on possible factors that may affect the number of contacts an individual may have in the metro system.

### 4.6.3 Validation

To validate the correctness of our generation model, we introduce Kolmogorov–Smirnov (KS) test [101] to compare the degree distribution of the MCN from the generation model and the MCN by the contact network generation algorithm. The null hypothesis of the KS test is that the two data samples for comparison are drawn from the same continuous distribution. Specifically, we binned the degree distribution of each MCN into 30 groups, using the same set of bin edges, and conduct KS test on the probability distribution of the binned data. This makes it possible to apply KS test

on both weighted degree distributions and unweighted degree distributions (discrete integers).

#### 4.6.4 Parameter fitting

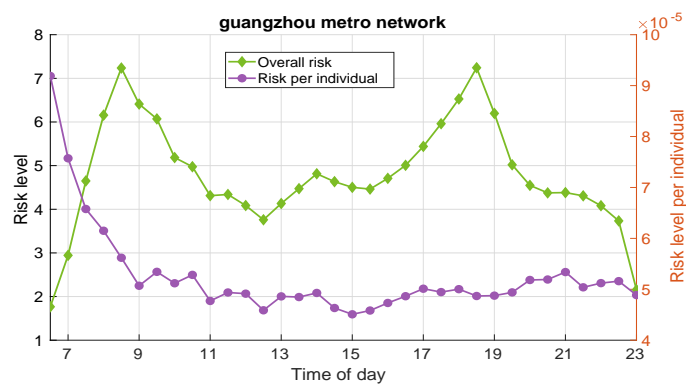
For each city, we consider  $\alpha$  being time invariant since it captures the impacts of metro network structure, and  $\gamma$  will change over time to reflect temporal variations of passenger trip patterns. We perform cross-validation to determine the optimal  $\alpha$  and  $\gamma$  for each city and for each time period, with the selection criteria being the parameter combination that gives the lowest sum of KS test threshold for weighted degree distribution and unweighted degree distribution of the MCNs. Note that since we fit both type of degree distributions, the optimal parameters can be uniquely determined since the number of parameters to fit matches with the degree of freedom (two different degree distributions with two model parameters).

### 4.7 Results

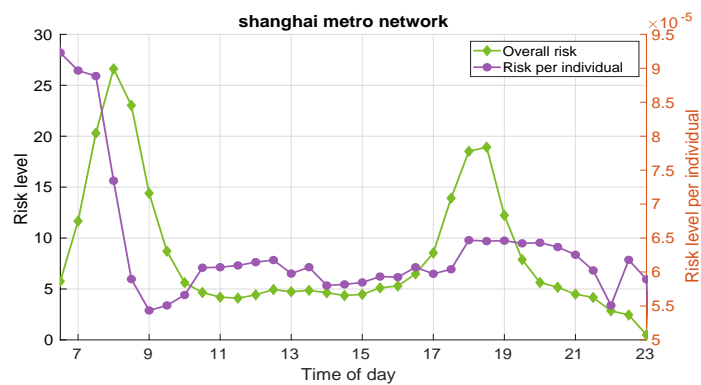
#### 4.7.1 Change of vulnerability over time

We set  $\beta = 0.001$  and investigate the change of vulnerability of metro network at different time of the day. All observations in the data are used to plot the variation of infectious disease risk in metro network for the three cities, and the results are shown in Figure 4.5. In the figure, the total risk level refers to the overall risk level of the metro network at the timestamp obtained from the ODMF model, and the individual risk level is calculated by dividing the total risk level with the total number of passengers travelling. In this regard, individual risk level can be considered as the relative chance of being infected for each individual traveler in the metro system. Based on the results in Figure 4.5, we notice that the total risk level is primarily driven by the total number of passengers traveling. Shanghai metro has the highest

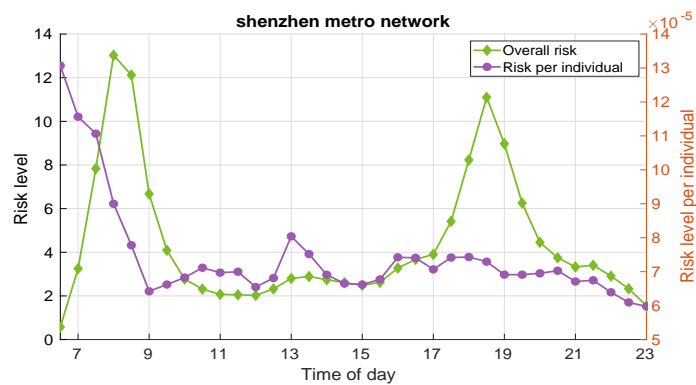
total risk, followed by Shenzhen metro and Guangzhou metro. While during peak hours, as shown in Figure 4.1(d), the peak demand of Shanghai metro is almost three times higher than that of Shenzhen network, the total risk level is only two times higher. The differences come from the risk level per individual, as a reflection of the trip purposes and metro network structure of the particular city. And the individual risk level for Shenzhen is 50% higher than Shanghai and 100% higher than Guangzhou. This explains the differences in total risk level during peak hours despite Shenzhen and Guangzhou have roughly the same passenger demand level. During off-peak hours, both individual risk level and total risk level are significantly lower than during peak hours, due to fewer passenger demand and more diverse trip purposes and directions, which reduce the chance that two passengers may meet in the metro system. In general, we report that the total risk level may be six times higher during peak hours than off peak periods (Shenzhen metro), and individuals may experience 30% 100% more risk while traveling during peak hours.



(a) Results of Guangzhou



(b) Results of Shanghai



(c) Results of Shenzhen

Figure 4.5.: Variation of risk level with respect to different time of the day, in all three cities. Both overall risk as well as the risk per individual are presented.

#### 4.7.2 Control the metro network

We consider four different control strategies and investigate their effectiveness in improving the vulnerability of metro network to infectious diseases. For MCN, the random control and target control are implemented. In addition, we introduce the path-based control which focuses on passengers of each OD pair, and the station level control where passengers that enter a particular station will be screened and vaccinated.

##### 1. Random control

Random control is the method to select individuals from the MCN at random and quarantine/vaccinate the selected person, so that he/she will not be infected.

##### 2. Target control

Target control refers to select individuals from the MCN based on their node degree in descending order. As a consequence, nodes with highest degree will be selected and quarantined.

##### 3. Path-based control

Path-based control is used at the OD-level, where the OD pairs contributing most to total risk level will be selected and all passengers on selected OD pairs will be considered as quarantined or vaccinated.

##### 4. Station-based control

Station based control refers to that we screen passengers at the entrance of each metro station and infectious individuals will be quarantined and vaccinated. In this experiment we consider 100% rate of success in identifying infectious people so that

all passengers enter a particular station are in susceptible state. The station-based control is the most practical method in real world. We consider the station level control is implemented based on the total passenger demand in descending order.

## 5. Results

The effectiveness of the control strategies is presented in Figure 4.6. Figure 4.6(a)-(b) suggest the existence of 20-80 rules within metro system, where 20% of the stations contribute to 80% of the passengers and 80% of total system risk is associated with 20% of the OD pairs. This may sounds promising when it comes to devise control strategies for metro system, as it seems that only minimal efforts are required to achieve a satisfactory control results based on the 20-80 rules. However, we observe that, in order to control disease spreading and improve the vulnerability of metro network, the most effective measure is the target control method, followed by the path based control. However, among the four methods, only the station level control and random control strategies are practical approaches in filtering infectious population, while it will be extremely expensive and unreliable in identifying the riskiest person for implementing target control or inquire each passenger of his trip destination for path-based control. We find that the in many cases, the station level control is even less effective as compared to the random control strategy. This clearly states the challenge associated with controlling the disease from spreading within metro system. The reasons behind the ineffectiveness of the station-level control are primarily due to that riskiest people in the metro system depart from various metro stations, and that eliminating a few of these people will not result in a significant reduction in risk level due to the degree-based exponentially decaying tails of the degree distributions. Based on the results, we conclude that though station level control strategy is shown to be effective during disease outbreaks (as shown in Part I of the dissertation), it is also among the most inefficient and expensive control strategies for mitigating the risk due to infectious diseases. It is therefore important to devise better strategies

from the operation of metro systems and by improving the structures of the metro networks.

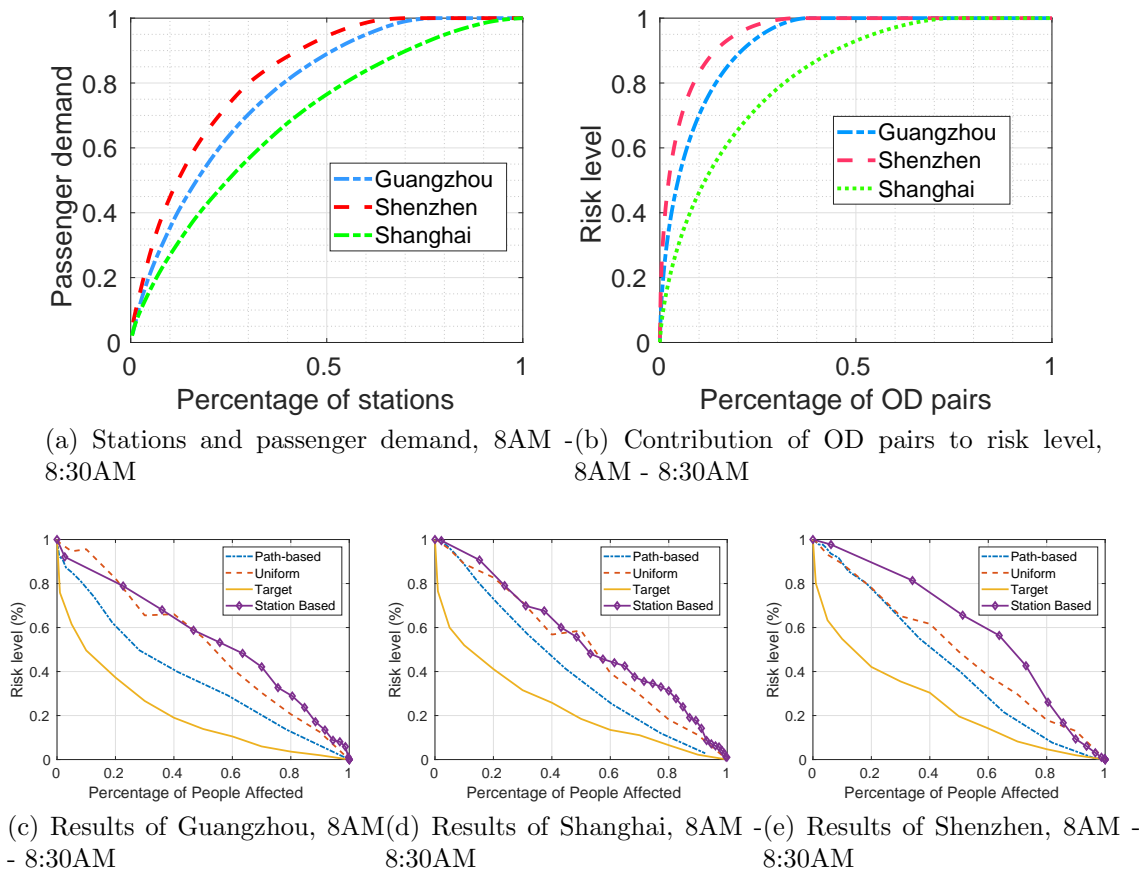


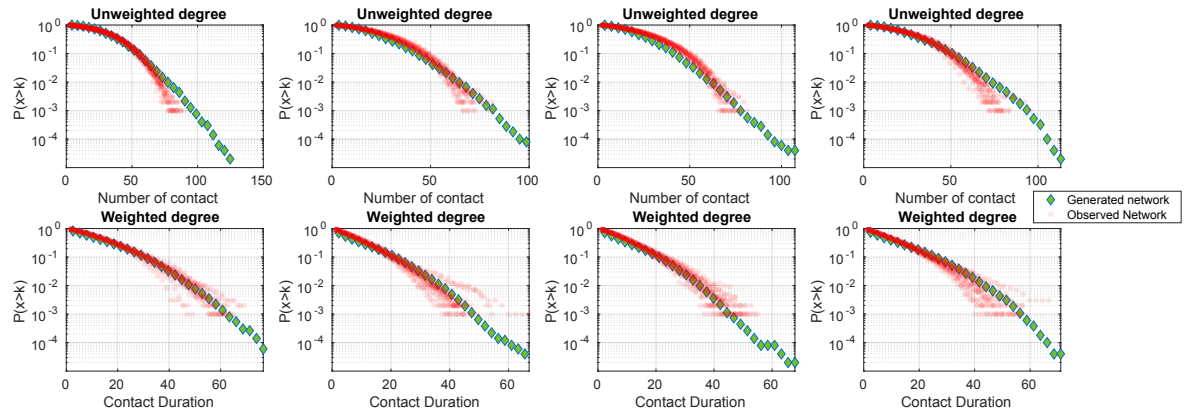
Figure 4.6.: Evaluations of effectiveness of various control strategies on improving the vulnerability of metro network to infectious diseases.

For each results, we consider 5000 passengers and compare the control strategies on individual contact networks, OD pairs, and at station level.

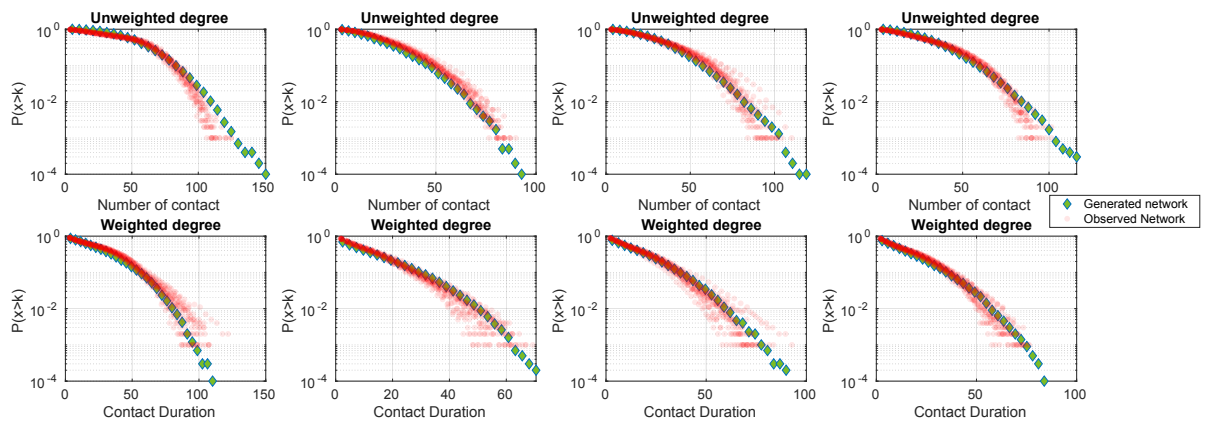
### 4.7.3 Fitting generation function to MCN

We choose four time periods of interest: 8:00-8:30, 12:00-12:30, 18:00-18:30, and 21:00-21:30 for each city, and report the fitting results of the generation model to the weighted and unweighted degree distribution of the MCNs generated. The fitted

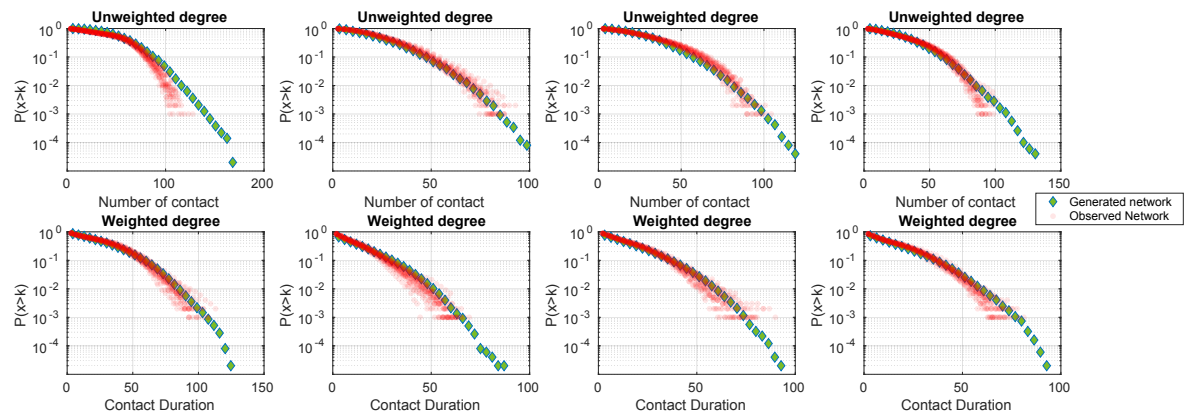
results of the three cities are shown in Figure 4.7. As discussed in previous sections, there are two parameters,  $\alpha$  for the metro structure and  $\gamma$  for the temporal factors, that need to be evaluated to finalize the generation model. These two factors are determined by first calibrating and fixing  $\alpha$ , then performing cross-validation to finalize  $\gamma$  based on the time of the day. For cross-validation, the KS statistic is used and the  $\gamma$  that results in the lowest combination of KS statistics for unweighted and weighted distributions is selected. The fitted statistics correspond to the results shown in Figure 4.7 are shown in Table 4.4. It can be observed that for all experiments, we fail to reject the null hypothesis for the two sample KS test with the lowest p-value among these cases being 0.51. Even this lowest value is way higher than the significant threshold for rejecting the null hypothesis (0.05), and in most of the cases the p value is greater than 0.9 for both weighted and unweighted distributions. The statistics along with the goodness of fits in Figure 4.7 are therefore strong evidences that the proposed generation function may well capture the underlying mechanisms that govern the meeting of passengers and the duration of exposures during their travels in metro system. And these evidences are further strengthened by varying the size of  $N$  and  $f$ , as shown in Figure 4.8. With the same set of parameters for  $\gamma$  and  $\alpha$ , we only vary the frequency of metro trains and the total number of passengers in the metro system. We observe that in all of these cases, the calibrated parameters fit well to different frequency and population levels. As a consequence, the proposed general model can be generalized to capture any operational frequency schedules and any passenger demand level. This means that our understanding on the functionality and structure of the MCNs is no longer restricted by the size of the passengers, and such generation model can therefore be used to provide guidance on designing operation strategies and structure improvements for more resilient metro networks against infectious diseases.



(a) Results of Guangzhou



(b) Results of Shanghai



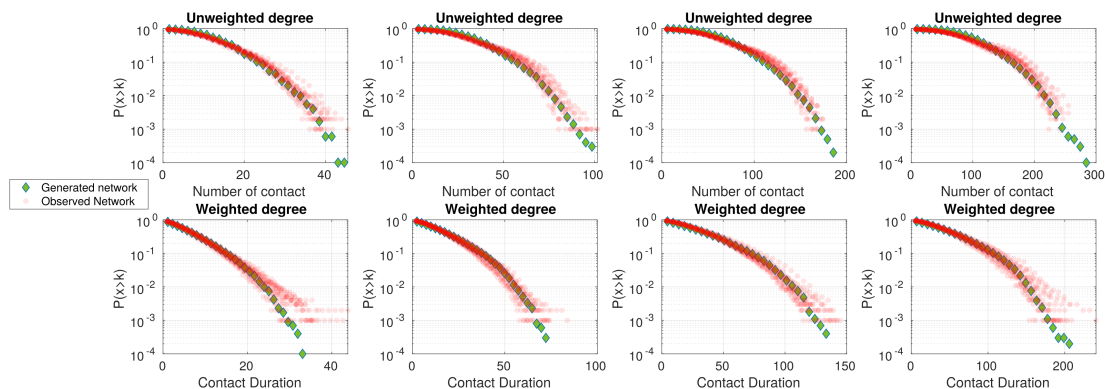
(c) Results of Shenzhen

Figure 4.7.: Visualization for the goodness of fit of the generation model to the MCNs generated from the smart card data.

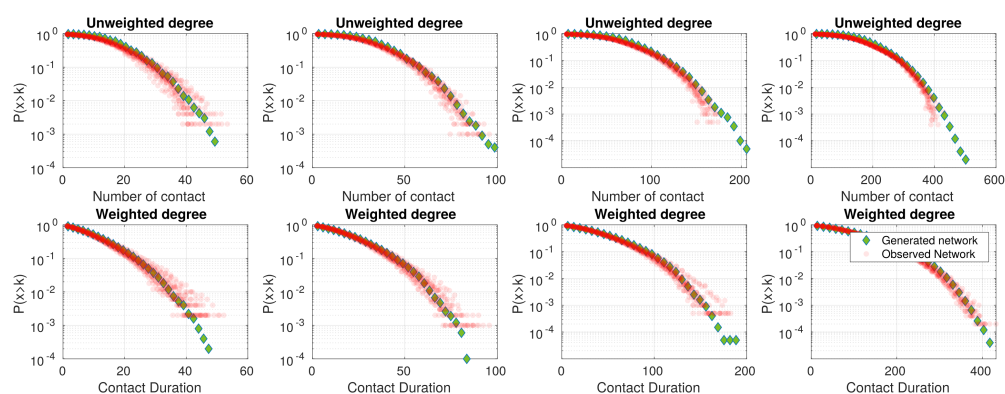
We consider four time periods of a day, which covers morning peak, off peak, evening peak, and night time. For each city, we fix  $\alpha$  and select  $\gamma$  using cross-validation. The results for generated network is based on the average of 20 realizations of the generation algorithm with the fitted parameter, and are compared with the scattered points representing the degree distribution of 20 randomly sampled MCNs. All scenarios fail to reject the null hypothesis of the K-S test with very high p-value, where detailed statistics of the K-S test can model parameters can be found in Table 4.4.

Table 4.4.: Summary of fitted results and model parameters from K-S test for three cities.

Shanghai				
time	8AM	12PM	6PM	9PM
unweighted p	0.95	0.68	0.84	0.84
weighted p	0.95	1.00	1.00	1.00
gamma	1.575	1.6	1.625	1.575
alpha	0.64	0.64	0.64	0.64
Guangzhou				
time	8AM	12PM	6PM	9PM
unweighted p	0.68	0.68	0.51	0.68
weighted p	1.00	1.00	1.00	0.95
gamma	1.67	1.61	1.595	1.665
alpha	0.69	0.69	0.69	0.69
Shenzhen				
time	8AM	12PM	6PM	9PM
unweighted p	0.84	0.95	0.51	0.84
weighted p	0.84	0.95	1.00	0.84
gamma	1.805	1.55	1.63	1.67
alpha	0.73	0.73	0.73	0.73



(a) Varying train frequency from 2min, 5min, 10min to 15min.



(b) Passenger demand from 500, 1000, 2000, to 5000

Figure 4.8.: Validation of the generation model by varying train frequency and number of passengers

#### 4.7.4 Discussion

It has been shown that the proposed generation model may well fit the data of the observed MCNs in all three cities across all time periods. The results indicate that the generation model is of high fidelity in describing the mechanism that drives the contact of two individuals as well as their contact duration. We next discuss the insights that can be obtained from the structure of the generation model.

Based on the analytical expression of the unweighted generation model (equation 4.6.5), there are two major factors that determine the shape of the degree dis-

tribution. One is the weight of each node  $w_i$ , which is given by the travel time of each passenger, and the other is the degree of each node  $k$ . The probability that a node has degree  $k$  drops rapidly with increasing node degree, which is much faster than that of a power-law or random graph. We term this as the node-degree based exponential decay, as the exponent term is the inverse of the node degree and the probability decays exponentially with the power term being the node degree as well. This analytical form is consistent with our observation of the fast decayed tail under semilog-scale plot, and explains the difficulties for controlling the MCNs against the spread of infectious disease. That is, while the node with highest degree dictates the risk level of the network, there are still many other nodes that are of slightly lower degree because of the degree-based exponential decay tail. Therefore, upon removing the riskiest person in the network, the functionality of the network will not be much affected. And only if a large amount of nodes being quarantined will we be able to significantly lower the risk level of the entire transportation system.

Based on the structure of the MCN, one important question is to identify the group of travelers who experience and introduce high risk exposure to the travel system. To gain insights into this issue, the correlations among the travel time distributions, distributions of number of contacts, and distributions of contact duration are plotted, and the results are shown in Figure 4.9. Each row in this figure corresponds to the observations of a particular city, and from top to bottom are the results of Guangzhou, Shanghai, and Shenzhen respectively. Despite some outliers in the results, we can easily observe that each pair of the three metrics of interests shows a strong positive correlation. And such observation is consistent across all three cities. Based on the results, we can see that there is a wide range of travel time for passengers having a high number of contact in the metro system. However, such range is much narrower for contact duration, and passengers who have the highest contact duration are those people who have the longest travel time. And the travel time of urban commuters is closely related to their work and home locations, their income levels, and eventually their lifestyle and health conditions. One recent study reported that

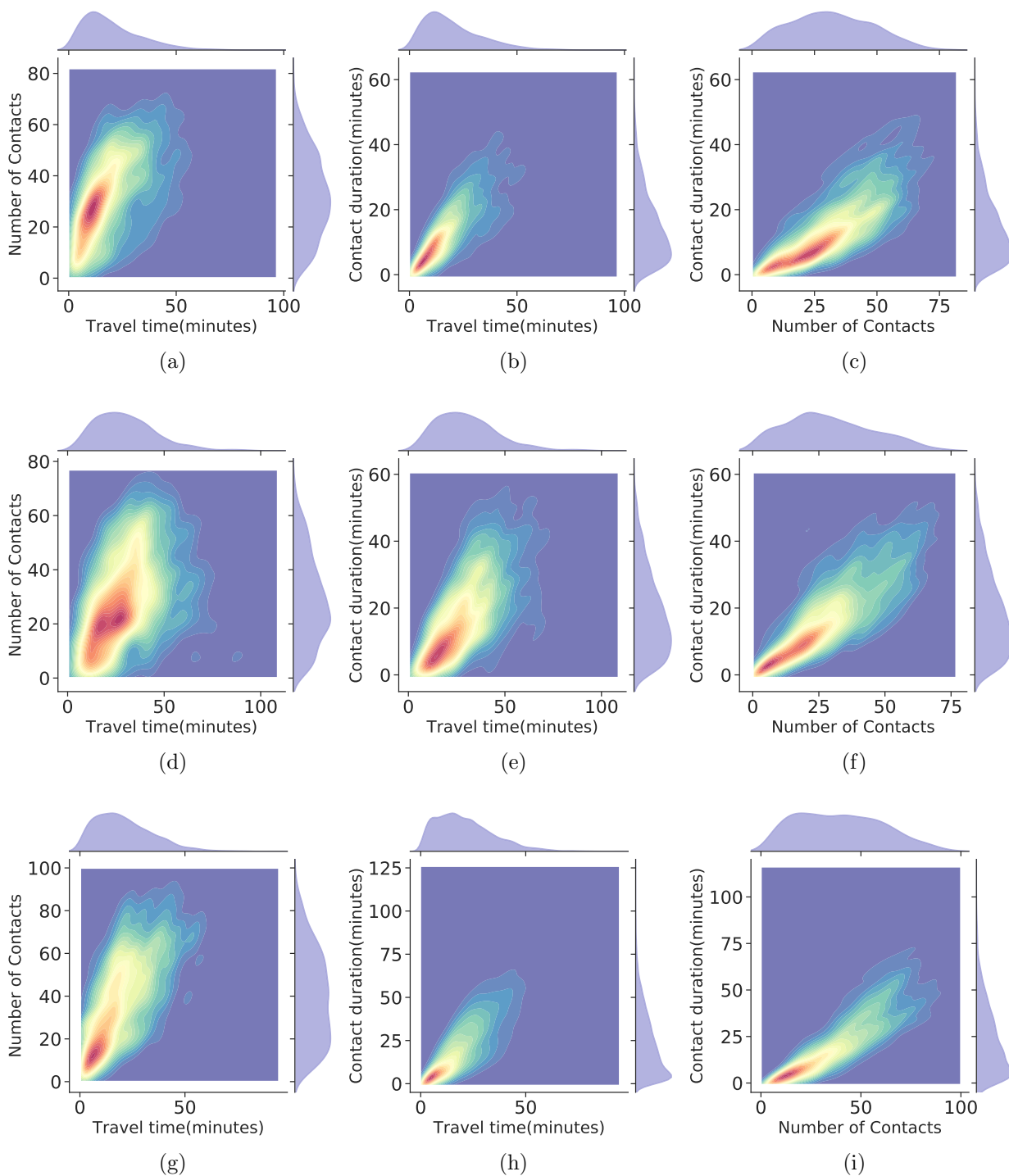


Figure 4.9.: The correlations among travel time, number of contacts, and total contagion duration in MCNs of three cities.

50 MCNs are generated for each plot using data from 8:00-8:30 AM, with each MCN having 1000 nodes. (a)-(c) are results of Guangzhou, (d)-(f) are results of Shanghai, and (g)-(i) are results of Shenzhen.

those commuters with the longest travel time in metro are likely to be low-income migrants and they may change their home and work locations more frequently than other urban commuters [102]. This finding suggests the another risk exposure for the MCNs. If commuters with long travel time overlap with the low-income population, then these people are more prone to infection when there is a disease outbreak. When compared to other population groups, they usually have a more stressful life and pay less attention to personal health and hygiene condition due to limited discretionary income. Consequently, the riskiest group of travelers in metro system are likely to be the most susceptible and vulnerable group of people during the disease outbreak. And this may inevitably raise additional challenges associated with disease contagion in urban transportation networks.

While it is difficult to stop the disease by controlling the passengers in the system, the generation model provides valuable insights in improving the resilience of transportation systems from the structure of the system. To reduce the risk of the MCNs is equivalent to reduce the probability of the MCNs having high degree nodes. As a consequence, the degree distribution that decays faster with increasing node degree will be preferred during disease outbreaks. Based on equation 4.6.5, we see that the possible approaches to reduce  $p(k)$  for large  $k$  are by lowering  $C$  value, reducing  $\alpha$  and  $\gamma$  values, and lowering  $w_i$  for all the travelers. The commonality of the these approaches is to segregate passengers during their trips to reduce the contact chance of two individuals. That is, one may increase the frequency of metro trains, which is linearly correlated with the value of  $C$  and thus having exponential contribution to lowering the probability of high degree nodes. We could also increase the number of transfer stations of reduce the detouring of passengers in the metro system to lower the value of  $\alpha$ , such as adding more ring lines to the metro system. Alternatively, we may provide travel guidance to passengers to induce those of similar travel routes and directions traveling at a different time, and motivate passengers with different travel directions to leave at the same time. This approach can therefore lower the  $\gamma$  parameter and therefore reducing the contact probability as well as the contact duration.

Finally, reducing the travel time of metro travelers eventually lead to the problem of urban planning. This finding is consistent with our results from the network model, where more decentralized urban structure will be less vulnerable to the risk of disease exposure. The decentralized urban structure implies that people are more likely to long distance travels across the city as they can find work or entertainment places that are more close to their home locations. While increasing metro frequency will only affect  $C$  value and the contact probability, the other two approaches will be more effective in reducing both contact probability as well as the contact duration, but would require much more efforts due to the changes needed in the structure of the metro networks and the urban shapes.

#### 4.8 Conclusion

This chapter develops the models for disease dynamics and the generation mechanism of contact patterns within urban transportation system at the individual level. The methods introduced in this chapter shed the light on the impacts of structural properties of individual contact network on the functionality of disease dynamics over the network. Moreover, the chapter provides the approach for understanding the factors that will affect the chance of two individuals meeting each other as well as the duration they will be exposed to each other. Real-world smart card transaction data are used to validate the developed models and comprehensive numerical experiments are conducted. Based on the results, we find that, despite having different metro network structures, the contact networks share many similar patterns across different cities at different time periods of the day. This suggests the existence of universal rule that governs the meeting pattern of individuals travel in metro network. Moreover, the analysis of IBMF model implies that the person with highest risk exposure dictates the vulnerability of the metro contact network, nevertheless, the shape of the contact network degree distribution also matters as it determines the level of difficulties in controlling the infectious diseases from spreading. While

IBMF model is computationally expensive and impractical for real-world sized case studies, the developed ODMF model addresses the computational bottleneck and is shown to be an effective tool in monitoring the real time variation of disease risks based on smart card data. The fitness of the generation model is further validated based on two sample KS-test, and all fitting results fail to reject the null hypothesis and reach high p-values. This implies that the proposed generation model is likely to be the actual rule governing the growth of MCNs and the generation model can therefore be used as a high-fidelity tool to guide the design and scheduling process of urban transportation system.

PART III: MULTIPLEX NETWORKS FOR INFORMATION AND DISEASE  
PERCOLATION AND CO-EVOLUTION



## 5. DISEASE SPREADING WITH LOCAL AND GLOBAL INFORMATION DISSEMINATION IN MULTIPLEX NETWORKS

### 5.1 Introduction

In the era of big data, people are more exposed to various information sources than ever before. This implies that they have much better access to the state of diseases during the disease outbreaks. And their behavior may therefore be different with the change of disease dynamics. This highlights the significance for considering the role of information dissemination while modeling the disease dynamics in urban networks.

The dynamics of the spread of infectious diseases in networks has been extensively investigated and there exists several discrepancies. Boguna et al. [65] modeled spreading diseases using SIS model in uncorrelated and correlated networks. The research yielded a concise equation for disease threshold in uncorrelated networks and used eigenvalue of the network matrix to describe the disease threshold when network is correlated. Correlation here implies degree correlation in the network. For correlation between networks, Dickison et al. [103] divided people into two groups and focuses on disease spreading inside and between the two networks. This model is suitable for certain two-group disease like sexual transmitted diseases. Sanz et al. [104] investigated two concurrent diseases. They introduced six parameters to depict the relationship of two diseases. Lacking realistic explanations to parameters is a shortcoming of the work. In addition, disease spreading in two networks with common nodes was researched by Buono et al. in 2014 [105]. This model was applied for specific situation where disease spread between two countries via frequent international travelers, but not under the scope of urban areas, or public transport.

Besides the differences in modeling structure to account for disease dynamics in networks, previous researchers also adopted different approaches to understand the co-evolution of information and disease dynamics. In summary, there were five main approaches: homogeneous mean field, heterogeneous mean field, individual-based, generating function, and pair-based approaches [106]. Youssef et al. [107] introduced the continuous Markov chain and individual-based SIR model. It was shown that epidemic threshold is inversely proportional to the eigenvalue of the network. This result agreed with those from other aggregated approaches. This conclusion was also achieved by Granell et al. with a microscopic Markov chain approach [108]. Wang et al. [109] modeled information and disease outbreak in communication and contact layers, respectively. For vaccination, they assumed that one will be vaccinated if and only if he is aware of the disease. Their extended work [110] introduced the analytical threshold of disease-infected neighborhoods and thus improved the original vaccination trigger. This change led to totally different conclusion: their early work [109] revealed that information spreading may raise disease threshold and the latter work [110] denied this result. In addition, Ruan et al. [111] used two parameters to depict human's response to diseases, and simulation was used for numerical results which lacked realistic explanations.

In this chapter, the heterogeneous mean field model (HMF) is introduced which is a widely used approach for understanding system dynamics in complex networks. Compared with previous studies, this work has the following advantages: 1) the model applies for most of the diseases; 2) both local information and global information (mass media) are modeled; 3) the multiplex network approach is introduced which avoids assuming overly-complicated individual behavior parameters; 4) three state: DAFA, DFE-A, and endemic are analyzed both theoretically and numerically.

The chapter is organized as follows. Section two introduces the mathematical notation used in this study. Section three describes the assumption made and section four gives an overview of the UA-SIS model. Section five presents the mathematical formulation of the UA-SIS model and section six delivers theoretical analysis of the

stable states and conditions for the UA-SIS model. Section seven shows the numerical experiments and insights obtained from the model. Section eight concludes the chapter with summary and key findings.

## 5.2 Notation

The mathematical notation used in this study is summarized in Table 5.1.

Table 5.1.: Table of notation

<b>Variables</b>	<b>Descriptions</b>
$k$	Nodes with degree $k$
$U_k$	Percentage of nodes in state $U$ with degree $k$ . U=unaware.
$\theta_{A,k}$	Percentage of nodes in state $A$ with degree $k$ . A=aware.
$S_k$	Percentage of nodes in state $S$ with degree $k$ . S=susceptible.
$\theta_{I,k}$	Percentage of nodes in state $I$ with degree $k$ . I=infectious.
$\beta_U$	Transmission probability when a node is in $U$ state.
$\beta_A$	Transmission probability when a node is in $A$ state. $\beta_A \ll \beta_U$ .
$\gamma_1$	Recovery rate of the aware state, $\gamma_1 \leq 1$ .
$\gamma_2$	Recovery rate of the given disease, $\gamma_2 \leq 1$ .
$p$	Probability of a node changes from $U$ to $A$ by observing that one of its neighbors is in $A$ state.
$\mathcal{N}(i)$	The set of neighbor nodes of node $i$ .

## 5.3 Assumption

The following assumptions are made to support the development of the UA-SIS model:

1. It is assumed that nodes of the same degree have the same behavior. So that we can make use of the heterogeneous mean field model (HMF), also known as the degree-based mean-field model, to understand UA-SIS dynamics.
2. The discussion is currently limited to HMF without degree correlation. But the framework discussed in this study can be easily adapt to account for correlated degree sequences.

3. It is considered that both UA process and SIS process have the same network structure for the numerical experiments. Various network structures in different layers will be considered in future work.

#### 5.4 UA-SIS model

In the UA-SIS model, individuals are modeled as nodes and their pairwise connections are captured by the edges. The UA-SIS model is capable of capturing the dynamics of three processes that take place simultaneously:

1. The physical contagion process, where individuals get in contact with others and the disease may spread upon contagion.
2. The observation process (local information), where individuals may observe the behavior of his/her neighbors, and accumulate knowledge of the diseases. Each valid observation will strengthen his understanding and increase the likelihood of an individual migrating from U state to A state. Meanwhile, individuals may move from A to U as time proceeds. This is known as the fading of memory.
3. The information gathering and dissemination process (global information). Different from many other studies, where information dissemination is assumed to take place among neighbors only, this chapter considers the existence of a central system which gathers the disease information from the population and disseminates the compiled information back to the population within reach.

The interactions among these three processes can therefore be captured by a multiplex network with three levels, as shown in Figure 5.1.

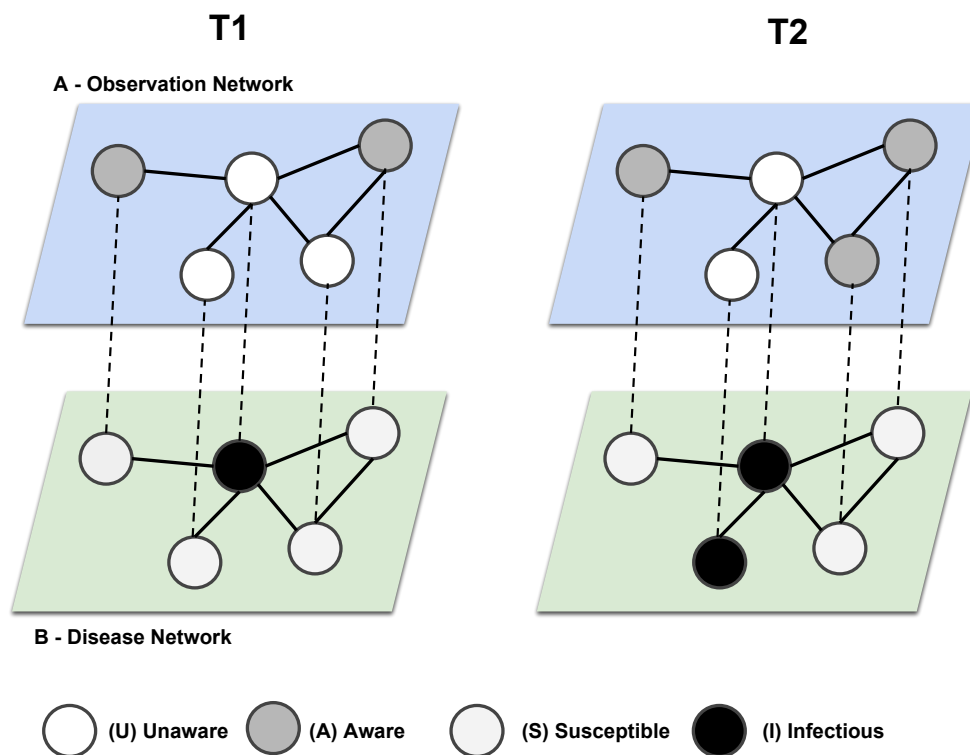


Figure 5.1.: Illustration of the UA-SIS modeling process.

In the figure, the system has two layers of networks: the disease network and the observation network. The SIS process takes place on disease network while the UA process is on the observation network. On the left (time= $T1$ ), the system starts with one infectious node and two out of four of its neighbors are aware of his illness. On the right (time= $T2$ ), the system evolves over time and one more node turns into A state. And the neighbor node who is still in U state is infected by the infectious node.

In Figure 5.1, there are two correlated networks that represent the disease dynamics and the observation dynamics. In the observation network, nodes observe their neighbors and obtain local information of the disease information. If one of the neighbors is in A, then the node has certain probability that it will evolve into A as well. As for the disease network, the classic SIS process is considered where the node is either in susceptible or infectious state. A susceptible node may turn into an infectious one upon physical contact with another infectious neighbor. However, since the two networks are inter-correlated and having the same topology, a susceptible node

may not be infected by its infectious neighbors in the disease network if it is in the aware state in the observation network. This illustrates why using SIS model itself may overestimate the outbreak scale of the disease and the necessity for including the information layer (observation as the case in our study).

Up to now, only local information dissemination upon physical contact is considered. However, one major source for the general public to obtain information is through online resources such as social medias and news agencies. People may value these information differently, among which the most reliable source is the official data and news. However, for any official media, it is in general difficult to understand the whole picture of the disease pattern. As a consequence, the other important research question is to understand how different levels of information may affect the disease spreading dynamics over the disease network. This process is described in Figure 5.2.

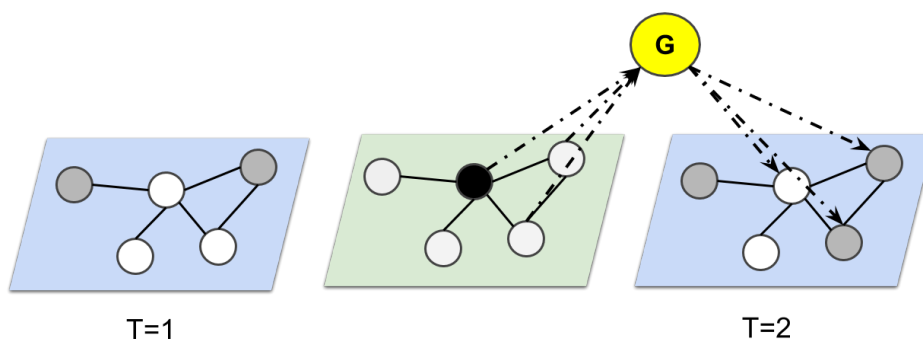


Figure 5.2.: Illustration of the UA-SIS information dissemination process.

During the process, the central system (node G in yellow) obtains the disease information from its neighbors in the disease layer at time  $T = 1$ , and the disseminates this information to the same set of nodes in the observation layer. This in combination with the observed information turns one of the nodes from U state to A state.

## 5.5 Formulation

The HMF method is used which assumes that nodes of same degree are homogeneous. Mathematically, the interplay among the three layers can be written as following.

### 5.5.1 Observation layer

The observation layer describes the dynamics where each individual observes from his or her physical contacts and accumulating awareness of the disease states:

$$\begin{aligned} \frac{dU_k}{dt} = & - [1 - (1 - p)^{k\Theta_A(t)} + \lambda_g(t) + \beta_U k \Theta_I(t)] U_k(t) \\ & + \gamma_1 \theta_{A,k}(t) \end{aligned} \quad (5.5.1)$$

$$\begin{aligned} \frac{d\theta_{A,k}}{dt} = & [1 - (1 - p)^{k\Theta_A(t)} + \lambda_g(t) + \beta_U k \Theta_I(t)] U_k(t) \\ & - \gamma_1 \theta_{A,k}(t) \end{aligned} \quad (5.5.2)$$

where  $\Theta_A(t)$  is the probability that the neighbor of a node is in state  $A$  at time  $t$ .  $1 - p$  denotes the probability that the node will remain in  $U$ , so that  $(1 - p)^{k\Theta_A(t)}$  gives the probability that node  $i$  will remain in  $U$  after observing all his neighbors in  $A$ . As a consequence, the first term in equation 5.5.1 refers to the proportion of nodes of degree  $k$  that migrates from state  $U$  to state  $A$ , and the second term describes the decreasing level of awareness so that people moves from  $A$  back to  $U$ .

### 5.5.2 Disease layer

In disease networks, individuals are considered to be in one of the two states: susceptible (S) and infectious (I). In particular, for individual in S, the chance of being infected depends on if they are in A or U states, with different transmission coefficient  $\beta_A$  and  $\beta_U$  respectively.

$$\begin{aligned} \frac{dS_k}{dt} = & -\beta_A k \Theta_I(t) S_k(t) \theta_{A,k}(t) - \beta_U k \Theta_I(t) S_k(t) (1 - \theta_{A,k}(t)) \\ & + \gamma_2 \theta_{I,k}(t) \end{aligned} \quad (5.5.3)$$

$$\begin{aligned} \frac{d\theta_{I,k}}{dt} = & \beta_A k \Theta_I(t) S_k(t) \theta_{A,k}(t) + \beta_U k \Theta_I(t) S_k(t) (1 - \theta_{A,k}(t)) \\ & - \gamma_2 \theta_{I,k}(t) \end{aligned} \quad (5.5.4)$$

where  $\Theta_I(t)$  is the probability that the neighbor of a node is in state  $I$  at time  $t$ . Equations and characterize the contagion dynamics for susceptible nodes in  $A$  and  $U$  states respectively.

### 5.5.3 Information layer

We next introduce the equation for the information layer, where it is assumed that there is a central system that collects the information over the network. In particular, we consider two types of information gathering schemes: the targeted information fetching and the random information fetching. It is considered that the central node can obtain the information over the disease network from the nodes that are adjacent to it, and then compile the information and send back to the same set of nodes on the observation network.

$$[Target] \quad \lambda_g(t) = \kappa \sum_{i \in \mathcal{T}} \Theta_{I,\mathcal{T}}(t) \quad (5.5.5)$$

$$[Random] \quad \lambda_g(t) = \kappa \alpha \sum_k \theta_{I,k}(t) P(k) \quad (5.5.6)$$

where  $\Theta_{I,\mathcal{T}}(t)$  denotes the probability that a node is infected within the target set  $\mathcal{T}$ ,  $\kappa$  is a discount factor that converts the total number of infectious nodes to the level

of dangerous, and  $\alpha$  is the ratio that accounts for the proportion of nodes that the central node has connection to.

#### 5.5.4 Probability of a node in infectious state

We now define the probability that a randomly selected neighbor of a node with degree  $k$  is in  $A$  or  $I$  states, namely  $\Theta_A(t)$  and  $\Theta_I(t)$ .

Define  $\theta_{A,k}(t)$  as the probability that a node with degree  $k$  is in  $A$  state at time  $t$ , we have:

$$\Theta_A(t) = \frac{\sum_{k'} k' P(k') \theta_{A,k'}(t)}{\langle k \rangle} \quad (5.5.7)$$

where  $\langle k \rangle$  is the average degree of the network. The reasoning behind this equation is that high degree node usually have a much higher chance of being in the infected states as compared to low degree nodes, so that such heterogeneity of node degree should be taken into consideration [60].

Similarly, for infectious population, we should have

$$\Theta_I(t) = \frac{\sum_{k'} k' P(k') \theta_{I,k'}(t)}{\langle k \rangle} \quad (5.5.8)$$

### 5.6 System equilibrium and stability analysis

SIS model is a well-studied epidemic model with two equilibrium states. One is the disease free equilibrium (DFE) where all individuals are susceptible. This can be analogous to that all individuals are in  $U$  and  $S$  states in our UA-SIS model, where such state is named as the disease and awareness free equilibrium (DAFE). The other equilibrium is known as the endemic equilibrium, where there will always be a proportion of nodes in infectious state, and the size of infectious population is equal to the size of the giant component in the graph. Finally, there is a special equilibrium point for the UA-SIS model, where the state is free from disease invasion

but the awareness itself is permanent and strictly positive. This regime is named as the disease free equilibrium with awareness (DFE-A).

### 5.6.1 Disease and awareness free equilibrium

We first discuss the first equilibrium state, the DAFE, so that when  $t \rightarrow 0$  we have  $\theta_{A,k}(t) = 0$  and  $\theta_{I,k}(t) = 0$  for all  $k$ . Equivalently, this gives  $U_k(t) = 1$  and  $S_k(t) = 1$  in their corresponding layers respectively. This reduces equations 5.5.2 and 5.5.4 to

$$\frac{d\theta_{A,k}}{dt} = 1 - (1-p)^{k\Theta_A(t)} + \lambda_g(t) - \gamma_1\theta_{A,k}(t) \quad (5.6.1)$$

$$\frac{d\theta_{I,k}}{dt} = \frac{\sum_{k'} \beta_U k k' P(k') \theta_{I,k'}(t)}{\langle k \rangle} - \gamma_2 \theta_{I,k}(t) \quad (5.6.2)$$

In the neighborhood of DFE, we further know that  $k\theta_A(t) \rightarrow 0$  and we should have

$$(1-p)^{k\Theta_A(t)} \approx 1 + \ln(1-p)k\Theta_A(t) \quad (5.6.3)$$

so that we can rewrite equation 5.6.1 as:

$$\begin{aligned} \frac{d\theta_{A,k}}{dt} &= -\ln(1-p)k\Theta_A(t) + \lambda_g(t) - \gamma_1\theta_{A,k}(t) \\ &= -\ln(1-p)k\Theta_A(t) + \kappa\alpha \sum_k \theta_{I,k}(t)P(k) - \gamma_1\theta_{A,k}(t) \end{aligned} \quad (5.6.4)$$

Let  $C^{OD}$  be the correlation matrix between observation layer and disease layer, and  $C^{OO}$  and  $C^{DD}$  be the matrices for observation layer and disease layer respectively, where.

$$C_{k_1, k_2}^{OO} = -\frac{\ln(1-p)k_1 k_2 P(k_2)}{\langle k \rangle} \quad (5.6.5)$$

$$C_{k_1, k_2}^{OD} = \kappa\alpha P(k_2) \quad (5.6.6)$$

$$C_{k_1, k_2}^{DD} = \frac{\beta_U k_1 k_2 P(k_2)}{\langle k \rangle} \quad (5.6.7)$$

We should therefore have

$$C = \begin{bmatrix} C^{OO} & C^{OD} \\ 0 & C^{DD} \end{bmatrix} \quad (5.6.8)$$

We can therefore write equations 5.6.2 and 5.6.4 as the following linear system:

$$\frac{d\theta}{dt} = C\theta - \gamma.\theta \quad (5.6.9)$$

where  $\theta = [\theta_{A,1}, \dots, \theta_{A,k_{max}}, \theta_{I,1}, \dots, \theta_{I,k_{max}}]^T$ .

We should have the following proposition:

**Proposition 5.6.1** *The DAFE of the UA-SIS system is asymptotically stable if the spectral radius of  $\rho(C)\gamma$ . In other words, if the maximum eigenvalue of  $C$  is smaller than  $\gamma$ , then the DFE is asymptotically stable.*

Since  $C$  is an upper-triangular matrix, we should have the maximum eigenvalue of  $C$  as

$$\lambda = \max(\lambda(C^{OO}), \lambda(C^{DD})) \quad (5.6.10)$$

When  $t \rightarrow 0$ , according to [25], the disease transmission thresholds for observation layer and disease layer can be written as:

$$\lambda_O = -\ln(1-p) \frac{\langle k^2 \rangle}{\langle k \rangle} \quad (5.6.11)$$

$$\lambda_D = \beta_U \frac{\langle k^2 \rangle}{\langle k \rangle} \quad (5.6.12)$$

where we immediately observe that the spreading spread of awareness decays exponential with the strength of individual perceptions of the disease, as shown in Figure 5.3

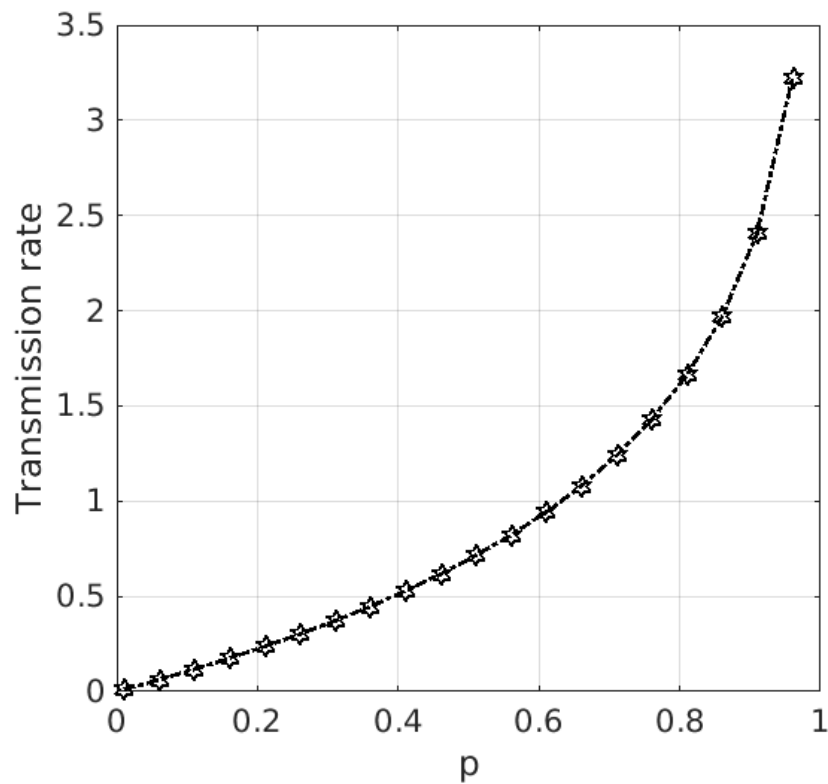


Figure 5.3.: Spreading rate of awareness with the change of individual perception of disease

The second observation from the structure of  $C$  is that the availability of global information does not affect the disease threshold in a network. That is,  $\lambda_g$  does not determine the value of  $\lambda_O$  and  $\lambda_D$ , and hence  $\lambda_C$ . This observation may sound counter-intuitive at first glance. However, when disease is approaching DFE, the value of  $\lambda_g$  is nearly zero as there are barely any infected people in the network. As a consequence, it is always of lower order as compared to the personal awareness of the disease, which plays a major role in the spreading process. The individual perception

level directly gives the duration that the awareness may persist, and therefore how likely that people may stay in a safer state.

### 5.6.2 Disease free equilibrium with awareness

By observing the system equations, there are actually two different DFEs rather than one for basic SIS model: the DAFE, which is disease and awareness free equilibrium, and DFE-A, which is the disease free equilibrium with positive awareness population. The DAFE state is discussed in the previous section. As for DFE-A, the equilibrium point of interest is  $\theta_{I,k} = 0$ ,  $\theta_{A,k} \geq 0$ .

To calculate the equilibrium point of interest, we first note that at DFE-A,  $\Theta_I = 0$  but  $\Theta_A > 0$ . By taking  $\frac{d\theta_{A,k}}{dt} = 0$  at DFE-A with above information, we should have

$$[1 - (1 - p)^{k\Theta_A}](1 - \theta_{A,k}) - \gamma_1\theta_{A,k} = 0 \quad (5.6.13)$$

and this yields

$$\theta_{A,k} = \frac{1 - (1 - p)^{k\Theta_A}}{1 - (1 - p)^{k\Theta_A} + \gamma_1} \quad (5.6.14)$$

Introducing this equation to the equation for  $\Theta_A(t)$ , we get a self-consistent equation for  $\Theta_A$  as

$$\Theta_A = \frac{1}{\langle k \rangle} \sum_{k'} kP(k') \frac{1 - (1 - p)^{k'\Theta_A}}{1 - (1 - p)^{k'\Theta_A} + \gamma_1} \quad (5.6.15)$$

where 0 is an trivial solution that corresponds to the DAFE equilibrium. The function

$$f(\Theta_A) = \frac{1}{\langle k \rangle} \sum_{k'} kP(k') \frac{1 - (1 - p)^{k'\Theta_A}}{1 - (1 - p)^{k'\Theta_A} + \gamma_1} - \Theta_A \quad (5.6.16)$$

is a concave function, where we have

$$\frac{1 - (1 - p)^{k'\Theta_A}}{1 - (1 - p)^{k'\Theta_A} + \gamma_1} < 1 \quad (5.6.17)$$

This suggest that  $f(1) < 0$  and  $\frac{df(x)}{dx}|_{x=0} > 0$ . As a consequence,  $\Theta_A$  admits a positive solution within the interval  $(0, 1)$ . Without loss of generality, consider the DFE-A solution being  $(\mu, 1 - \mu, 1, 0)$  where

$$\mu_k = \frac{\gamma_1}{1 - (1 - p)^{k\Theta_A^*} + \gamma_1} \quad (5.6.18)$$

And the solution with positive awareness is stable as long as  $\rho(C) > \gamma_1$ , based on our analysis for the stability of DAFE. Now we know that  $\frac{\gamma_1}{1+\gamma_1} \leq \mu_k \leq 1$ . More importantly, for nodes with higher degree,  $\mu_k \rightarrow \frac{\gamma_1}{1+\gamma_1}$ . Meanwhile, the higher the  $p$  is, the lower the  $\mu_k$  will be. And the value of  $\mu_k$  is sensitive to  $\gamma_1$  value, which is the fading rate of memory. If it takes longer for a disease to be forgot, then the  $\gamma_1$  value should be smaller and there will be fewer people in  $U$  state.

We now linearize the UA-SIS system at DFE-A as:

$$\frac{d\theta_{A,k}}{dt} = [1 - (1 - p)^{k\Theta_A(t)} + \lambda_g(t) + \beta_U k \Theta_I(t)] \mu_k - \gamma_1 \theta_{A,k}(t) \quad (5.6.19)$$

$$\frac{d\theta_{I,k}}{dt} = \beta_A k \Theta_I(t) (1 - \mu_k) + \beta_U k \Theta_I(t) \mu_k - \gamma_2 \theta_{I,k}(t) \quad (5.6.20)$$

Rearranging the right hand side gives:

$$\frac{d\theta_{I,k}}{dt} = \beta_A k \Theta_I(t) + (\beta_U - \beta_A) \mu_k k \Theta_I(t) - \gamma_2 \theta_{I,k}(t) \quad (5.6.21)$$

To ensure that the DFE-A is a.s.s, I just need to ensure that  $I = 0$  is stable solution, which is equivalent to that

$$\lambda_{DFE-A} = \beta_A \frac{\langle k^2 \rangle}{\langle k \rangle} + (\beta_U - \beta_A) \frac{\langle \mu_k k^2 \rangle}{\langle k \rangle} < \gamma_2 \quad (5.6.22)$$

If we consider that  $\beta_A = 0$ , which is equivalent to that those people who are aware of the disease will be totally vaccinated or quarantined. Se know that  $\lambda_D^{DFE-A}$  is proportionally to  $(\beta_U - \beta_A) \frac{\langle \mu_k k^2 \rangle}{\langle k \rangle}$ . This demonstrates that the local information contributes significantly to lowering the disease threshold as compared to the state

when there is no information available. But the marginal gain will be considerably weaker as we keep increasing the value of  $p$ .

Based on these analysis, there will be two conditions for the disease to reach DFE-A state. The first is the trivial case, where the disease system itself will stay in the DFE state and the aware population is positive:

$$\lambda_O > \gamma_1, \lambda_D < \gamma_2 \quad (5.6.23)$$

The second case is more interesting where the disease itself may eventually reach endemic without awareness outbreak. However, the strength of the disease is weakened by the spread of awareness so that the previously endemic disease will eventually be eliminated. Mathematically, this requires the following condition to be satisfied:

$$\lambda_{DFE-A} < \gamma_2, \lambda_O > \gamma_1, \lambda_D > \gamma_2 \quad (5.6.24)$$

### 5.6.3 Size of endemic state

We are not only interested in DFE of the diseases, but also would like to explore how local observation and global information may affect the speed of the infectious diseases, and consequently the size of the outbreak (endemic state). This motivates us to conduct further analysis.

When  $\lambda_D^{DFE-A} > \gamma_2$  and  $\lambda_O > \gamma_1$ , the disease will eventually reach the endemic state. Following [60], we first calculate the size of the endemic disease. At endemic, we should have the equilibrium point being  $(\mu, 1 - \mu, s, 1 - s)$ . As a consequence, we should have

$$\begin{aligned} \frac{d\theta_{I,k}}{dt} = & (\beta_A k \Theta_I(t) + (\beta_U - \beta_A) \mu_k k \Theta_I(t)) (1 - \theta_{I,k}(t)) \\ & - \gamma_2 \theta_{I,k}(t) \end{aligned} \quad (5.6.25)$$

At endemic state, we should have  $\frac{d\theta_{I,k}}{dt} = 0$ , so that

$$\gamma_2\theta_{I,k} = [\beta_A + (\beta_U - \beta_A)\mu_k](1 - \theta_{I,k})k\Theta_I \quad (5.6.26)$$

$$\theta_{I,k} = \frac{\alpha_k k \Theta_I}{\gamma_2 + \alpha_k k \Theta_I} \quad (5.6.27)$$

where  $\alpha_k = \beta_A + (\beta_U - \beta_A)\mu_k$ . And

$$\Theta_I = \frac{\sum_{k'} k' P(k') \theta_{I,k'}}{\langle k \rangle} \quad (5.6.28)$$

$$\Theta_I = \frac{1}{\langle k \rangle} \sum_{k'} k' P(k') \frac{\alpha'_k k' \Theta_I}{\gamma_2 + \alpha'_k k' \Theta_I} \quad (5.6.29)$$

Following the same analysis as for  $\Theta_A$  for DFE-A, we know that there will be a positive  $\Theta_I$  in the interval  $(0, 1)$  which satisfies above equation.

Meanwhile, for  $\theta_{A,k}$ , by setting

$$[1 - (1 - p)^{k\Theta_A(t)} + \lambda_g(t) + \beta_U k \Theta_I(t)](1 - \theta_{A,k}(t)) = \gamma_1 \theta_{A,k}(t) \quad (5.6.30)$$

$$\theta_{A,k} = 1 - \frac{\gamma_1}{1 - (1 - p)^{k\Theta_A} + \lambda_g + \beta_U k \Theta_I + \gamma_1} \quad (5.6.31)$$

Let  $G(k) = 1 - (1 - p)^{k\Theta_A} + \lambda_g$ , we have

$$\theta_{A,k} = 1 - \frac{\gamma_1}{G(k) + \gamma_1 + \beta_U k \Theta_I} \quad (5.6.32)$$

$$\mu_k = \frac{\gamma_1}{G(k) + \gamma_1 + \beta_U k \Theta_I} \quad (5.6.33)$$

Finally, we have

$$\Theta_A = \frac{1}{\langle k \rangle} \sum_{k'} k' P(k') (1 - \mu'_k) \quad (5.6.34)$$

$$\Theta_I = \frac{1}{\langle k \rangle} \sum_{k'} k' P(k') \left(1 - \frac{\gamma_2}{\gamma_2 + (\beta_A + (\beta_U - \beta_A)\mu'_k)k' \Theta_I}\right) \quad (5.6.35)$$

Based on the equations, we observe that, for high degree nodes, the value of  $u_k$  is dominated by  $\beta_U \theta_I$  rather than the strength of the personal awareness. But for nodes

with low degree, the strength of information dictates the value of  $\mu_k$ . This suggests that at endemic state, high degree nodes are less prone to being infected, while low degree nodes are more vulnerable to the risk of infectious diseases.

### 5.7 Numerical experiments

The ODE45 solver in MATLAB is used to simulate the UA-SIS model described in the dissertation. Unless otherwise mentioned, we consider the network follows the scale-free network with  $p(k) \propto k^{-\gamma}$ , and the exponent is set to 3.5.

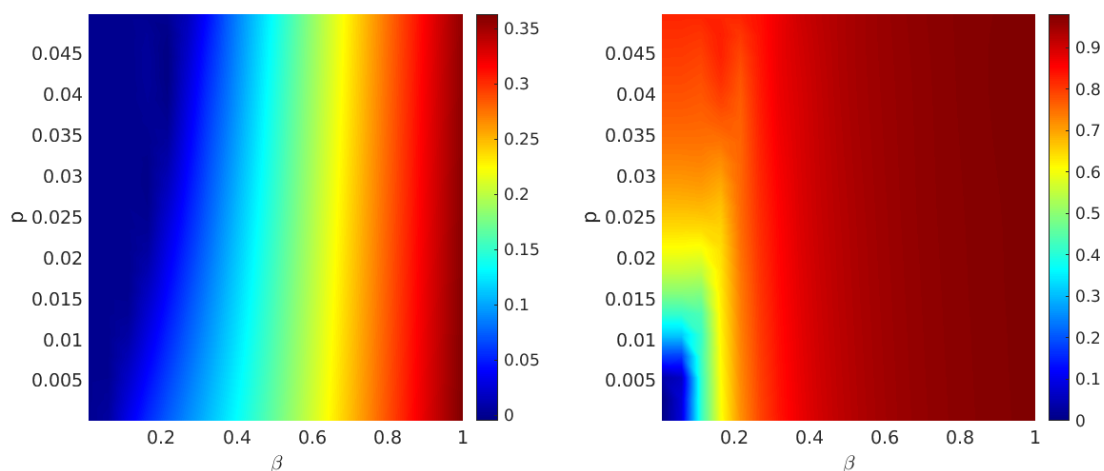


Figure 5.4.: Infectious population (left) and aware population (right) with varying  $\beta$  and  $p$ .

Figure 5.4 shows how varying  $\beta$  and  $p$  may affect the final infectious and awareness population. The figure depicts the state transition among the three equilibrium states with different  $\beta$  and  $p$  values. In particular, when  $\beta < 0.1$ , the DFE can be achieved without the help of information dissemination. Meanwhile, when  $\beta < 0.1$  and  $p < 0.01$ , the strength of the awareness is not strong enough to promote a local information outbreak. Under such circumstance, the system is in DAFE state with disease and awareness population being 0. When  $\beta$  increases beyond 0.1, the local disease outbreak starts to emerge, but may be eliminated with higher  $p$  value. Such

state corresponds to the  $DFE-A$  equilibrium, where the awareness is strictly positive but the disease is eradicated. Finally, when the disease strength exceeds  $\lambda_{DFE-A}$ , the system will transit into endemic state and both disease and awareness are permanent in the population.

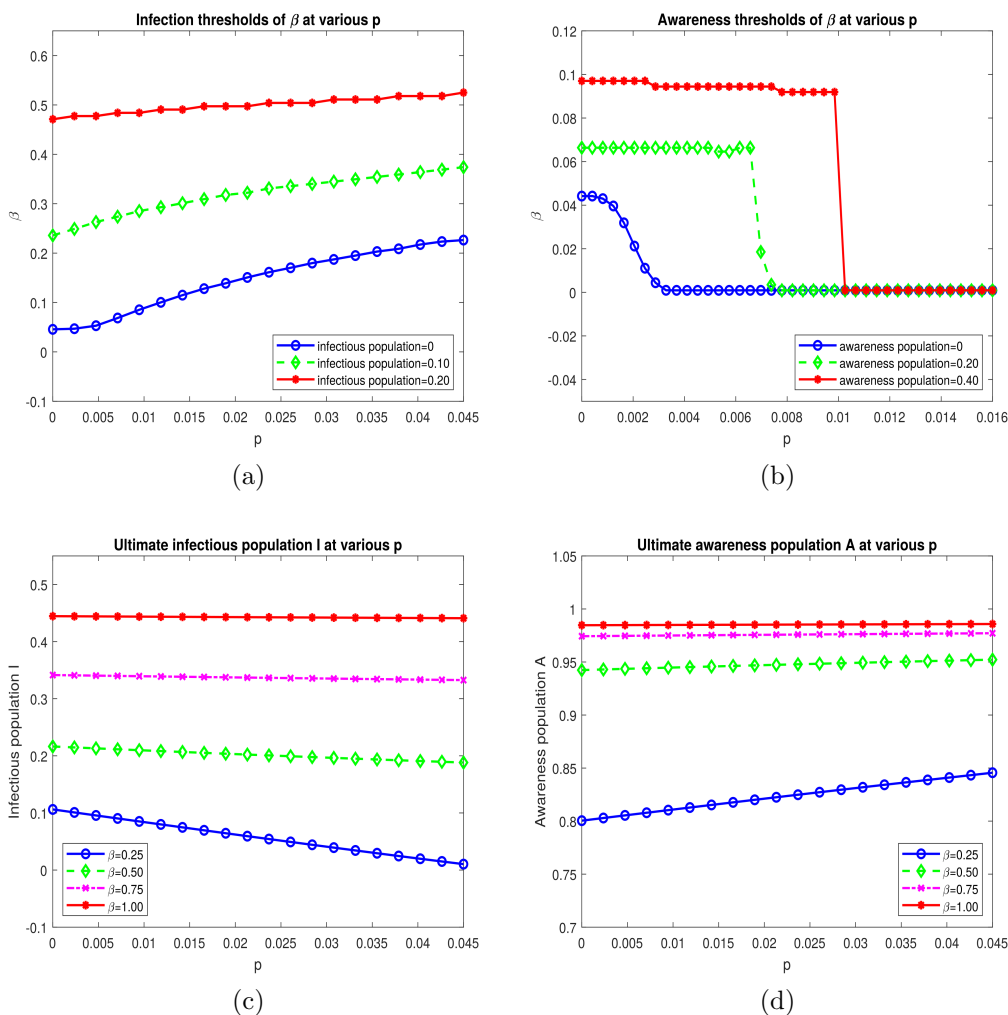


Figure 5.5.: The impact of local information on disease spreading dynamics

Figure 5.5 reveals the effect of local information transmission on spreading dynamics. The blue line in Figure 5.5(a) presents that local information efficiently suppresses disease outbreak, for the threshold increases as  $p$  increases. This conclusion can also be drawn via equation 5.6.22 where  $\mu_k$  is less than 1. For reaching

higher infectious population ( $I = 0.1$  and  $0.2$ ), increasing individual awareness is observed to be less effective, as shown in green and red lines. Figure 5.5(b) shows that increasing transmission probability  $\beta$  lowers the awareness outbreak threshold. An interesting observation is the existence of “threshold drop”, which happens at around  $p = 0.002$  (awareness = 0),  $0.007$  (awareness = 0.20) and  $0.01$  (awareness = 0.40). When  $p$  increases from lower value to above the observed threshold, the information threshold drops rapidly. After the “threshold drop”, even a small percent of infection will lead to awareness spreading very quickly. This finding demonstrates the essential role of local information transmission related to infectious disease outbreak. On the other hand, the blue line in Figure 5.5(c)-(d) present that local information transmission reduces the limiting size of infectious population and increases the limiting size of aware population. This asymmetrical phenomenon is consistent with the results shown in Figure 5.5(a)-(b). When  $\beta$  is high,  $p$  has little impact on final infectious and aware population. In that case,  $\beta$  dominates the system dynamics for both infectious and aware population.

Figure 5.6 reveals the role of global information. Figure 5.6(a) and (c) show that global information has no impact on disease threshold. In particular, global information is zero when there is no infectious population. This is because media agencies release global information based on monitoring the progress of social events in a reactive manner. After infectious disease breaks out, only very strong global information is able to restrain disease efficaciously (e.g, when global information strength increased by 10000 times). As  $\beta$  becomes larger, even strong global information is no longer effective to inhibit diseases. Figure 5.6(b) and (d) display the similar results. Global information exerts no influence on information outbreak threshold and only increases ultimate awareness population when  $\beta$  is not very high. In summary, global information is not as useful as local information to control disease and stimulate information spreading. And both local information and global information are no longer effective for highly infectious diseases.

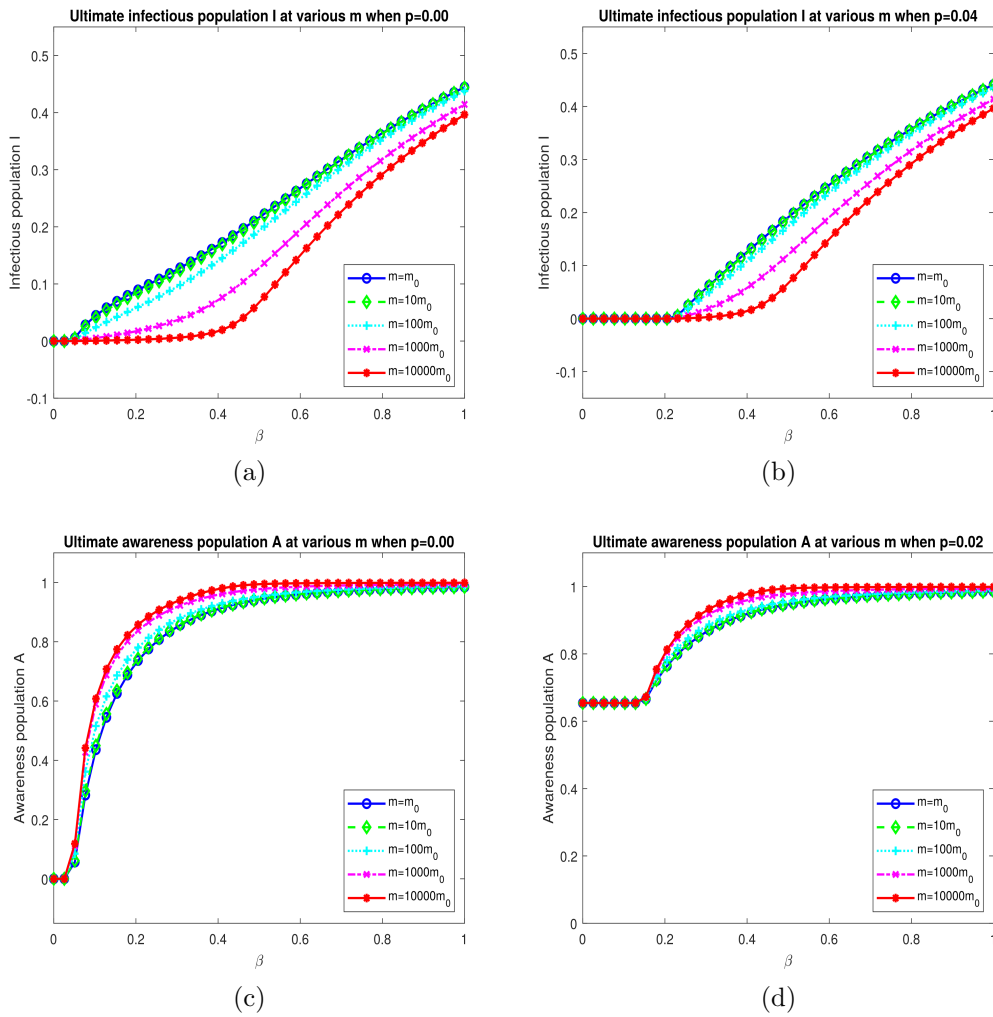


Figure 5.6.: The impact of global information on disease spreading dynamics

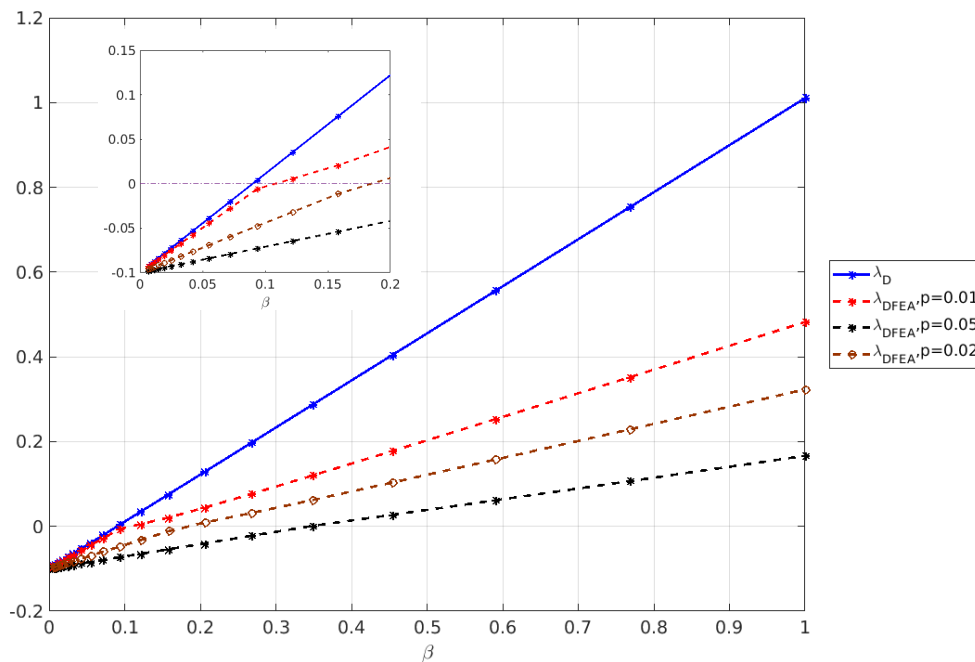
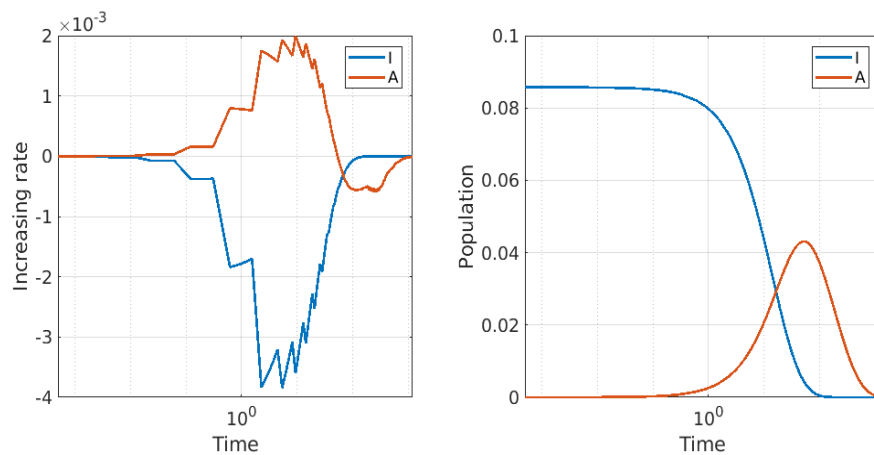
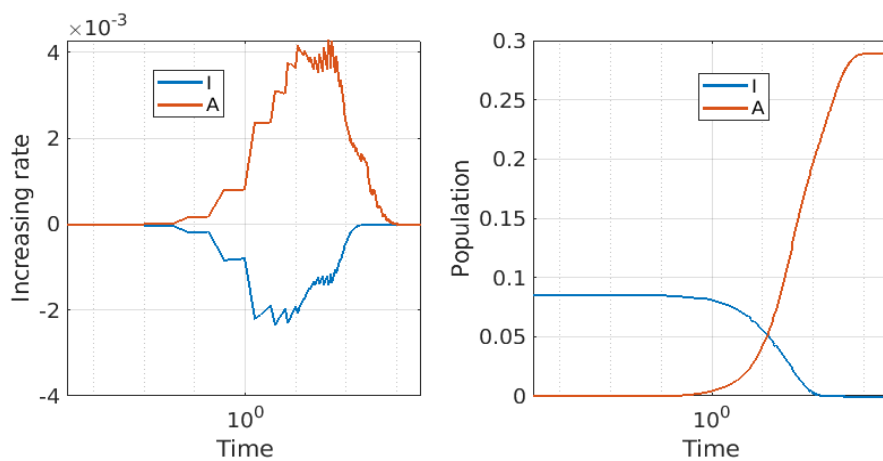


Figure 5.7.: Comparison between  $\lambda_D$  and  $\lambda_{DFEA}$ . DFE is achieved when  $\lambda < 0$ , otherwise the disease process will reach the endemic state.

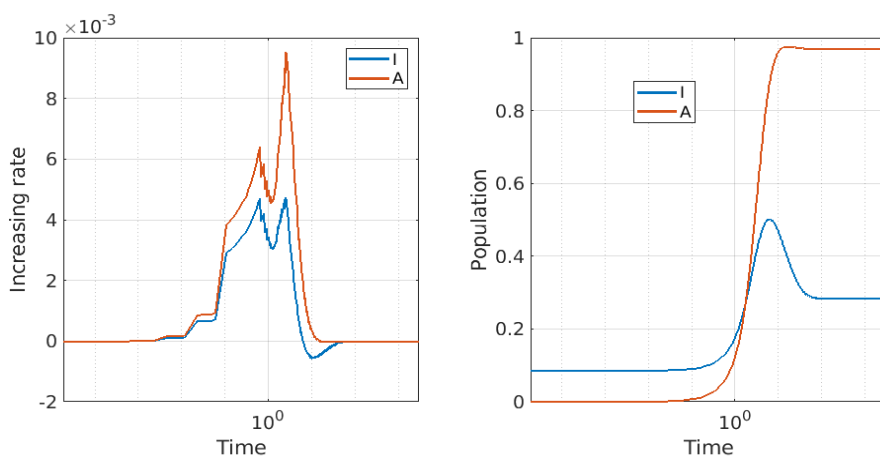
Figure 5.7 demonstrates the correctness of the derivation for  $\lambda_{DFE-A}$  and how the strength of local observation may eventually change the disease threshold. We observe that stronger local awareness  $p$  value will drive the disease from endemic to the disease free equilibrium state, particularly when the transmission rate  $\beta$  is low as shown in the figure ( $\beta < 0.35$ ). When the disease outbreaks and one can not turn endemic into disease free equilibrium, stronger local observation also contributes to significantly lowering the actual threshold value. This in return reduces the speed of the disease contagion as well as the final size of the disease outbreaks.



(a) DAFE



(b) DFE-A



(c) Endemic

Figure 5.8.: The rate of change for S and I in three different equilibrium states

Figure 5.8 presents the relative growth rates and dynamics of I and A population under different equilibrium states. For both DFE-A and DAFE, the information population will reach its peak shortly after the increase rate of infectious population reaches its minimum. Note that the synchronizations and disease dynamics during DFE-A and DAFE are different even though the disease gets eliminated in both cases. Under DAFE, the increasing rate of disease is in general faster than that of awareness. When disease population reaches zero, we observe that the amount of information also starts to drop. This implies that the growth of awareness population is primarily driven by the disease spreading itself, and the strength of the information awareness is not strong enough to persist. On the other hand, under DFE-A, we observe that the growth of awareness population is faster than the infectious population, and the relative growth rate of awareness population is always positive. And the increase rate also drops with decreasing number of infectious population. Nevertheless, we observe that the growth rates of awareness and infectious population are positively correlated, and there exists a time lag for the two growth rates to be positively correlated. This time lag is found to be shorter under DAFE, and much longer under DFE-A. Finally, the synchronizations and dynamics when the disease is endemic also differ from both DAFE and DFE-A. In particular, the growth of awareness and the growth of infectious population are found to be almost perfectly synchronized, but with awareness always spreading faster than the disease. This finding is found to be consistent with the real world observation reported in [110], where the growth rate of patient visit data (corresponding to infectious population) is perfectly synchronized with the trend of Google Flu index (corresponding to awareness population). Based on these findings, we conclude that when there is a large number of people that are aware of the disease, the disease either should be either of minimum risk or it has almost reached its endemic state.

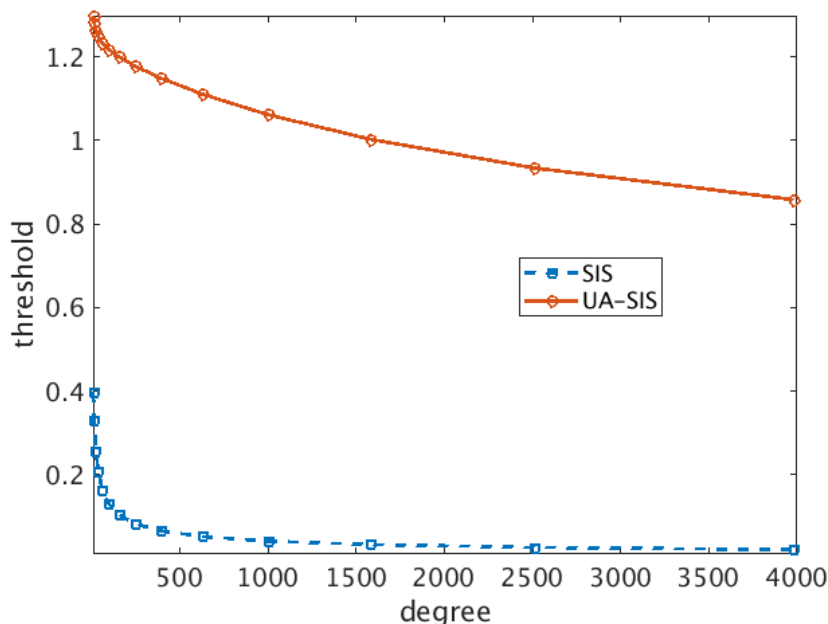


Figure 5.9.: Decay of disease threshold in scale free network with increasing number of nodes (increasing maximum degree). ( $\gamma = -2.5$ )

Finally, Figure 5.9 presents how disease threshold changes with the size of the network. An important and well-known finding for scale-free networks is that there is a lack of disease threshold if the power term of the degree distribution  $2 \leq \gamma < 3$ . The reason behind is that the moment of the variance of degree distribution diverges with the growing size of the network. Nevertheless, with the help of information dissemination, even a small amount of local information will significantly improve the resilience of the network and the disease threshold is found to be no longer diminishing. This is a particularly important observation and articulates the effectiveness of local information in preventing target attacks.

### 5.8 Conclusion

In this chapter, the multiplex network model for modeling co-evolution of information and disease dynamics over the networks is presented. In particular, travelers are assumed to change their behavior based on their observations of the states of

their neighbors, and by obtaining information from global sources such as news agencies and social medias. This percolation of information will have a direct impact on the disease dynamics over the disease network, meanwhile, the state of the disease spreading also affects the level of information released by global sources and the state and behavior of each individual travelers. The HMF method is used to model the co-evolution of the two dynamics, and obtained three possible stable states. Based on these findings, threshold values for disease and information percolation that may result in one of the three stable states are also discussed and validated by the numerical experiments.



## 6. CONCLUSION AND FUTURE WORK

### 6.1 Conclusion

This dissertation makes initial efforts to connect urban mobility and urban transportation systems with the spread of infectious diseases, and conducts thorough analyses to understand the relationship between them. In particular, their relationship is examined from the macroscopic level where travels within urban areas are modeled as passenger flow between zones, to the microscopic level where the contagion process is modeled among individual travelers. To support the modeling of infectious diseases at different aggregation levels, the dissertation introduces hybrid system modeling, reachability analysis, data-driven methods, and complex network theories, along with domain knowledge in transportation engineering and the-state-of-the-art methods of disease modeling, which combined with real-world datasets, to investigate how urban transportation system may facilitate and further the spread of infectious diseases. Based on theoretical analyses and comprehensive numerical experiments, the dissertation draws three major conclusions.

First, while the development of urban transportation systems improves the mobility level for urban commuters, it also increases the pace of the spread of infectious diseases, the highest number of people being infected, as well as the final size of disease outbreaks. These findings are supported by the results from regional level models which consider the inter-dependency among various transportation mode and selfish behavior of urban travelers. In particular, the increase in spreading pace is reflected by sooner time it takes to reach the disease peak and also the faster synchronization of disease dynamics among different urban areas. As for the size of the disease outbreaks, existing urban transportation systems may turn certain diseases that will

eventually reach DFE into endemic among urban population. It may also increase the total number of infected urban population as well as the peak size of infected people during disease outbreaks. These findings assert the emerging need to rethink the philosophy behind the planning of urban transportation system, and encourage the consideration of resilience for the design and operation of urban transportation systems.

Second, there are multiple measures that can be taken to mitigate or even eradicate infectious diseases by properly designing urban transportation networks and operating the systems. One possible measure is to place entrance control to decrease the number of infected people getting into this system so as to lower the risk exposure of urban commuters. But as indicated by the results from chapter four, such measure is barely effective considering the efforts and costs that it takes during practical implementation, and the results are only comparable to random control strategies at individual level. Instead, it will be more effective and sustainable to reduce the risk of infectious diseases through redesign of transportation networks, or even structure of urban forms. The results of chapter three and chapter four all suggest that the key idea to reduce the risk exposure is by decreasing the chance and duration that individual travelers get into contact, which may significantly improve the vulnerability of urban transportation systems because it will directly alter the degree distributions of individual contact networks during travel.

Finally, the availability of information on disease states and the dissemination of information among the population are observed to have significant impacts on both dynamics and final outcomes of infectious diseases in urban areas. The dissertation introduces the multiplex network approach to model the co-evolution of information and disease percolations on complex networks. The results indicate that personal awareness of the risk of diseases will directly change the state of disease outbreaks, from endemic to the state free of diseases. And the personal awareness can be improved through general education on the prevention and treatment of the diseases, which could be achieved at much lower cost as compared to directly measures for

controlling diseases. However, increasing level of personal awareness also has exponentially decayed marginal gain with increasing disease transmission rate. As a consequence, it is less effective to prevent the spread of diseases that are highly infectious. On the other hand, the available of global information is found to have no effect on altering the state of infectious diseases, nevertheless, it is effective to reduce the size of disease outbreaks significantly and slow down the spread speed of infectious diseases.

## 6.2 Future work

Based on the results and methods developed, there are two possible future directions which may further the works in this dissertation.

The first direction is to explore additional factors of urban transportation systems that may contribute to the spread of infectious diseases. For instance, the investigation on contact networks can be extended to incorporate adaptive networks as well as temporally varying networks. The adaptive nature of networks may model the change of travel behavior due to awareness of the diseases, which results in change of network topology as the disease proceeds. Moreover, the contact network may have different characteristics at different time periods of the day, and the introduction of temporal varying networks can model the transition of network structures over time to capture more accurate disease dynamics. In addition to introducing different network representation methods, the current modeling framework for individual contact networks can be extended to incorporate more accurate and complicated network models such as SEIR to further our understanding on the network structure on more refined disease dynamics.

The second direction is to extend the research framework in this dissertation to study research questions of similar characteristics. One particular example will be to extend the modeling approach (individual based disease modeling framework) to study the evolution of congestion on road networks. Note that the percolation of

traffic congestion follows a similar process as the disease spread process, but with different medias (from human beings to road segments). In addition, the multiplex network method can be used to model interdependency among different urban infrastructures. In this setting, we not only can model the dynamics for each individual network, but also be able to capture the internal impacts of the dynamics of one network on the others.

## REFERENCES

## REFERENCES

- [1] The Economist. Open-air computers, October 2012. [Accessed Nov, 2017].
- [2] Howard Frumkin. Urban sprawl and public health. *Public health reports*, 117(3):201, 2002.
- [3] Russ Lopez. Urban sprawl and risk for being overweight or obese. *American Journal of Public Health*, 94(9):1574–1579, 2004.
- [4] Reid Ewing, Tom Schmid, Richard Killingsworth, Amy Zlot, and Stephen Raudenbush. Relationship between urban sprawl and physical activity, obesity, and morbidity. In *Urban Ecology*, pages 567–582. Springer, 2008.
- [5] Billie Giles-Corti, Anne Vernez-Moudon, Rodrigo Reis, Gavin Turrell, Andrew L Dannenberg, Hannah Badland, Sarah Foster, Melanie Lowe, James F Sallis, Mark Stevenson, et al. City planning and population health: a global challenge. *The lancet*, 388(10062):2912–2924, 2016.
- [6] Mark Stevenson, Jason Thompson, Thiago Hérick de Sá, Reid Ewing, Dinesh Mohan, Rod McClure, Ian Roberts, Geetam Tiwari, Billie Giles-Corti, Xiaoduan Sun, et al. Land use, transport, and population health: estimating the health benefits of compact cities. *The Lancet*, 388(10062):2925–2935, 2016.
- [7] Wikipedia. 2015–16 zika virus epidemic, 2017. [Accessed Nov, 2017].
- [8] Wikipedia. Severe acute respiratory syndrome, 2017. [Accessed Nov, 2017].
- [9] World Health Organization. The ten leading causes of death by broad income group, 2017. World Health Organization Fact Sheet. [Accessed Nov, 2017].
- [10] Barney Cohen. Urbanization in developing countries: Current trends, future projections, and key challenges for sustainability. *Technology in society*, 28(1):63–80, 2006.
- [11] Wikipedia. List of infectious diseases, 2017. [Accessed Nov, 2017].
- [12] Chris Morris. The \$5.8 billion hidden cost of the flu on the us economy, Oct 2016. CNBC News. [Accessed Nov, 2017].
- [13] Degrees and Radians. Sars infographic, November 2012. [Accessed Nov, 2017].
- [14] Hector De Arazoza, Rachid Lounes, Thu Hoang, and Yannet Interian. Modeling hiv epidemic under contact tracing—the cuban case. *Computational and Mathematical Methods in Medicine*, 2(4):267–274, 2000.
- [15] David Fisman, Edwin Khoo, and Ashleigh Tuite. Early epidemic dynamics of the west african 2014 ebola outbreak: estimates derived with a simple two-parameter model. *PLoS currents*, 6, 2014.

- [16] SALLY GOLDENBERG. Report: Commute time for nyc residents longest in the nation, March 2015. Politico. [Accessed Nov, 2017].
- [17] Katie Nelson. Beijing's commutes worst in china, followed by shanghai's, Jan 2015. Shanghaiist. [Accessed Nov, 2017].
- [18] Hong Kong Special Administrative Region Government . Hong kong: The facts, April 2015. [Accessed Nov, 2017].
- [19] Alexandra Mangili and Mark A Gendreau. Transmission of infectious diseases during commercial air travel. *The Lancet*, 365(9463):989–996, 2005.
- [20] Duygu Balcan, Vittoria Colizza, Bruno Gonçalves, Hao Hu, José J Ramasco, and Alessandro Vespignani. Multiscale mobility networks and the spatial spreading of infectious diseases. *Proceedings of the National Academy of Sciences*, 106(51):21484–21489, 2009.
- [21] Kamran Khan, Julien Arino, Wei Hu, Paulo Raposo, Jennifer Sears, Felipe Calderon, Christine Heidebrecht, Michael Macdonald, Jessica Liauw, Angie Chan, et al. Spread of a novel influenza a (h1n1) virus via global airline transportation. *N Engl J Med*, 2009(361):212–214, 2009.
- [22] William O Kermack and Anderson G McKendrick. A contribution to the mathematical theory of epidemics. In *Proceedings of the Royal Society of London A: mathematical, physical and engineering sciences*, volume 115, pages 700–721. The Royal Society, 1927.
- [23] William O Kermack and Anderson G McKendrick. Contributions to the mathematical theory of epidemics. ii. the problem of endemicity. *Proceedings of the Royal Society of London. Series A, containing papers of a mathematical and physical character*, 138(834):55–83, 1932.
- [24] Romualdo Pastor-Satorras and Alessandro Vespignani. Epidemic spreading in scale-free networks. *Physical review letters*, 86(14):3200, 2001.
- [25] Yamir Moreno, Romualdo Pastor-Satorras, and Alessandro Vespignani. Epidemic outbreaks in complex heterogeneous networks. *The European Physical Journal B-Condensed Matter and Complex Systems*, 26(4):521–529, 2002.
- [26] Herbert W Hethcote. The mathematics of infectious diseases. *SIAM review*, 42(4):599–653, 2000.
- [27] Odo Diekmann and Johan Andre Peter Heesterbeek. *Mathematical epidemiology of infectious diseases: model building, analysis and interpretation*, volume 5. John Wiley & Sons, 2000.
- [28] Roy M Anderson, Robert M May, and B Anderson. *Infectious diseases of humans: dynamics and control*, volume 28. Wiley Online Library, 1992.
- [29] Fred Brauer, Carlos Castillo-Chavez, and Carlos Castillo-Chavez. *Mathematical models in population biology and epidemiology*, volume 40. Springer, 2001.
- [30] Julien Arino, Fred Brauer, Pauline van den Driessche, James Watmough, and Jianhong Wu. Simple models for containment of a pandemic. *Journal of the Royal Society Interface*, 3(8):453–457, 2006.

- [31] Abba B Gumel, Shigui Ruan, Troy Day, James Watmough, Fred Brauer, P Van den Driessche, Dave Gabrielson, Chris Bowman, Murray E Alexander, Sten Ardal, et al. Modelling strategies for controlling sars outbreaks. *Proceedings of the Royal Society of London B: Biological Sciences*, 271(1554):2223–2232, 2004.
- [32] Dieter Schenzle. An age-structured model of pre-and post-vaccination measles transmission. *Mathematical Medicine and Biology: A Journal of the IMA*, 1(2):169–191, 1984.
- [33] David Greenhalgh. Analytical results on the stability of age-structured recurrent epidemic models. *Mathematical Medicine and Biology: A Journal of the IMA*, 4(2):109–144, 1987.
- [34] Carlos Castillo-Chavez, Herbert W Hethcote, Viggo Andreasen, Simon A Levin, and Wei M Liu. Epidemiological models with age structure, proportionate mixing, and cross-immunity. *Journal of mathematical biology*, 27(3):233–258, 1989.
- [35] Sonia Altizer, Andrew Dobson, Parvize Hosseini, Peter Hudson, Mercedes Pascual, and Pejman Rohani. Seasonality and the dynamics of infectious diseases. *Ecology letters*, 9(4):467–484, 2006.
- [36] Stavros Busenberg and Kenneth Cooke. *Vertically transmitted diseases: models and dynamics*, volume 23. Springer Science & Business Media, 2012.
- [37] Z Agur, L Cojocar, G Mazar, RM Anderson, and YL Danon. Pulse mass measles vaccination across age cohorts. *Proceedings of the National Academy of Sciences*, 90(24):11698–11702, 1993.
- [38] Boris Shulgin, Lewi Stone, and Zvia Agur. Pulse vaccination strategy in the sir epidemic model. *Bulletin of mathematical biology*, 60(6):1123–1148, 1998.
- [39] Alberto d’Onofrio. On pulse vaccination strategy in the sir epidemic model with vertical transmission. *Applied Mathematics Letters*, 18(7):729–732, 2005.
- [40] Julien Arino and P Van den Driessche. A multi-city epidemic model. *Mathematical Population Studies*, 10(3):175–193, 2003.
- [41] Roy M Anderson and Robert M May. Vaccination and herd immunity. *Nature*, 318:28, 1985.
- [42] Odo Diekmann, Johan Andre Peter Heesterbeek, and Johan AJ Metz. On the definition and the computation of the basic reproduction ratio  $r_0$  in models for infectious diseases in heterogeneous populations. *Journal of mathematical biology*, 28(4):365–382, 1990.
- [43] O Diekmann, JAP Heesterbeek, and MG Roberts. The construction of next-generation matrices for compartmental epidemic models. *Journal of the Royal Society Interface*, page rsif20090386, 2009.
- [44] Michael Y Li and James S Muldowney. Global stability for the seir model in epidemiology. *Mathematical biosciences*, 125(2):155–164, 1995.

- [45] Edoardo Beretta and Yasuhiro Takeuchi. Global stability of an sir epidemic model with time delays. *Journal of mathematical biology*, 33(3):250–260, 1995.
- [46] Alberto d’Onofrio. Stability properties of pulse vaccination strategy in seir epidemic model. *Mathematical biosciences*, 179(1):57–72, 2002.
- [47] Andrei Korobeinikov and Graeme C Wake. Lyapunov functions and global stability for sir, sirs, and sis epidemiological models. *Applied Mathematics Letters*, 15(8):955–960, 2002.
- [48] Wei-min Liu, Herbert W Hethcote, and Simon A Levin. Dynamical behavior of epidemiological models with nonlinear incidence rates. *Journal of mathematical biology*, 25(4):359–380, 1987.
- [49] Herbert W Hethcote and P Van Den Driessche. Some epidemiological models with nonlinear incidence. *Journal of Mathematical Biology*, 29(3):271–287, 1991.
- [50] Leonid A Rvachev and Ira M Longini. A mathematical model for the global spread of influenza. *Mathematical biosciences*, 75(1):3–22, 1985.
- [51] Steven Riley, Christophe Fraser, Christl A Donnelly, Azra C Ghani, Laith J Abu-Raddad, Anthony J Hedley, Gabriel M Leung, Lai-Ming Ho, Tai-Hing Lam, Thuan Q Thach, et al. Transmission dynamics of the etiological agent of sars in hong kong: impact of public health interventions. *Science*, 300(5627):1961–1966, 2003.
- [52] Christophe Fraser, Christl A Donnelly, Simon Cauchemez, William P Hanage, Maria D Van Kerkhove, T Déirdre Hollingsworth, Jamie Griffin, Rebecca F Baggaley, Helen E Jenkins, Emily J Lyons, et al. Pandemic potential of a strain of influenza a (h1n1): early findings. *science*, 324(5934):1557–1561, 2009.
- [53] Lauren Meyers. Contact network epidemiology: Bond percolation applied to infectious disease prediction and control. *Bulletin of the American Mathematical Society*, 44(1):63–86, 2007.
- [54] Lauren Ancel Meyers, Babak Pourbohloul, Mark EJ Newman, Danuta M Skowronski, and Robert C Brunham. Network theory and sars: predicting outbreak diversity. *Journal of theoretical biology*, 232(1):71–81, 2005.
- [55] Cristopher Moore and Mark EJ Newman. Epidemics and percolation in small-world networks. *Physical Review E*, 61(5):5678, 2000.
- [56] Romualdo Pastor-Satorras and Alessandro Vespignani. Epidemic dynamics and endemic states in complex networks. *Physical Review E*, 63(6):066117, 2001.
- [57] Mark EJ Newman. Spread of epidemic disease on networks. *Physical review E*, 66(1):016128, 2002.
- [58] Romualdo Pastor-Satorras and Alessandro Vespignani. Immunization of complex networks. *Physical Review E*, 65(3):036104, 2002.
- [59] Marián Boguná, Romualdo Pastor-Satorras, and Alessandro Vespignani. Absence of epidemic threshold in scale-free networks with degree correlations. *Physical review letters*, 90(2):028701, 2003.

- [60] Romualdo Pastor-Satorras, Claudio Castellano, Piet Van Mieghem, and Alessandro Vespignani. Epidemic processes in complex networks. *Reviews of modern physics*, 87(3):925, 2015.
- [61] Yang Wang, Deepayan Chakrabarti, Chenxi Wang, and Christos Faloutsos. Epidemic spreading in real networks: An eigenvalue viewpoint. In *Reliable Distributed Systems, 2003. Proceedings. 22nd International Symposium on*, pages 25–34. IEEE, 2003.
- [62] Deepayan Chakrabarti, Yang Wang, Chenxi Wang, Jurij Leskovec, and Christos Faloutsos. Epidemic thresholds in real networks. *ACM Transactions on Information and System Security (TISSEC)*, 10(4):1, 2008.
- [63] Sergio Gómez, Alexandre Arenas, J Borge-Holthoefer, Sandro Meloni, and Yamir Moreno. Discrete-time markov chain approach to contact-based disease spreading in complex networks. *EPL (Europhysics Letters)*, 89(3):38009, 2010.
- [64] Joel C Miller. Epidemic size and probability in populations with heterogeneous infectivity and susceptibility. *Physical Review E*, 76(1):010101, 2007.
- [65] Marián Boguná, Romualdo Pastor-Satorras, and Alessandro Vespignani. Epidemic spreading in complex networks with degree correlations. *arXiv preprint cond-mat/0301149*, 2003.
- [66] Thilo Gross, Carlos J Dommar D’Lima, and Bernd Blasius. Epidemic dynamics on an adaptive network. *Physical review letters*, 96(20):208701, 2006.
- [67] Márton Karsai, Mikko Kivelä, Raj Kumar Pan, Kimmo Kaski, János Kertész, A-L Barabási, and Jari Saramäki. Small but slow world: How network topology and burstiness slow down spreading. *Physical Review E*, 83(2):025102, 2011.
- [68] Juliette Stehlé, Nicolas Voirin, Alain Barrat, Ciro Cattuto, Vittoria Colizza, Lorenzo Isella, Corinne Régis, Jean-François Pinton, Nagham Khanafer, Wouter Van den Broeck, et al. Simulation of an seir infectious disease model on the dynamic contact network of conference attendees. *BMC medicine*, 9(1):87, 2011.
- [69] Guangming Ren and Xingyuan Wang. Epidemic spreading in time-varying community networks. *Chaos: An Interdisciplinary Journal of Nonlinear Science*, 24(2):023116, 2014.
- [70] UN DESA. United nations, department of economic and social affairs, population division: World urbanization prospects, the 2014 revision, 2015.
- [71] Michael Brauer, Gerard Hoek, Patricia Van Vliet, Kees Meliefste, Paul H Fischer, Alet Wijga, Laurens P Koopman, Herman J Neijens, Jorrit Gerritsen, Marjan Kerkhof, et al. Air pollution from traffic and the development of respiratory infections and asthmatic and allergic symptoms in children. *American journal of respiratory and critical care medicine*, 166(8):1092–1098, 2002.
- [72] Arie Oosterlee, Marjon Drijver, Erik Lebet, and Bert Brunekreef. Chronic respiratory symptoms in children and adults living along streets with high traffic density. *Occupational and environmental medicine*, 53(4):241–247, 1996.

- [73] Rafael Lozano, Mohsen Naghavi, Kyle Foreman, Stephen Lim, Kenji Shibuya, Victor Aboyans, Jerry Abraham, Timothy Adair, Rakesh Aggarwal, Stephanie Y Ahn, et al. Global and regional mortality from 235 causes of death for 20 age groups in 1990 and 2010: a systematic analysis for the global burden of disease study 2010. *The Lancet*, 380(9859):2095–2128, 2013.
- [74] Matthew Chambers, Justyna Goworowska, and Sonya Smith. Passenger travel facts and figures 2015. 2015.
- [75] Global Market Forecast. Flying by numbers 2015–2034, 2015.
- [76] Hal L Smith, Liancheng Wang, and Michael Y Li. Global dynamics of an seir epidemic model with vertical transmission. *SIAM Journal on Applied Mathematics*, 62(1):58–69, 2001.
- [77] Herbert W Hethcote, Harlan W Stech, and Pauline van den Driessche. Periodicity and stability in epidemic models: a survey. *Differential Equations and Applications in Ecology, Epidemics and Population Problems*, Academic Press, New York, pages 65–82, 1981.
- [78] Leon Danon, Ashley P Ford, Thomas House, Chris P Jewell, Matt J Keeling, Gareth O Roberts, Joshua V Ross, and Matthew C Vernon. Networks and the epidemiology of infectious disease. *Interdisciplinary perspectives on infectious diseases*, 2011, 2011.
- [79] Alun L Lloyd and Robert M May. Spatial heterogeneity in epidemic models. *Journal of theoretical biology*, 179(1):1–11, 1996.
- [80] Lisa Sattenspiel and Klaus Dietz. A structured epidemic model incorporating geographic mobility among regions. *Mathematical biosciences*, 128(1-2):71–91, 1995.
- [81] Pauline Van den Driessche and James Watmough. Reproduction numbers and sub-threshold endemic equilibria for compartmental models of disease transmission. *Mathematical biosciences*, 180(1-2):29–48, 2002.
- [82] R. Alur, C. Courcoubetis, N. Halbwachs, T. A. Henzinger, P.-H. Ho, X. Nicollin, A. Olivero, J. Sifakis, and S. Yovine. The algorithmic analysis of hybrid systems. *Theor. Comput. Sci.*, 138(1):3–34, 1995.
- [83] X. Chen, E. Abraham, and S. Sankaranarayanan. Flow\*: An analyzer for non-linear hybrid systems. In *Proc. of CAV'13*, volume 8044 of *LNCS*, pages 258–263. Springer, 2013.
- [84] R. E. Moore, R. B. Kearfott, and M. J. Cloud. *Introduction to Interval Analysis*. SIAM, 2009.
- [85] M. Berz. *Modern Map Methods in Particle Beam Physics*, volume 108 of *Advances in Imaging and Electron Physics*. Academic Press, 1999.
- [86] K. Makino and M. Berz. Taylor models and other validated functional inclusion methods. *J. Pure and Applied Mathematics*, 4(4):379–456, 2003.

- [87] M. Berz and K. Makino. Verified integration of ODEs and flows using differential algebraic methods on high-order Taylor models. *Reliable Computing*, 4:361–369, 1998.
- [88] X. Chen. *Reachability Analysis of Non-Linear Hybrid Systems Using Taylor Models*. PhD thesis, RWTH Aachen University, 2015.
- [89] X. Chen, E. Ábrahám, and S. Sankaranarayanan. Taylor model flowpipe construction for non-linear hybrid systems. In *Proc. of RTSS'12*, pages 183–192. IEEE Computer Society, 2012.
- [90] Ashleigh R Tuite, Amy L Greer, Michael Whelan, Anne-Luise Winter, Brenda Lee, Ping Yan, Jianhong Wu, Seyed Moghadas, David Buckeridge, Babak Pourbohloul, et al. Estimated epidemiologic parameters and morbidity associated with pandemic h1n1 influenza. *Canadian Medical Association Journal*, 182(2):131–136, 2010.
- [91] Xinghuo Pang, Zonghan Zhu, Fujie Xu, Jiyong Guo, Xiaohong Gong, Donglei Liu, Zejun Liu, Daniel P Chin, and Daniel R Feikin. Evaluation of control measures implemented in the severe acute respiratory syndrome outbreak in beijing, 2003. *Jama*, 290(24):3215–3221, 2003.
- [92] Center for Disease Control and Prevention. Frequently asked questions about sars. [Online; Accessed 15-DEC-2017].
- [93] Vittoria Colizza, Alain Barrat, Marc Barthélemy, and Alessandro Vespignani. Predictability and epidemic pathways in global outbreaks of infectious diseases: the sars case study. *BMC medicine*, 5(1):34, 2007.
- [94] Tuen Wai Ng, Gabriel Turinici, and Antoine Danchin. A double epidemic model for the sars propagation. *BMC Infectious Diseases*, 3(1):19, 2003.
- [95] Xin Chen and Sriram Sankaranarayanan. Decomposed reachability analysis for nonlinear systems. In *Real-Time Systems Symposium (RTSS), 2016 IEEE*, pages 13–24. IEEE, 2016.
- [96] Vanja Dukic, Hedibert F Lopes, and Nicholas G Polson. Tracking epidemics with google flu trends data and a state-space seir model. *Journal of the American Statistical Association*, 107(500):1410–1426, 2012.
- [97] Gaode Map API. <http://map.amap.com/subway/>, 2018. Accessed: 2018-09-30.
- [98] Shanghai Metro Schedule. <http://service.shmetro.com/en/hcskb/240.htm>, 2018. Accessed: 2018-09-30.
- [99] Gene H Golub and Charles F Van Loan. *Matrix computations*, volume 3. JHU Press, 2012.
- [100] Ana Lajmanovich and James A Yorke. A deterministic model for gonorrhoea in a nonhomogeneous population. *Mathematical Biosciences*, 28(3-4):221–236, 1976.
- [101] Frank J Massey Jr. The kolmogorov-smirnov test for goodness of fit. *Journal of the American statistical Association*, 46(253):68–78, 1951.

- [102] Jie Huang, David Levinson, Jiaoe Wang, Jiangping Zhou, and Zi-jia Wang. Tracking job and housing dynamics with smartcard data. *Proceedings of the National Academy of Sciences*, page 201815928, 2018.
- [103] Mark Dickison, Shlomo Havlin, and H Eugene Stanley. Epidemics on interconnected networks. *Physical Review E*, 85(6):066109, 2012.
- [104] Joaquín Sanz, Cheng-Yi Xia, Sandro Meloni, and Yamir Moreno. Dynamics of interacting diseases. *Physical Review X*, 4(4):041005, 2014.
- [105] Camila Buono, Lucila G Alvarez-Zuzek, Pablo A Macri, and Lidia A Braunstein. Epidemics in partially overlapped multiplex networks. *PloS one*, 9(3):e92200, 2014.
- [106] Zi-Ke Zhang, Chuang Liu, Xiu-Xiu Zhan, Xin Lu, Chu-Xu Zhang, and Yi-Cheng Zhang. Dynamics of information diffusion and its applications on complex networks. *Physics Reports*, 651:1–34, 2016.
- [107] Mina Youssef and Caterina Scoglio. An individual-based approach to sir epidemics in contact networks. *Journal of theoretical biology*, 283(1):136–144, 2011.
- [108] Clara Granell, Sergio Gómez, and Alex Arenas. Competing spreading processes on multiplex networks: awareness and epidemics. *Physical review E*, 90(1):012808, 2014.
- [109] Wei Wang, Ming Tang, Hui Yang, Younghae Do, Ying-Cheng Lai, and Gyu-Won Lee. Asymmetrically interacting spreading dynamics on complex layered networks. *Scientific reports*, 4:5097, 2014.
- [110] Wei Wang, Quan-Hui Liu, Shi-Min Cai, Ming Tang, Lidia A Braunstein, and H Eugene Stanley. Suppressing disease spreading by using information diffusion on multiplex networks. *Scientific reports*, 6:29259, 2016.
- [111] Zhongyuan Ruan, Ming Tang, and Zonghua Liu. Epidemic spreading with information-driven vaccination. *Physical Review E*, 86(3):036117, 2012.

VITA

## VITA

Xinwu Qian graduated in 2012 with a B.S. degree in Transportation Engineering from Tongji University in China. He received a M.S.E degree in Civil Engineering in 2014 from Purdue University. He pursued his Ph.D. study under the supervision of Prof. Satish Ukkusuri in Transportation Engineering at Purdue University. His research interests include big data analytics in transportation, urban computing, complex networks, and transportation network modeling. He authored more than 19 peer-reviewed journal and conferences papers, 3 book chapters, and 2 project reports. In 2018, Xinwu was awarded his Ph.D. degree from Purdue University.